Supplementary Material on

"Temperature-gradient induced massive augmentation of solute dispersion in viscoelastic micro-flows"

Siddhartha Mukherjee,[1], Sunando DasGupta[1,2], Suman Chakraborty[1,3*]

[1]*Advanced Technology Development Center, Indian Institute of Technology Kharagpur, Kharagpur, India-721302*
[2]*Department of Chemical Engineering, Indian Institute of Technology Kharagpur, Kharagpur, India-721302*
[3]*Department of Mechanical Engineering, Indian Institute of Technology Kharagpur, Kharagpur, India-721302*

Section A. Analytical solution procedure

In this section, the solution methodology is discussed in detail. As evident from its definition, hydrodynamic dispersion coefficient depends strongly on the flow velocity which in turn is influenced by the pertinent electrokinetic and thermo-electric forcing. Here, the temperature distribution is discussed first which is followed by the potential distribution. Then these two are further employed in the momentum equation to obtain the velocity distribution.

A1 *Temperature distribution*

Unlike conventional streaming field-induced electrokinetic flow, here temperature (T) within the microchannel does not remain constant which is given by the energy equation

$$\rho C_p\left(u\frac{\partial T}{\partial x}+v\frac{\partial T}{\partial y}\right)=\frac{\partial}{\partial x}\left(k\frac{\partial T}{\partial x}\right)+\frac{\partial}{\partial y}\left(k\frac{\partial T}{\partial y}\right)+Q_{gen}+Q_{vd} \tag{S1}$$

where ρ, C_p and k are density, specific heat capacity and thermal conductivity of the fluid respectively. The left-hand side of equation (S1) represents the advective component of the thermal transport, whereas the first and second terms on the right side represent the axial and transverse conductive components. Q_{gen} is the heat generation term due to the induced streaming field and Q_{vd} is the viscous dissipation term. Q_{gen} can be expressed as $Q_{gen} \sim \sigma E_x^{\,2}$ where $E_x=-\partial\phi/\partial x$ is the induced streaming field and σ bulk electrical conductivity, $\sigma=2z^2e^2Dn_\infty/k_BT$ with z, e, D, n_∞ and k_B being the valence of ions, elementary electronic charge, average diffusivity of ions, bulk ionic number density and Boltzmann constant respectively. Besides, for a Newtonian fluid, the viscous dissipation term $\left(Q_{vd}\right)$ in equation (S1) can be written as $\mu\left[2\left\{\left(\frac{\partial u}{\partial x}\right)^2+\left(\frac{\partial v}{\partial y}\right)^2\right\}+\left(\frac{\partial u}{\partial y}+\frac{\partial v}{\partial x}\right)^2\right]-\frac{2}{3}\mu\left(\nabla\cdot\boldsymbol{v}\right)^2$ where $\mu\left(T\right)$ is the viscosity of the fluid. Here, we have neglected the variation of ρ and C_p with temperature while obtaining

*Corresponding author, email: suman@mech.iitkgp.ernet.in

the temperature distribution, whereas other thermo-physical properties like viscosity (μ), electrical permittivity (ε) and thermal conductivity (k) are considered to be temperature-dependent. The following forms of temperature dependencies are assumed: $\mu = \mu_{ref} \exp\left[-\omega_1\left(T - T_{ref}\right)\right]$, $\varepsilon = \varepsilon_{ref} \exp\left[-\omega_2\left(T - T_{ref}\right)\right]$ and $k = k_{ref} \exp\left[\omega_3\left(T - T_{ref}\right)\right]$ where the subscript "*ref*" denotes the reference value of the property evaluated at reference temperature T_{ref} with ω_is being individual temperature sensitivities. The reason for assuming constant ρ and C_p is that the relative change of ρ and C_p with temperature is insignificant as compared to the change of other parameters (μ, ε, k) (Dietzel & Hardt 2017). For incompressible flow, $\nabla \cdot \boldsymbol{v}$ becomes zero and the expression of Q_{vd} gets simplified. Now, to obtain the temperature field, we have non-dimensionalized the energy equation (S1) by using the following variables

$$\bar{u} = \frac{u}{u_c},\ \bar{v} = \frac{v\,l}{u_c\,h},\ \theta = \frac{T - T_C}{\Delta T_{ref}},\ \bar{\phi} = \frac{z\,e\,\phi}{k_B\,T_C}$$

where u_c and $T_C = T_{ref}$ are taken as characteristic scales of velocity and temperature with $\Delta T_{ref} = \left(T_H - T_C\right)/2$ being the characteristic temperature difference. The dimensionless form of equation (S1) reads

$$\left.\begin{aligned}\beta\,Pe_T\left(\bar{u}\frac{\partial\theta}{\partial\bar{x}} + \bar{v}\frac{\partial\theta}{\partial\bar{y}}\right) = \beta^2\frac{\partial}{\partial\bar{x}}\left(\frac{k}{k_{ref}}\frac{\partial\theta}{\partial\bar{x}}\right) + \frac{\partial}{\partial\bar{y}}\left(\frac{k}{k_{ref}}\frac{\partial\theta}{\partial\bar{y}}\right) + \beta^2\frac{\varepsilon\,\kappa^2 D}{k_{ref}\,\Delta T_{ref}}\left(\frac{k_B\,T_C}{z\,e}\right)^2\left(\frac{\partial\bar{\phi}}{\partial\bar{x}}\right)^2 \\ + \frac{\mu\,u_c^{\,2}}{k_{ref}\,\Delta T_{ref}}\left[2\beta^2\left\{\left(\frac{\partial\bar{u}}{\partial\bar{x}}\right)^2 + \left(\frac{\partial\bar{v}}{\partial\bar{y}}\right)^2\right\} + \left(\frac{\partial\bar{u}}{\partial\bar{y}} + \beta^2\frac{\partial\bar{v}}{\partial\bar{x}}\right)^2\right]\end{aligned}\right\} \quad \text{(S2)}$$

In equation (S2), $\beta = h / l$ is the aspect ratio of the microchannel, $Pe_T = u_c\,h/\alpha_{ref}$ thermal Peclet number with thermal diffusivity $\alpha_{ref} = k_{ref}/\rho\,C_p$ and $\kappa = \sqrt{2z^2e^2n_\infty/\varepsilon k_B T}$ is the inverse of the electrical double layer (EDL) thickness. Similarly, temperature-dependent thermo-physical properties are also rewritten as $\bar{\mu} = \mu/\mu_{ref} = \exp\left(-\gamma C_\mu \theta\right)$, $\bar{\varepsilon} = \varepsilon/\varepsilon_{ref} = \exp\left(-\gamma C_\varepsilon \theta\right)$ and $\bar{k} = k/k_{ref} = \exp\left(\gamma C_k \theta\right)$ respectively where $C_\mu = \omega_1 T_C$, $C_\varepsilon = \omega_2 T_C$, $C_k = \omega_3 T_C$ and $\gamma = \Delta T/T_C$ is the ratio of the imposed temperature difference to the reference temperature. Here, the values of l and h are taken as ~ 1 mm and 1 μm respectively thus making β ~ O(10^{-3}), i.e. << 1. The characteristic velocity scale is chosen as the scale that is typically used for pressure-driven flow $u_c \sim \frac{\Delta p_0\,\beta\,h}{3\mu_{ref}}$. Assuming viscosity, μ_{ref} ~ 10^{-3} Pa. s. and pressure drop Δp_0 ~ O(10^2) Pa, u_c turns out to be of the order of ~ 10^{-4} ms^{-1}. For bulk ionic number density $n_\infty = 6.023\times10^{20}$ mol^{-1}), the inverse of EDL thickness κ becomes O(10^7) m. For typical values of parameters ρ ~ 10^3 kg m^{-3}, C_p ~ 4200 J kg^{-1} K^{-1}, k_{ref} ~ 0.6 W m^{-1} K^{-1}, the value of thermal Peclet number $\left(Pe_T\right)$ becomes ~ O(10^{-4}). Since Pe_T is already multiplied by another small quantity β, thus, one can safely neglect the advective component in the energy equation (S2) and therefore, any alteration in the hydrodynamics due to the application of thermal gradient has no effect on the temperature distribution. Similarly, heat generation term involves a quantity $\varepsilon\kappa^2 D k_B^{\,2} T_c^{\,2}/\left(k_{ref}\Delta T_{ref}\,z^2e^2\right)$ which, for ΔT_{ref} ~ O(10) K, ε ~ O(10^{-10}) Fm^{-1}, D ~ 10^{-9} m^{2}s^{-1}, κ ~ O(10^7) m^{-1} becomes O(10^{-9})

which is further multiplied by the quantity β^2 where $\beta << 1$ and hence, the heat generation due to streaming field can be neglected. Also, most of the terms in viscous dissipation component involve $\beta^2$and diminish for $\beta << 1$. The remaining term is $\frac{\mu\, u_c^{\,2}}{k_{ref}\,\Delta T_{ref}}\left(\frac{\partial \bar{u}}{\partial \bar{y}}\right)^2$, which in our analysis comes out to be O(10^{-8}) and remains insignificant in determining the temperature distribution.

Case (a): *Temperature gradient applied in the axial direction*

For axially applied temperature gradient, the simplified energy equation subjected to the aforesaid assumptions is given below

$$\frac{\partial}{\partial \bar{x}}\left(\bar{k}\,\frac{\partial \theta}{\partial \bar{x}}\right)=0 \tag{S3}$$

where the dimensionless form of thermal conductivity is written as $\bar{k}=k/k_{ref}=\exp\left(\gamma C_k\,\theta\right)$ with k_{ref} being the reference thermal conductivity at T_{ref}. We have obtained both closed-form and approximate analytical solution of the temperature distribution. For approximate analytical solution, the well-known asymptotic approach has been followed (typically employed to capture small perturbation to the system) where any variable φ can be expanded in the following way

$$\varphi=\varphi_0+\gamma\,\varphi_1+\gamma^2\varphi_2+\ldots\ldots \tag{S4}$$

where $\gamma=\Delta T/T_C$ is the thermal perturbation parameter used in the regular perturbation approach (S4) which implies the ratio of the imposed temperature difference of the domain to the cold side temperature (so, $\gamma\to 0$ represents the scenario of isothermal condition). The exact solution of equation (S3) subjected to axial temperature difference (i.e. at $\bar{x}=0,\ \theta=0$ and at $\bar{x}=1,\ \theta=2$) is given by

$$\theta=\ln\left\{-C_k C_{T1}\gamma\left(C_{T2}+x\right)\right\}\Big/\gamma C_k \tag{S5}$$

where $C_{T1}=-\left(e^{2\gamma C_k}-1\right)\Big/\gamma C_k$, $C_{T2}=1\Big/\left(e^{2\gamma C_k}-1\right)$. Meanwhile, the governing equations and the solution for the asymptotic approach read as

governing equations:

$$\begin{aligned}&\mathrm{O}(1):\ \frac{\partial^2\theta_0}{\partial \bar{x}^2}=0 \qquad\qquad \left(\text{leading order}\right)\\ &O(\gamma):\ \frac{\partial^2\theta_1}{\partial \bar{x}^2}+C_k\,\theta_0\,\frac{\partial^2\theta_0}{\partial \bar{x}^2}+C_k\left(\frac{\partial\theta_0}{\partial \bar{x}}\right)^2=0 \quad \left(\text{first order}\right)\end{aligned} \tag{S6}$$

and solution:

$$\theta=\theta_0+\gamma\,\theta_1=2\,\bar{x}+2\,C_k\,\gamma\left(\bar{x}-\bar{x}^2\right) \tag{S7}$$

The comparison between the exact solution and asymptotic solution for temperature distribution is presented in figure S1 where the lines show the results of the exact solution with symbols representing the predictions of asymptotic approach. With increasing C_k, enhanced temperature sensitivity of the fluid thermal conductivity results in a departure from the linear variation of temperature in the axial direction. At higher C_k (i.e. at C_k = 10), this distribution becomes parabolic in nature where a deviation between the asymptotic and exact solution can be noticed (as shown in the inset). However, as reported in the literature, the relative change of thermal conductivity with temperature in the typical electrolyte solution is $\left(1/k\right)\cdot\left(\partial k/\partial T\right)=2.41\times10^{-3}$ K^{-1} (Dietzel & Hardt 2017) for which the value of C_k turns out to be

of the order of unity and hence, a linear temperature distribution can be assumed safely as an approximation. Throughout our analysis, we maintain $C_k = 1$ while presenting the results.

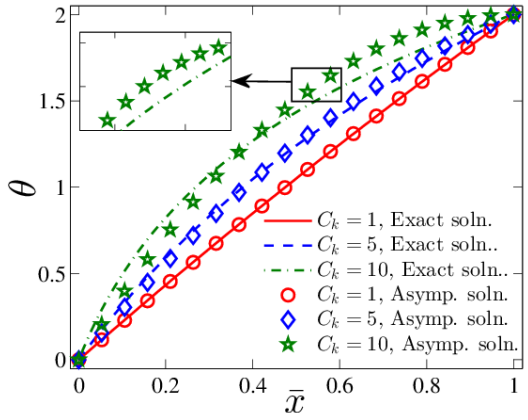

FIGURE S1. Dimensionless temperature profile in the *x*-direction for different C_k. Lines show exact solutions while asymptotic solutions are shown by symbols. Inset shows zoomed view at $C_k = 10$.

A2 *Potential distribution*

In contrast to the conventional electrokinetics problem, in presence of thermal gradient, ions no longer remain in equilibrium and one cannot consider Boltzmann distribution assumption while obtaining the potential distribution. Here, we need to find the ionic number concentration first which can be obtained by employing the classical Nernst-Planck (NP) equation. The electrolyte solution is considered to be dilute such that effects like ion-ion correlation or finite-size effect (also known as steric effect) can be neglected. Under steady-state and in absence of any chemical reaction, the NP equation for the transport of ionic species reads as $\nabla \cdot J_i = 0$ i.e. the divergence of net ionic flux is zero. This ionic flux $\left(J_i\right)$ consists of 4 components, namely, advection $\left(n_i \boldsymbol{v}\right)$, diffusion $\left(D_i \nabla n_i\right)$, thermo-diffusion $\left(n_i D_{Ti} \nabla T\right)$, and electro-migration $\left(n_i \, u_i^* \nabla \phi\right)$ components

$$J_i = n_i \boldsymbol{v} - D_i \nabla n_i - n_i D_{Ti} \nabla T - n_i \mu_i^* \nabla \phi \tag{S8}$$

In equation (S8), D_i is the diffusivity, D_{Ti} and μ_i^* are the thermophoretic and electrophoretic mobilities respectively with $\mu_i^* = e z_i D_i / \left(k_B T\right)$. Using $\bar{n}_i = n_i / n_0$, $\bar{\phi} = z e \phi / \left(k_B T_C\right)$, $\bar{z}_i = z_i / z$, dimensionless form of $\nabla \cdot J_i = 0$ is written below

$$\beta^2 Pe_i \left(\bar{u} \frac{\partial \bar{n}_i}{\partial \bar{x}} + \bar{v} \frac{\partial \bar{n}_i}{\partial \bar{y}} \right) = \beta^2 \frac{\partial}{\partial \bar{x}} \left[\frac{D_i}{D} \left(\frac{\partial \bar{n}_i}{\partial \bar{x}} + \bar{n}_i \bar{S}_{Ti} \gamma \frac{\partial \theta}{\partial \bar{x}} + \frac{\bar{z}_i \bar{n}_i}{1 + \gamma \theta} \frac{\partial \bar{\phi}}{\partial \bar{x}} \right) \right] + \frac{\partial}{\partial \bar{y}} \left[\frac{D_i}{D} \left(\frac{\partial \bar{n}_i}{\partial \bar{y}} + \bar{n}_i \bar{S}_{Ti} \gamma \frac{\partial \theta}{\partial \bar{y}} + \frac{\bar{z}_i \bar{n}_i}{1 + \gamma \theta} \frac{\partial \bar{\phi}}{\partial \bar{y}} \right) \right] \tag{S9}$$

Here, $\bar{S}_{Ti}$ is the Soret coefficient of ions defined as $\bar{S}_{Ti} = \left(D_{Ti} / D_i\right) T_C$ and Pe_i is the ionic Peclet number $\left(Pe_i = u_c l / D\right)$ which should not exceed unity for a diffusion-dominated problem like this and therefore, the advective term (i.e. left side of equation (S9)) becomes ~ O (β^2). Since, $\beta << 1$, this term and the first term on the right side can be neglected while finding $\bar{n}_i$. Potential $\bar{\phi}$ consists of two terms $\bar{\phi} = \bar{\phi}\left(\bar{x}\right) + \psi\left(\bar{x}, \bar{y}\right)$ where $\bar{\phi}\left(\bar{x}\right)$ is the induced streaming field with $\bar{\psi}\left(x, y\right)$ being the potential induced within EDL. Considering this, the distribution of $\bar{n}_i$ subjected to the symmetry condition at the channel centreline (i.e., at $\bar{y} = 0$, $\partial \bar{n}_i / \partial \bar{y} = 0$) and

number density being equal to the bulk number concentration in electroneutral region ($\bar{n}_i = \bar{n}_{i\infty}$ at $\bar{\psi} = 0$) results

$$\bar{n}_i = \bar{n}_{i\infty} \exp\left(-\frac{\bar{\psi}}{1+\gamma\theta} \right) \tag{S10}$$

where $\bar{\psi} = z\, e\psi / \left(k_B T_C \right)$. Since this shows an exponential dependence, it may seem like similar to the well-known Boltzmann distribution. However, the bulk ionic concentration $\left(\bar{n}_{i\infty} \right)$ is not constant, instead, it is varying axially in the presence of the axial temperature gradient. To obtain this dependence, one need to equate the first term of the right side of equation (S9) with zero, so that

$$\frac{\partial \bar{n}_i}{\partial \bar{x}} + \bar{n}_i\, \bar{S}_{Ti}\, \gamma \frac{\partial \theta}{\partial \bar{x}} + \frac{\bar{z}_i\, \bar{n}_i}{1+\gamma\theta} \frac{\partial \bar{\phi}}{\partial \bar{x}} = 0 \tag{S11}$$

Since electro-neutrality is prevalent in the bulk (i.e. $\partial \bar{\phi} / \partial \bar{x} = 0$), equation (S11) gets simplified and we obtain the following expression for $\bar{n}_{i\infty}$

$$\bar{n}_{i\infty} = \exp\left(-\bar{S}_{Tavg}\, \gamma\theta \right) \tag{S12}$$

The ionic number concentration described by the equations (S10)-(S12) is further used in the Poisson equation to evaluate the potential distribution which reads as $\nabla \cdot \left(\varepsilon \nabla \phi \right) = -\rho_e = -e \sum_i z_i\, n_i$. The dimensionless form of the Poisson equation is given below

$$\bar{\varepsilon} \frac{\partial^2 \bar{\psi}}{\partial \bar{y}^2} = \bar{\kappa}_{eff}^2 \sinh\left(\frac{\bar{\psi}}{1+\gamma\theta} \right) \tag{S13}$$

Contrary to the traditional electrokinetic studies, here the EDL thickness (i.e. the inverse of $\bar{\kappa}_{eff}$) no longer remains constant and becomes a function of the axial co-ordinate $\bar{\kappa}_{eff}^2 = \bar{\kappa}_0^2 \exp\left(-\bar{S}_{Tavg}\, \gamma\theta \right)$ which yields $\bar{\varepsilon} \frac{\partial^2 \bar{\psi}}{\partial \bar{y}^2} = \bar{\kappa}_0^2 \sinh\left[\bar{\psi} / \left(1+\gamma\theta \right) \right] \exp\left(-\bar{S}_{Tavg}\, \gamma\theta \right)$. For small values of surface potential and γ (i.e. small imposed temperature difference), we can use Debye-Hückel linearization where $\sinh\left[\bar{\psi} / \left(1+\gamma\theta \right) \right]$ is approximated as $\bar{\psi} / \left(1+\gamma\theta \right)$; along with the exponential term being linearized as $\exp\left(-\bar{S}_{Tavg}\, \gamma\theta \right) \approx 1 - \bar{S}_{Tavg}\, \gamma\theta + \left(\bar{S}_{Tavg}\, \gamma\theta \right)^2 / 2$.

$$\left.\begin{aligned} \mathrm{O}(1):\ & \frac{\partial^2 \bar{\psi}_0}{\partial \bar{y}^2} = \bar{\kappa}_0^2\, \bar{\psi}_0 && \left(\text{leading order} \right) \\ \mathrm{O}(\gamma):\ & \frac{\partial^2 \bar{\psi}_1}{\partial \bar{y}^2} - C_\varepsilon \theta_0 \frac{\partial^2 \bar{\psi}_0}{\partial \bar{y}^2} = \bar{\kappa}_0^2 \left(\bar{\psi}_1 - \bar{\psi}_0\, \theta_0 - \bar{\psi}_0\, \bar{S}_{Tavg}\, \theta_0 \right) && \left(\text{first order} \right) \end{aligned}\right\} \tag{S14}$$

In this context, it is worth mentioning that in the presence of a thermal gradient, the surface potential (or zeta-potential) no longer remains constant. Instead, it becomes a strong function of the imposed temperature difference by following a linear relationship. Some previous experimental studies have demonstrated this temperature-dependence of zeta potential where it not only depends on temperature but also other factors like surface reactions (Ghonge *et al.* 2013; Ishido & Mizutani 1981; Reppert 2003; Revil *et al.* 2003). However, this surface reaction has a relatively weaker influence on altering the non-isothermal flow dynamics, as highlighted in

a recent study by Dietzel et al. (Dietzel & Hardt 2016). Consideration of this surface equilibrium and other associated reaction kinetics will unnecessarily complicate the present theoretical framework and hence, the only linear dependence of zeta-potential with temperature is considered, i.e. at $\bar{y} = \pm 1$, $\bar{\psi} = \psi/\zeta = \left[1 + C_\zeta \gamma \theta\right]$ with C_ζ being the temperature sensitivity of zeta potential. Equation (S14) subjected to the constant zeta potential boundary condition (i.e. $C_\zeta = 0$) results in the following two equations for the potential distribution

$$\bar{\psi}_0 = \frac{\cosh\left(\bar{\kappa}_0 \bar{y}\right)}{\cosh\left(\bar{\kappa}_0\right)} \tag{S15}$$

$$\bar{\psi}_1 = f_1 \exp\left(\bar{\kappa}_0 \bar{y}\right) + f_2 \exp\left(-\bar{\kappa}_0 \bar{y}\right) - \frac{C_{\varepsilon eff}\left\{\exp\left(-\bar{\kappa}_0 \bar{y}\right) - 4\bar{\kappa}_0 \bar{y} \sinh\left(\bar{\kappa}_0 \bar{y}\right) + 2\cosh\left(\bar{\kappa}_0 \bar{y}\right)\right\}}{8\cosh\left(\bar{\kappa}_0\right)} \tag{S16}$$

where $f_1 = \frac{1}{8}\frac{C_{\varepsilon eff}}{\cosh\left(\bar{\kappa}_0\right)} - \frac{\bar{\kappa}_0}{4}\frac{C_{\varepsilon eff}\tanh\left(\bar{\kappa}_0\right)}{\cosh\left(\bar{\kappa}_0\right)}$, $f_2 = \frac{1}{8}\frac{C_{\varepsilon eff}\left\{\sinh\left(2\bar{\kappa}_0\right) + 2\bar{\kappa}_0 - 2\bar{\kappa}_0 \cosh\left(2\bar{\kappa}_0\right)\right\}}{\cosh\left(\bar{\kappa}_0\right)\sinh\left(2\bar{\kappa}_0\right)}$ and $C_{\varepsilon eff} = \left\{C_\varepsilon - \left(1 + \bar{S}_{Tavg}\right)\right\}\theta_0$. Now, considering the temperature-dependence of zeta-potential as boundary condition, the modified form of O(γ) potential distribution (i.e. $\bar{\psi}_1$) is given by

$$\bar{\psi}_1 = f_3 \exp\left(\bar{\kappa}_0 \bar{y}\right) + f_4 \exp\left(-\bar{\kappa}_0 \bar{y}\right) - \frac{C_{\varepsilon eff}\left\{\exp\left(-\bar{\kappa}_0 \bar{y}\right) - 4\bar{\kappa}_0 \bar{y} \sinh\left(\bar{\kappa}_0 \bar{y}\right) + 2\cosh\left(\bar{\kappa}_0 \bar{y}\right)\right\}}{8\cosh\left(\bar{\kappa}_0\right)} \tag{S17}$$

where $f_3 = f_1 + \frac{\theta_0 C_\zeta}{2\cosh\left(\bar{\kappa}_0\right)}$ and $f_4 = f_2 + \frac{\theta_0 C_\zeta}{2\cosh\left(\bar{\kappa}_0\right)}$.

Reported experimental results of the temperature dependence of zeta potential (Reppert 2003) is depicted in figure S2 (i) which clearly shows that zeta potential (ζ) is indeed strongly dependent on temperature by following a linear relationship. These data are fitted in the form of $\zeta/\zeta_{ref} = m\left(T - T_{ref}\right)$ (this is the same form of zeta potential variation with temperature which we present as $\bar{\psi} = \left[1 + C_\zeta \gamma \theta\right]$) and this approximates quite well with the experimental data. As can be seen from this figure, depending on electrolyte concentration, this sensitivity with temperature is increased almost twice as the slope (m) of the fitted line increases from 0.0112 to 0.0214. So, in the dimensionless form, the value of C_ζ turns out to be varying from ~ 3 to 6 (approximately). Accordingly, in our analysis, we have chosen C_ζ to lie between 0 and 4 while presenting the results, with $C_\zeta = 0$ representing the case of constant zeta potential. Figure S2 (ii) shows the potential distribution in the transverse direction where the inset clearly shows the effect of C_ζ on the potential distribution. The effect of C_ζ is noticeable only in the close vicinity of channel walls (where the EDL is located) while remains ineffective in the electro-neutral region. As C_ζ is increased, more is the ionic redistribution within EDL and the magnitude of zeta potential may increase up to twice (at $\gamma = 0.1$ as shown in the inset) as observed in figure S2 (iii) for $C_\zeta = 4$.

Another key factor in altering the potential distribution is C_ε representing the change in electrical permittivity with temperature. Increasing C_ε from 1 to 10 indicates a significant reduction in electrical permittivity with temperature whose effect is reflected in the charge distribution via the permittivity-induced component $C_\varepsilon \theta_0 \left(\partial^2 \bar{\psi}_0 / \partial \bar{y}^2\right)$. As observed in figure S2 (iv), increasing C_ε creates a deviation in potential profile close to the channel walls while

remains unaffected in the bulk.

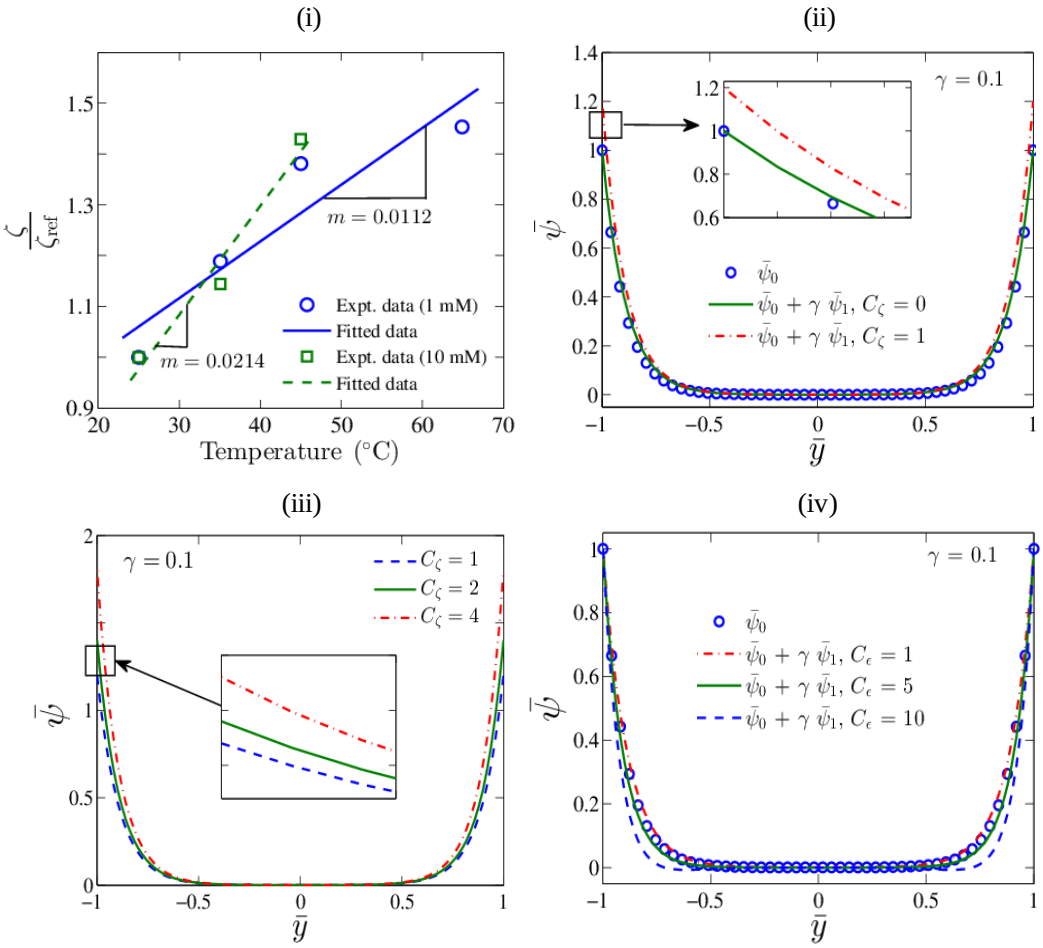

FIGURE S2. (i) Reported experimental results of zeta potential variation with temperature (Reppert 2003), (ii) potential distribution in the *y*-direction for both constant and temperature-dependent zeta potential, variation of the same for (iii) different C_ζ and for (iv) different C_ε.

A3 *Velocity distribution*

Because of the applied temperature gradient (ΔT), a thermo-electric field is induced within the microchannel by virtue of the difference in Soret coefficients between cations and anions. Besides, another form of thermoelectricity can be induced due to the difference in ionic diffusivities of the ions even if their Soret coefficients remain the same. Also, since the thermo-physical properties of the fluid are strongly dependent on temperature, there will be drastic alteration in the hydrodynamics in the presence of ΔT. For example, the variation of electrical permittivity with temperature is manifested through the contribution of dielectrophoretic body force with accompanying axial pressure gradient thereby strongly influencing the advection motion of the fluid. For steady, incompressible flow, the velocity distribution for a Newtonian fluid is described by continuity equation $\nabla \cdot \boldsymbol{v} = 0$ along with the following momentum equation

$$0 = -\nabla p + \nabla \cdot \mu \left[\nabla \boldsymbol{v} + \left(\nabla \boldsymbol{v} \right)^T \right] + F_{EK} + F_{DEP} \tag{S18}$$

The left-hand side of equation (S18) is zero because of negligible inertial effect consideration which occurs only when the Reynolds number (*Re*) associated with flow is very less compared to

unity, i.e. *Re* << 1. Here, *p* is the hydrodynamic pressure, $\mu\left[\nabla\boldsymbol{v}+\left(\nabla\boldsymbol{v}\right)^{T}\right]$ viscous stress, $F_{EK}=-\rho_e\nabla\phi$ electrokinetic force, and $F_{DEP}=-\left(1/2\right)\left(\nabla\phi\right)^2\nabla\varepsilon$ dielectrophoretic force respectively. In the momentum equation, the effect of electrostriction force (i.e. the variation of electrical permittivity with fluid density) is not considered because of the assumption of the constant density of the fluid. Evaluating F_{EK} and F_{DEP} from the previously-obtained potential distribution, substituting those in momentum equation and employing β << 1, we get

$$\left.\begin{aligned} x-\text{component}:\ 0&=-\frac{\partial\bar{p}}{\partial\bar{x}}+\bar{\mu}\frac{\partial^2\bar{u}}{\partial\bar{y}^2}+\frac{\lambda\,\bar{\varepsilon}}{\bar{\kappa}_{eff}^2}\left[\frac{\partial^2\bar{\psi}}{\partial\bar{y}^2}\frac{\partial\bar{\phi}}{\partial\bar{x}}+\frac{1}{2}\gamma C_{\varepsilon}\left(\frac{\partial\bar{\psi}}{\partial\bar{y}}\right)^2\frac{\partial\theta}{\partial\bar{x}}\right]\\ y-\text{component}:\ 0&=-\frac{\partial\bar{p}}{\partial\bar{y}}+\frac{\lambda\,\bar{\varepsilon}}{\bar{\kappa}_{eff}^2}\frac{\partial^2\bar{\psi}}{\partial\bar{y}^2}\frac{\partial\bar{\psi}}{\partial\bar{y}}\end{aligned}\right\} \qquad \text{(S19)}$$

In equation (S19), λ represents the ratio of induced velocity due to osmotic pressure to the characteristic flow velocity $\lambda=2\beta h n_{\infty}k_B T_c/\mu_{ref}\,u_c$.

First, we solve the pressure distribution from the *y*-component of the momentum equation. Here, the axial pressure-gradient consists of two terms, one is the externally imposed pressure gradient while the other part is induced in non-isothermal condition. If one looks into the *x*-component of the momentum equation, then one can notice the term $\bar{\kappa}_{eff}$ i.e. the effective thickness of the inverse of the electrical double layer (EDL) which takes the form $\bar{\kappa}_{eff}=\bar{\kappa}_0\sqrt{\exp\left(-\bar{S}_{Tavg}\,\gamma\theta\right)}$. Since temperature ($\theta$) is varying in the axial direction, $\bar{\kappa}_{eff}$ becomes a function of the axial coordinate. Also, the dimensionless forms of the physical properties like dynamic viscosity $\left(\bar{\mu}\right)$ and electrical permittivity $\left(\bar{\varepsilon}\right)$ are function of the temperature distribution as $\bar{\mu}=\mu/\mu_{ref}=\exp\left(-\gamma C_{\mu}\theta\right)$ and $\bar{\varepsilon}=\varepsilon/\varepsilon_{ref}=\exp\left(-\gamma C_{\varepsilon}\theta\right)$. Considering these aspects one can understand that the resulting flow dynamics in the present analysis is two-dimensional in nature and fundamentally different from that typically occurring in classical streaming field-induced unidirectional flow. Using the expressions of $\bar{\kappa}_{eff}$ and $\frac{\partial\bar{p}}{\partial\bar{x}}$ (pressure gradient), the modified form of the *x*-component of the momentum equation becomes

$$\bar{\mu}\frac{\partial^2\bar{u}}{\partial\bar{y}^2}=\frac{\partial\bar{p}_0}{\partial\bar{x}}+\frac{\lambda}{\bar{\kappa}_0^2}\exp\left(\bar{S}_{Tavg}\gamma\theta\right)\left\{\bar{\varepsilon}\frac{\partial^2\bar{\psi}}{\partial\bar{y}^2}\bar{E}_x+\frac{1}{2}\frac{\partial\bar{\varepsilon}}{\partial\bar{x}}\left(\frac{\partial\bar{\psi}}{\partial\bar{y}}\right)^2\right\}+\frac{\lambda}{2}\frac{\partial\theta}{\partial\bar{x}}\frac{\partial_{\theta}\bar{n}_{\infty}}{\bar{n}_{\infty}}\frac{\bar{\psi}^2}{\left(1+\gamma\theta\right)}-\frac{\lambda}{2}\frac{\partial\theta}{\partial\bar{x}}\gamma\frac{\bar{\psi}^2}{\left(1+\gamma\theta\right)^2} \qquad \text{(S20)}$$

where $\bar{E}_x=-\partial\bar{\phi}/\partial\bar{x}$. Equation (S20) is now solved by following the aforesaid asymptotic approach where the governing equations at different orders of perturbations are as follows

$$\left.\begin{aligned} \mathrm{O}(1):\quad & \frac{\partial^2 \bar{u}_0}{\partial \bar{y}^2} = \frac{\partial \bar{p}_0}{\partial \bar{x}} + \frac{\lambda}{\bar{\kappa}_0^2}\frac{\partial^2 \bar{\psi}_0}{\partial \bar{y}^2}\bar{E}_{x0}, \\ \mathrm{O}(\gamma):\frac{\partial^2 \bar{u}_1}{\partial \bar{y}^2} - C_\mu\,\theta_0\frac{\partial^2 \bar{u}_0}{\partial \bar{y}^2} &= \frac{\lambda}{\bar{\kappa}_0^2}\left[\begin{array}{l} \dfrac{\partial^2 \bar{\psi}_0}{\partial \bar{y}^2}\left\{\bar{E}_{x0}\,\theta_0\left(\bar{S}_{Tavg} - C_\varepsilon\right) + \bar{E}_{x1}\right\} \\ \dfrac{\partial^2 \bar{\psi}_1}{\partial \bar{y}^2}\bar{E}_{x0} - \dfrac{1}{2}C_\varepsilon\dfrac{\partial \theta_0}{\partial \bar{x}}\left(\dfrac{\partial \bar{\psi}_0}{\partial \bar{y}}\right)^2 \end{array}\right] - \frac{\lambda}{2}\bar{\psi}_0^2\frac{\partial \theta_0}{\partial \bar{x}}\left(1+\bar{S}_{Tavg}\right) \end{aligned}\right\} \quad \text{(S21)}$$

To obtain the flow field, equation (S21) is subjected to no-slip condition at the surface $\left(\bar{u}=0 \text{ at } \bar{y}=1\right)$ and symmetry condition $\left(\partial\bar{u}/\partial\bar{y}=0 \text{ at } \bar{y}=0\right)$ at the channel centreline. Using this, the velocity distributions are given in the following two equations

$$\bar{u}_0 = \frac{1}{2}\frac{\partial \bar{p}_0}{\partial \bar{x}}\left(\bar{y}^2-1\right) + \frac{\lambda}{\bar{\kappa}_0^2}\bar{E}_{x0}\left[\frac{\cosh\left(\bar{\kappa}_0\,\bar{y}\right)}{\cosh\left(\bar{\kappa}_0\right)} - 1\right] \quad \text{(S22)}$$

$$\begin{aligned} \bar{u}_1 = {} & \beta_2\frac{\partial \bar{p}_0}{\partial \bar{x}}\frac{\bar{y}^2}{2} + \beta_2\frac{\lambda}{\bar{\kappa}_0^2}\bar{E}_{x0}\frac{\cosh\left(\bar{\kappa}_0\,\bar{y}\right)}{\cosh\left(\bar{\kappa}_0\right)} + \beta_3\left(\beta_1\bar{E}_{x0} + \bar{E}_{x1}\right)\frac{\cosh\left(\bar{\kappa}_0\,\bar{y}\right)}{\cosh\left(\bar{\kappa}_0\right)} - \frac{\beta_5\,\bar{\kappa}_0^2\,F_1\left(\bar{y}\right) + \beta_6\,F_2\left(\bar{y}\right)}{\bar{\kappa}_0\cosh^2\left(\bar{\kappa}_0\right)} \\ & + \beta_4\,\bar{E}_{x0}\left[\frac{\beta_7}{\bar{\kappa}_0^2}\exp\left(\bar{\kappa}_0\,\bar{y}\right) + \frac{\left(\beta_8-\beta_{11}\right)}{\bar{\kappa}_0^2}\exp\left(-\bar{\kappa}_0\,\bar{y}\right) + \beta_9\,F_3\left(\bar{y}\right) + \beta_{10}\,F_4\left(\bar{y}\right)\right] + c_1\,\bar{y} + c_2 \end{aligned} \quad \text{(S23)}$$

Equation (S22) represents the perturbation-free flow field which is the well-known expression for combined pressure-driven and streaming field-induced electrokinetic flow while equation (S23) indicates the contribution of the thermal perturbation to the flow field. The coefficients of the velocity distribution described by equation (S23) are given below

$$c_1 = -\beta_4\frac{\bar{E}_{x0}}{\bar{\kappa}_0}\beta_{12}, c_2 = -\frac{\beta_2}{2}\frac{\partial \bar{p}_0}{\partial \bar{x}} + \frac{\bar{E}_{x0}}{\bar{\kappa}_0}\left(\beta_4\,\beta_{12} - \frac{\beta_2\,\lambda}{\bar{\kappa}_0} - \beta_4\,\beta_{18}\,\bar{\kappa}_0\right) - \beta_3\left(\beta_1\,\bar{E}_{x0} + \bar{E}_{x1}\right) + \beta_5\,\beta_{13} + \beta_6\,\beta_{14},$$

$$\beta_1 = \theta_0\left(\bar{S}_{Tavg} - C_\varepsilon\right), \beta_2 = C_\mu\,\theta_0, \beta_3 = \frac{\lambda}{\bar{\kappa}_0^2}, \beta_4 = \beta_3, \beta_5 = \frac{\beta_3}{2}C_\varepsilon\frac{\partial \theta_0}{\partial \bar{x}}, \beta_6 = \frac{\lambda}{2}\left(1+\bar{S}_{Tavg}\right)\frac{\partial \theta_0}{\partial \bar{x}}, \beta_7 = f_1\,\bar{\kappa}_0^2,$$

$$\beta_8 = f_2\,\bar{\kappa}_0^2, \beta_9 = \frac{3}{4}\beta_{19}, \beta_{10} = \frac{1}{2}\beta_{19}\,\bar{\kappa}_0, \beta_{11} = \frac{\beta_{19}}{8}, \beta_{12} = \left(\beta_7 - \beta_8 + \beta_{11}\right), \beta_{13} = \frac{\beta_{20}}{4\,{\beta_{23}}^2}, \beta_{14} = \frac{\beta_{21}}{4\,\bar{\kappa}_0^2\,{\beta_{23}}^2},$$

$$\beta_{15} = \frac{\beta_{22}}{\bar{\kappa}_0^2}, \beta_{16} = \frac{\beta_9\,\beta_{23}}{\bar{\kappa}_0^2}, \beta_{17} = \frac{\beta_{11}}{\bar{\kappa}_0^2}\exp\left(-\bar{\kappa}_0\right), \beta_{18} = \left(\beta_{15} + \beta_{16} - \beta_{17}\right), \beta_{19} = \frac{C_{\varepsilon eff}\,\bar{\kappa}_0^2}{\beta_{23}}, \beta_{20} = \left({\beta_{23}}^2 - \bar{\kappa}_0^2\right),$$

$$\beta_{21} = \left({\beta_{23}}^2 + \bar{\kappa}_0^2\right), \beta_{22} = \left[\beta_7\exp\left(\bar{\kappa}_0\right) + \beta_8\exp\left(-\bar{\kappa}_0\right)\right], \beta_{23} = \cosh\left(\bar{\kappa}_0\right), F_1\left(\bar{y}\right) = \frac{\left\{\cosh^2\left(\bar{\kappa}_0\,\bar{y}\right) - \bar{\kappa}_0^2\,\bar{y}^2\right\}}{4\,\bar{\kappa}_0},$$

$$F_2\left(\bar{y}\right) = F_1\left(\bar{y}\right) + \frac{1}{2}\bar{\kappa}_0\,\bar{y}^2, F_3\left(\bar{y}\right) = \frac{\cosh\left(\bar{\kappa}_0\,\bar{y}\right)}{\bar{\kappa}_0^2}, F_4\left(\bar{y}\right) = \frac{\bar{\kappa}_0\,\bar{y}\,\sinh\left(\bar{\kappa}_0\,\bar{y}\right) - 2\cosh\left(\bar{\kappa}_0\,\bar{y}\right)}{{\bar{\kappa}_0}^3}$$

Still, the completion of the flow field requires the knowledge of the induced streaming potential for which the electroneutrality condition (i.e. vanishing net current condition) is invoked, i.e. $I_{\text{net}} = I_{\text{streaming}} + I_{\text{advection}} = 0$. The governing equation of electroneutrality employed for streaming potential evaluation is given below

$$-\bar{E}_x\left(\frac{1+C_D\gamma\theta}{1+\gamma\theta}\right)\int_{-1}^{1}\left[\cosh\left(\frac{\bar{\psi}}{1+\gamma\theta}\right)-\chi\sinh\left(\frac{\bar{\psi}}{1+\gamma\theta}\right)\right]d\bar{y}-\frac{1}{2}\frac{\partial\theta}{\partial\bar{x}}\gamma\left(1+\chi\right)\left(1+C_D\gamma\theta\right)\Delta\bar{S}_T\int_{-1}^{1}\exp\left(-\frac{\bar{\psi}}{1+\gamma\theta}\right)d\bar{y}$$
$$-\frac{\partial\theta}{\partial\bar{x}}\frac{\gamma\left(1+C_D\gamma\theta\right)}{\left(1+\gamma\theta\right)^2}\int_{-1}^{1}\bar{\psi}\left[\cosh\left(\frac{\bar{\psi}}{1+\gamma\theta}\right)-\chi\sinh\left(\frac{\bar{\psi}}{1+\gamma\theta}\right)\right]d\bar{y}+Pe_i\int_{-1}^{1}\bar{u}\sinh\left(\frac{\bar{\psi}}{1+\gamma\theta}\right)d\bar{y} \quad \text{(S24)}$$
$$+\frac{\partial\theta}{\partial\bar{x}}\left(\bar{S}_{T-}+\frac{\partial_\theta\bar{n}}{\bar{n}}\right)\left(1+C_D\gamma\theta\right)\int_{-1}^{1}\left[\sinh\left(\frac{\bar{\psi}}{1+\gamma\theta}\right)-\chi\cosh\left(\frac{\bar{\psi}}{1+\gamma\theta}\right)\right]d\bar{y}=0$$

Equation (S24) is then expanded similarly (as described earlier in the asymptotic approach)

$$\mathrm{O}(1):-\bar{E}_{x0}\int_{-1}^{1}d\bar{y}-\frac{1}{2}\bar{E}_{x0}\int_{-1}^{1}\bar{\psi}_0^2\,d\bar{y}+\chi\bar{E}_{x0}\int_{-1}^{1}\bar{\psi}_0\,d\bar{y}+Pe_i\int_{-1}^{1}\bar{u}_0\;\bar{\psi}_0\,d\bar{y}=0 \quad \text{(S25)}$$

$$\mathrm{O}(\gamma):-\bar{E}_{x0}\int_{-1}^{1}\left\{-\theta_0\bar{\psi}_0^2+\bar{\psi}_0\bar{\psi}_1-\chi\left(\bar{\psi}_1-\theta_0\bar{\psi}_0\right)\right\}-\bar{E}_{x1}\int_{-1}^{1}\left(1+\frac{1}{2}\bar{\psi}_0^2-\chi\bar{\psi}_0\right)d\bar{y}$$

$$\text{and}\quad -\frac{\partial\theta_0}{\partial\bar{x}}\int_{-1}^{1}\left(\bar{\psi}_0+\frac{1}{2}\bar{\psi}_0^3-\chi\bar{\psi}_0^2\right)d\bar{y}-\frac{1}{2}\left(1+\chi\right)\Delta\bar{S}_T\frac{\partial\theta_0}{\partial\bar{x}}\int_{-1}^{1}\left(1-\bar{\psi}_0\right)d\bar{y}+Pe_i\int_{-1}^{1}\left(\bar{\psi}_1\bar{u}_0+\bar{\psi}_0\bar{u}_1-\bar{\psi}_0\bar{u}_0\theta_0\right)d\bar{y} \quad \text{(S26)}$$
$$+\left(\bar{S}_{T-}-\bar{S}_{Tavg}\right)\frac{\partial\theta_0}{\partial\bar{x}}\int_{-1}^{1}\left(\bar{\psi}_0-\chi-\frac{1}{2}\chi\bar{\psi}_0^2\right)d\bar{y}+\bar{E}_{x0}\,\theta_0\left(1-C_D\right)\int_{-1}^{1}\left(1-\chi\bar{\psi}_0+\frac{1}{2}\bar{\psi}_0^2\right)d\bar{y}=0$$

Now, we get the final expression of the streaming fields at different degree of perturbations

$$\bar{E}_{x0}=\frac{2\,Pe_i\,\dfrac{\partial\bar{p}_0}{\partial\bar{x}}\left\{\tanh\left(\bar{\kappa}_0\right)-\bar{\kappa}_0\right\}}{\left[2\bar{\kappa}_0^3+\bar{\kappa}_0^2\left\{\dfrac{\bar{\kappa}_0}{2\cosh^2\left(\bar{\kappa}_0\right)}+\dfrac{1}{2}\tanh\left(\bar{\kappa}_0\right)\right\}-2\chi\bar{\kappa}_0^2\tanh\left(\bar{\kappa}_0\right)-Pe_i\,\lambda\left\{\dfrac{\bar{\kappa}_0}{\cosh^2\left(\bar{\kappa}_0\right)}-\tanh\left(\bar{\kappa}_0\right)\right\}\right]} \quad \text{(S27)}$$

$$\text{and}\qquad \bar{E}_{x1}=\left(-\gamma_{48}\frac{\partial\theta_0}{\partial\bar{x}}-Pe_i\;\gamma_{47}-\bar{E}_{x0}\,\gamma_{45}\right)\Big/\gamma_{46} \quad \text{(S28)}$$

The coefficients of equation (S28) is reported in Section F1 of the supplementary material. Here, it is necessary to mention the two parameters involved in the final expression of the streaming potential described by equations (S27)-(S28), χ and C_D. χ represents the diffusivity difference between the co-ions and counter-ions $\chi=\left(D_+-D_-\right)/\left(D_++D_-\right)$ while C_D represents the sensitivity of diffusivity of ions with temperature (here diffusivity D is assumed to be obeying the following relationship $D=D_{ref}\left[1+\omega_4\left(T-T_{ref}\right)\right]$, i.e. $\bar{D}=D/D_{ref}=\left[1+C_D\gamma\theta\right]$ (D. R. Lide 2005; Ghonge *et al.* 2013)). While results for varying χ are reported in the main paper, corresponding results for varying C_D are presented in Section B of the supplementary material for the sake of brevity.

Now, to show the two-dimensional nature of the flow, we have plotted the distribution of the $\bar{u}$ component in the transverse direction $\left(\bar{y}\right)$ at different axial locations $\left(\bar{x}\right)$ as shown in figure S3. The dotted line (blue-coloured), solid line (green-coloured) and dash-dot (red-coloured) line correspond to $\bar{x}$ = 0, $\bar{x}$ = 0.5 and $\bar{x}$ = 1 respectively. Velocity profiles are

evaluated at $-\frac{\partial \bar{p}_0}{\partial \bar{x}}$ = 0.01 while the inset shows the variation of the same at a lower strength of pressure gradient, i.e. $-\frac{\partial \bar{p}_0}{\partial \bar{x}}$ = 0.001. With increasing the value of $\bar{x}$, the magnitude of the flow velocity starts to increase with the maximum increment occurred at the channel centreline (i.e. at $\bar{y}$ = 0). This increment in the flow velocity gets strengthened with increasing strength of pressure gradient. As we increase the pressure gradient 10 folds from $-\frac{\partial \bar{p}_0}{\partial \bar{x}}$ = 0.001 to $-\frac{\partial \bar{p}_0}{\partial \bar{x}}$ = 0.01, the maximum enhancement of $\bar{u}$ increases from ~ 1.06 times to ~ 1.16 times thereby indicating stronger axial dependence of flow.

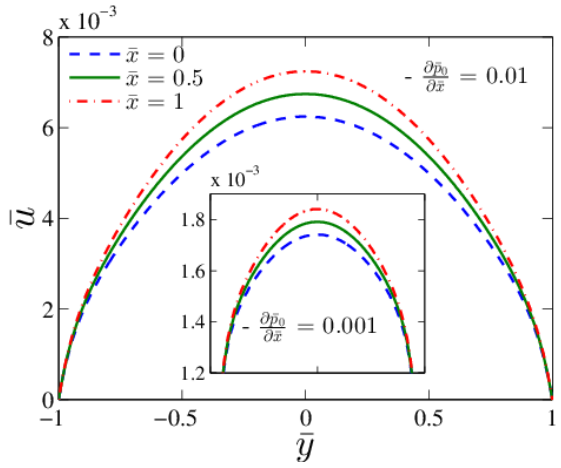

FIGURE S3. Velocity distribution $\bar{u}$ in the transverse direction $(\bar{y})$. Plots are shown at different axial locations $(\bar{x})$ for $-\frac{\partial \bar{p}_0}{\partial \bar{x}}$ = 0.01. Inset shows the variation of the same for $-\frac{\partial \bar{p}_0}{\partial \bar{x}}$ = 0.001.

Equations (S22) and (S23) along with the knowledge of O(1) and O(γ) streaming potentials $\bar{E}_{x0}$ and $\bar{E}_{x1}$ completes the velocity distribution $\bar{u} = \bar{u}_0 + \gamma \bar{u}_1$. Once the velocity field is known, one can differentiate it with respect to the axial coordinate $(\bar{x})$ which, according to the incompressibility constraint, becomes

$$\frac{\partial \bar{u}}{\partial \bar{x}} = -\frac{\partial \bar{v}}{\partial \bar{y}} \tag{S29}$$

Now, one can obtain the transverse velocity component $(\bar{v})$ by integrating the expression of $\frac{\partial \bar{u}}{\partial \bar{x}}$ in the transverse direction $(\bar{y})$. The expression of the $\bar{v}$ component is given in the following

$$\bar{v} = \gamma \left[-\frac{\partial \bar{p}_0}{\partial \bar{x}} \left[\begin{array}{l} -\frac{\beta_3 \sinh(\bar{\kappa}_0 \bar{y})}{\beta_{23} \bar{\kappa}_0 \gamma_{46}} (Pe_i C_3 + C_1 C_4) - C_1 \left(\frac{2 C_\mu \lambda}{\bar{\kappa}_0^{\,2}} + 2\beta_3 C_2 \right) \bar{y} - C_\mu \bar{y} + \frac{1}{3} C_\mu y^3 \\ + \frac{2 C_\mu \lambda C_1 \sinh(\bar{\kappa}_0 \bar{y})}{\bar{\kappa}_0^{\,3} \beta_{23}} + \frac{2\beta_3 \sinh(\bar{\kappa}_0 \bar{y}) C_1 C_2}{\beta_{23} \bar{\kappa}_0} - (Pe_i C_3 + C_1 C_4) \frac{\gamma_{41} \bar{y}}{\gamma_{46}} \end{array} \right] + C_5 \right] \tag{S30}$$

where C_5 is the integration constant which can be obtained by invoking the impermeability conditions at the channel walls (i.e. $\bar{v}$ = 0 at $\bar{y}$ = ±1). The other coefficients are listed below

$$C_1 = \bar{E}_{x0} = \frac{2\,Pe_i\left\{\tanh\left(\bar{\kappa}_0\right)-\bar{\kappa}_0\right\}}{\left[2\bar{\kappa}_0^3+\bar{\kappa}_0^2\left\{\frac{\bar{\kappa}_0}{2\cosh^2\left(\bar{\kappa}_0\right)}+\frac{1}{2}\tanh\left(\bar{\kappa}_0\right)\right\}-2\chi\,\bar{\kappa}_0^2\tanh\left(\bar{\kappa}_0\right)-Pe_i\,\lambda\left\{\frac{\bar{\kappa}_0}{\cosh^2\left(\bar{\kappa}_0\right)}-\tanh\left(\bar{\kappa}_0\right)\right\}\right]},$$

$$C_2 = \left(\bar{S}_{Tavg}-C_\varepsilon\right),\; C_3 = -\frac{2\,\beta_{25}}{\beta_{23}\,\bar{\kappa}_0^{\,3}}+\frac{2\tanh\left(\bar{\kappa}_0\right)}{\bar{\kappa}_0}+\frac{2C_\mu\,\beta_{25}}{\beta_{23}\,\bar{\kappa}_0^{\,3}}-2\gamma_{38}\,C_\mu\tanh\left(\bar{\kappa}_0\right),$$

$$C_4 = \left[\begin{array}{l} -\dfrac{8\,\chi\tanh\left(\bar{\kappa}_0\right)}{\bar{\kappa}_0}+4+\dfrac{2\,\beta_{24}\left(\beta_{23}+2\right)}{\bar{\kappa}_0\;\beta_{23}^{\,2}}+\dfrac{4\,Pe_i\,\lambda\,\sinh\left(\bar{\kappa}_0\right)}{\beta_{23}\;\bar{\kappa}_0^{\,3}} \\ -4\gamma_{38}\,Pe_i\left(\dfrac{C_\mu\,\lambda}{\bar{\kappa}_0^{\,2}}+\beta_3\,C_2\right)\tanh\left(\bar{\kappa}_0\right)+\dfrac{4\,Pe_i\,\beta_{24}}{\beta_{23}^{\,2}}\left(\dfrac{C_\mu\,\lambda}{\bar{\kappa}_0^{\,3}}+\dfrac{\beta_3\,C_2}{\bar{\kappa}_0}\right) \end{array}\right]$$

The variation of the transverse velocity component $\left(\bar{v}\right)$ in the *y*-direction is shown in figure S4. In figure S4(a), the effect of the thermal perturbation parameter γ on $\bar{v}$ is shown for three different values of γ. As one increases the value of γ, more is the thermal perturbation to the flow field, more is the alteration in the thickness of the electrical double layer (EDL), more is the deviation of the ionic number concentration from its equilibrium distribution thus leads to establishing stronger axial dependence of primary flow component $\left(\bar{u}\right)$. This results in more generation of the secondary component to maintain the flow continuity condition as reflected in figure S4(a). The maximum increment (at $\bar{y}$ = 0) of the velocity magnitude is ~ 4 times as γ is changing from 0.025 to 0.1 (i.e. linear dependence with γ as the asymptotic solution is correct up to O(γ)). Similarly, at a fixed γ and pressure gradient, increasing C_μ indicates the lessening of the viscous resistance in the flow which leads to more generation of the $\bar{v}$ component. The

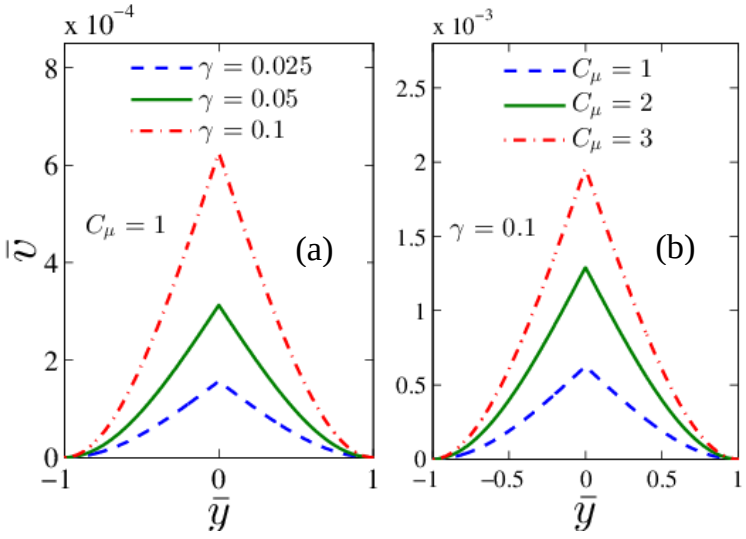

FIGURE S4. Velocity distribution $\bar{v}$ in the transverse direction $\left(\bar{y}\right)$. Plots are shown for different values of (a) γ and (b) C_μ respectively (evaluated at $\bar{x}$ = 1, $-\dfrac{\partial\bar{p}_0}{\partial\bar{x}}$ = 0.01).

enhancement of the velocity magnitude is ~ 3.13 times as C_μ is increased from 1 to 3 (shown in figure S4(b)). Once the velocity field is known, we can obtain the volumetric flow rate $\left(\bar{Q}\right)$ through the microchannel by integrating the flow velocity cross-sectionally

$$\bar{Q} = \bar{Q}_0 + \gamma \bar{Q}_1 = \int_{-1}^{1} \bar{u}\, d\bar{y} = \int_{-1}^{1} \left(\bar{u}_0 + \gamma \bar{u}_1\right) d\bar{y} \tag{S31}$$

In the traditional pressure-driven flow of electrolyte solution, the induced streaming field creates a flow in the reverse direction, thus leading to a suppression of the net volumetric flow rate of the pressure-driven flow. Now, in the presence of thermal gradient, net throughput through the channel depends on whether the induced thermo-electric streaming field assists or opposes the pressure-gradient induced streaming field. Here, we have presented some results of the flow rate ratio (Q_r) which is defined as the ratio of the net flow due to combined action of external pressure gradient and temperature gradient to the throughput because of sole action of the pressure gradient. For solely temperature gradient driven flow, as $\Delta\bar{S}_T$ is increasing, the reduction in net streaming potential results in a significant enhancement in flow rate in absence of pressure gradient, .i.e. increment up to ~ 2.1 times can be observed (as shown in Figure S5 (i)). This rate gets attenuated in the presence of a pressure gradient (at $-\partial\bar{p}_0/\partial\bar{x} = 0.01$). One interesting thing to notice that there is a cross-over between the graphs for $-\partial\bar{p}_0/\partial\bar{x} = 0$ and $-\partial\bar{p}_0/\partial\bar{x} = 0.01$ at $\Delta\bar{S}_T = 0.66$. Below this critical $\Delta\bar{S}_T$, Q_r is higher in presence of pressure gradient and beyond this, reverse trend has been observed. In solely ΔT driven flow, at lower $\Delta\bar{S}_T$, axial separation between ions is not that higher thus creating lower reduction of streaming potential whereas at higher $\Delta\bar{S}_T$, this occurs relatively faster thus giving rise to more augmnetation in flow rate as compared to the case of $-\partial\bar{p}_0/\partial\bar{x} = 0.01$. Increasing $\Delta\bar{S}_T$ has almost vanishing effect in higher strength of pressure gradient. As shown in figure S5 (i) slight increase in flow rate ratio is seen for $-\partial\bar{p}_0/\partial\bar{x} = 0.1$ while for $-\partial\bar{p}_0/\partial\bar{x} = 1$, the profile of Q_r remains constant at 1.2.

The variation of Q_r with χ is shown in figure S5 (ii). Decreasing χ results in lowering the induced streaming potential because of the enhanced migration of co-ions in the upstream section. However, the dependence of Q_r on χ is very weak as a slight increment in the flow rate ratio is observed when χ is decreased from 0 to -0.2. The magnitude of the flow rate ratio (Q_r) becomes higher (from 1 to ~ 1.55) as one introduces a pressure gradient $\left(-\partial\bar{p}_0/\partial\bar{x} = 0.01\right)$. Now, increasing the strength of pressure gradient results in a reduction of the magnitude of Q_r with χ becoming increasingly insignificant (Q_r vs. χ plot remains constant).

Now, the flow rate ratio (Q_r) dependence on C_μ is depicted in figure S5 (iii) where increasing C_μ denotes a reduction in the fluid viscosity with temperature. The subsequent lowering in the viscous resistance of flow results in significant augmentation of the volumetric flow rate. However, as described earlier in the variation of streaming potential ratio (E_r), increasing C_μ also ensures faster migration of the ions caused by the imposed pressure gradient or the induced concentration gradient which also generates more electrokinetic flow in the reverse direction. Therefore, the net throughput depends on the rate of lessening of viscous resistance as well as the enhanced induced streaming field. For lower strength of pressure gradient ($-\partial\bar{p}_0/\partial\bar{x} = 0.01$), an enhancement in the flow rate ratio (Q_r) up to ~ 3.35 times is observed as C_μ is increased from 1 to 10. Increasing the strength of the pressure gradient lowers the magnitude of the net flow rate with the dependence on C_μ remaining qualitatively similar.

The alteration in the flow rate ratio (Q_r) with increasing C_ε is highlighted in figure S5 (iv) where the reduction in the streaming potential owing to the temperature-sensitivity of electrical permittivity causes significant enhancement (~ 2.87 times) in the net throughput for purely thermally driven flow. However, the impact of C_ε on Q_r becomes less in the presence of pressure gradient and interestingly, a cross-over between plots of $-\partial\bar{p}_0/\partial\bar{x}=0$ and $-\partial\bar{p}_0/\partial\bar{x}=0.1$ has been observed at C_ε = 5. Higher the strength of pressure gradient, C_ε becomes less important and the profile of Q_r remains flat at a constant value of ~ 1.21.

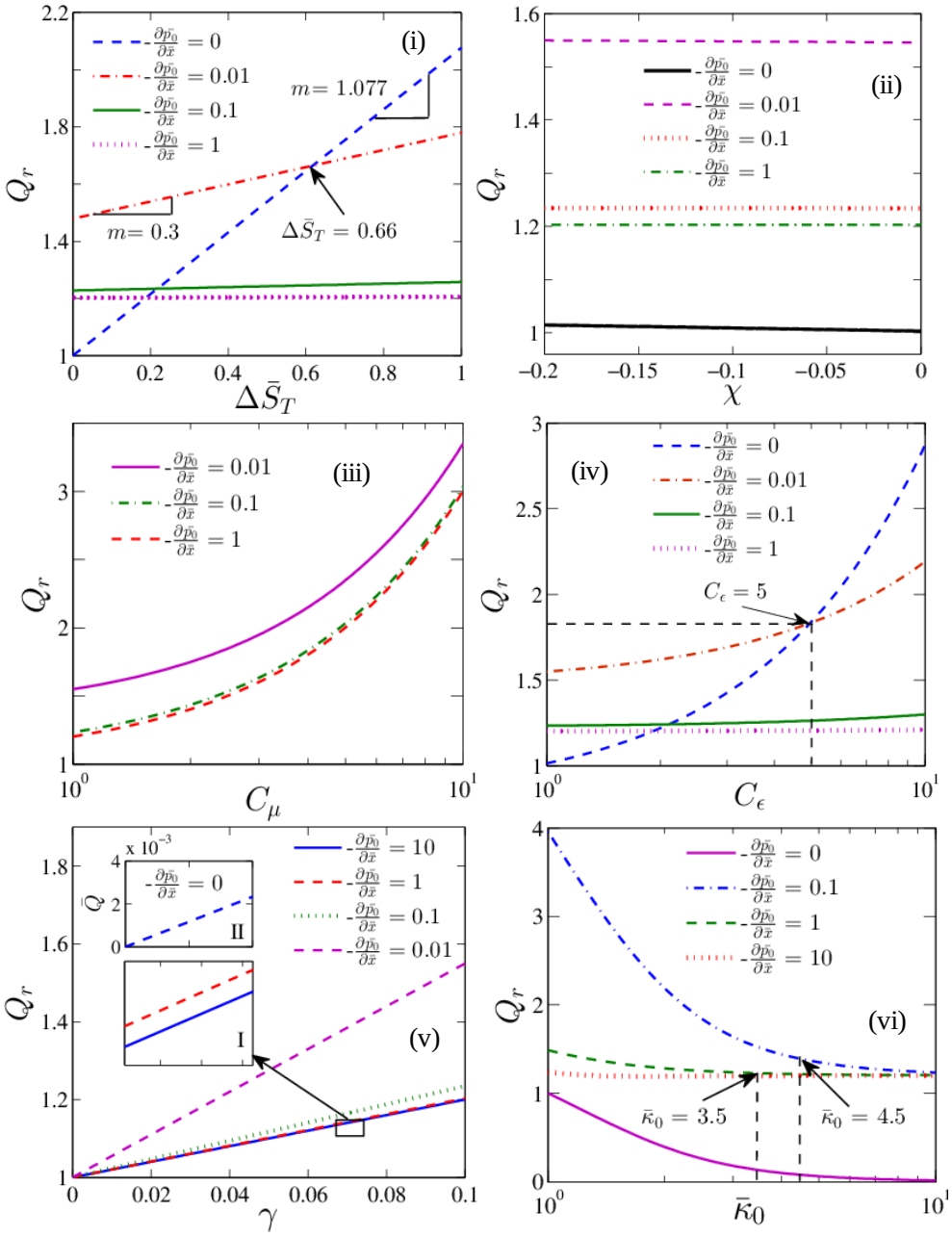

FIGURE S5. Flow rate ratio with (i) $\Delta\bar{S}_T$, (ii) χ, (iii) C_μ, (iv) C_ε, (v) γ and (vi) $\bar{\kappa}_0$ (at $\bar{x}$ = 1).

The dependence of Q_r on γ is shown in figure S5 (v) where the higher value of γ implies a higher degree of thermal perturbation which is more pronounced at a lower strength of pressure gradient $\left(-\partial\overline{p}_0/\partial\overline{x}=0.01\right)$. This influence of γ gets weakened with increasing pressure gradient. As clear from figure S5 (v), the slope of Q_r vs. γ becomes almost half of the previous case as the strength of pressure gradient increases 10 times from $-\partial\overline{p}_0/\partial\overline{x}=0.01$ to $-\partial\overline{p}_0/\partial\overline{x}=0.1$. At higher strength, the graphs are identical with a zoomed view of a portion (inset I of figure S5 (v)) indicating a negligible difference in Q_r with γ. For completeness, inset II of figure S5 (v) shows the variation of dimensionless flow rate for purely ΔT driven flow which also shows linear dependence with increasing thermal perturbation.

Figure S5c (vi) shows the variation of the flow rate ratio (Q_r) with decreasing channel confinement (i.e. increasing $\overline{\kappa}_0$). For purely thermally driven flow (i.e. $-\partial\overline{p}_0/\partial\overline{x}=0$), Q_r decreases sharply from its reference value and approaches towards zero as one increases $\overline{\kappa}_0$ from 1 to 10. At higher $\overline{\kappa}_0$, the net flow through the channel gets completely arrested. This also highlights the importance of channel confinement on the hydrodynamics of purely thermally driven flow. As the pressure gradient is introduced $\left(-\partial\overline{p}_0/\partial\overline{x}=0.1\right)$, the reduction in Q_r becomes so rapid that it falls from 4 times to approach a constant value of ~ 1.2 beyond $\overline{\kappa}_0=4.5$. Now, increasing the strength of the pressure gradient makes it predominant to dictate the flow physics. Therefore, the rate of reduction of Q_r with $\overline{\kappa}_0$ gets dampened and approaches to the same constant value earlier (at $\overline{\kappa}_0=3.5$) as compared to the case of $-\partial\overline{p}_0/\partial\overline{x}=0.1$. Also, the plots for $-\partial\overline{p}_0/\partial\overline{x}=1$ and $-\partial\overline{p}_0/\partial\overline{x}=10$ becomes identical at higher $\overline{\kappa}_0$ indicating the vanishing effect of $\overline{\kappa}_0$ on the flow field.

Similarly, the dispersion coefficient can also be expressed as

$$\overline{D}_{eff}=\overline{D}_0+\overline{D}_1 \tag{S32}$$

where the estimation of $\overline{D}_1$ (i.e. dispersion coefficient at O(γ)) involves the knowledge of O(γ) flow velocity $\overline{u}_1$. The expressions of the flow field and streaming potential for the exact solution in case of the axial temperature gradient is too large to be presented in the supplementary material. The MATLAB script file containing the expressions for the exact solution can be made available upon request.

In this context, it is worth mentioning that, for a two-dimensional flow, in addition to the dispersion coefficient, there is a contribution to the mean advection speed of the solute plug which depends on both longitudinal $\left(\overline{u}\right)$ as well as transverse $\left(\overline{v}\right)$ components of flow (Chu et al. 2019). Since our definition of dispersion coefficient requires the knowledge of the average flow velocity, we mainly focus on the alterations in the velocity distribution utilizing the pertinent variables involved. However, if one conducts the multiple-scale perturbation analysis, one can not only evaluate the dispersion coefficient, but also the concentration distribution of the species. As employed by Chu et al. and other researchers (Chu *et al.* 2019; Ng 2006), the transport of species can be described by the following advection-diffusion equation (Chu *et al.* 2019)

$$\frac{\partial C}{\partial t}+u\frac{\partial C}{\partial x}+v\frac{\partial C}{\partial y}=D\left(\frac{\partial^2 C}{\partial x^2}+\frac{\partial^2 C}{\partial y^2}\right) \tag{S33}$$

where D is the molecular diffusivity. In the multiple-scale perturbation analysis, the aspect ratio of the microchannel $\beta = h/l$ (which is very small as compared to unity, i.e. $\beta << 1$) can be chosen as the perturbation parameter and therefore, the three times scales, i.e. (i) diffusion time scale across the channel height, (ii) advection time scale across the channel length and (iii) diffusion time scale across the channel length takes the following form (Chu *et al.* 2019)

$$t_0 = t, \quad t_1 = \beta\, t \ \text{ and } \ t_2 = \beta^2 t$$

Now choosing a reference concentration scale C_{ref}, length scales l and h in the axial and transverse directions and time scale $t_c = \frac{h^2}{D}$ one can non-dimensionalize the advection-diffusion equation (S33) (Chu *et al.* 2019) as

$$\frac{\partial \bar{C}}{\partial \bar{t}}+\beta\, Pe\left(\bar{u}\frac{\partial \bar{C}}{\partial \bar{x}}+\bar{v}\frac{\partial \bar{C}}{\partial \bar{y}}\right)=\beta^2\frac{\partial^2 \bar{C}}{\partial \bar{x}^2}+\frac{\partial^2 \bar{C}}{\partial \bar{y}^2} \tag{S34}$$

where Pe is the Peclet number, $Pe = \frac{u_c h}{D}$. Now, following Chu et al., we expand the temporal derivative in the following manner $\frac{\partial}{\partial \bar{t}} = \frac{\partial}{\partial \bar{t}_0}+\beta\frac{\partial}{\partial \bar{t}_1}+\beta^2\frac{\partial}{\partial \bar{t}_2}$ and the concentration distribution is expressed as (Chu *et al.* 2019)

$$\bar{C}\left(\bar{x},\bar{y},\bar{t}\right)=\bar{C}_0\left(\bar{x},\bar{y},\bar{t}_1,\bar{t}_2\right)+\beta\,\bar{C}_1\left(\bar{x},\bar{y},\bar{t}_0,\bar{t}_1,\bar{t}_2\right)+\beta^2\bar{C}_2\left(\bar{x},\bar{y},\bar{t}_0,\bar{t}_1,\bar{t}_2\right) \tag{S35}$$

where $\bar{C}_0$, $\bar{C}_1$ and $\bar{C}_2$ are the leading order (i.e. O(1)), O(β) and O(β^2) concentration distributions respectively. This concentration field is subjected to the impermeability boundary conditions at the channel walls (i.e. $\frac{\partial \bar{C}}{\partial \bar{y}}$ = 0 at $\bar{y}$ = ±1). Similar to Chu et al., here also, the leading order concentration profile ($\bar{C}_0$) indicates that it is independent of the transverse coordinate ($\bar{y}$) and function of $\bar{x}$, $\bar{t}_1$ and $\bar{t}_2$ only. The governing equation of the first order concentration field $\bar{C}_1$ after time-averaging followed by the cross-sectional averaging becomes (Chu *et al.* 2019)

$$\frac{\partial \bar{C}_1}{\partial \bar{t}_0}+Pe\left(\bar{u}-\bar{u}_{avg}\right)\frac{\partial \bar{C}_0}{\partial \bar{x}}=\frac{\partial^2 \bar{C}_1}{\partial \bar{y}^2} \tag{S36}$$

The solution of equation (S36) can be chosen in the form $\bar{C}_1 = Pe\,A\left(\bar{x},\bar{y}\right)\frac{\partial \bar{C}_0}{\partial \bar{x}}$. Substituting this form of $\bar{C}_1$ on both sides of equation (36) and equating the coefficients of $\frac{\partial \bar{C}_0}{\partial \bar{x}}$ on both sides one can find the following governing equation for the function $A\left(\bar{x},\bar{y}\right)$ (Chu *et al.* 2019)

$$\frac{\partial^2 A}{\partial \bar{y}^2}=\bar{u}-\bar{u}_{avg} \tag{S37}$$

subjected to the boundary condition $\frac{\partial A}{\partial \bar{y}} = 0$ at $\bar{y} = \pm 1$. In a similar way, one can obtain the governing equation for O(β^2) concentration field. Now, combining these three concentration fields, using $\frac{\partial}{\partial \bar{t}} = \frac{\partial}{\partial \bar{t}_0} + \beta \frac{\partial}{\partial \bar{t}_1} + \beta^2 \frac{\partial}{\partial \bar{t}_2}$, the time-averaged and cross-sectionally averaged transport equation becomes (Chu *et al.* 2019)

$$\frac{\partial \bar{C}_0}{\partial \bar{t}} + Pe\left(\beta\, \bar{u}_{avg} + \beta^2 Pe\, K_s\right)\frac{\partial \bar{C}_0}{\partial \bar{x}} = \beta^2\left[1 + Pe^2 \bar{D}_{eff}\right]\frac{\partial^2 \bar{C}_0}{\partial \bar{x}^2} \tag{S38}$$

where K_s is the correction to the mean advection speed of the solute plug. The expression of K_s is given by $K_s = \langle \bar{u}\, A_x \rangle + \langle \bar{v}\, A_y \rangle$ where the operator $\langle\ \rangle$ is the average across the channel cross-section, A_x and A_y are the derivates of the function A with respect to x and y respectively.

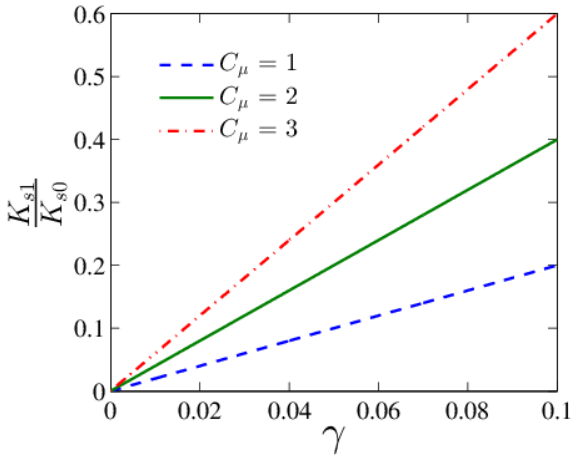

FIGURE S6. Variation of the ratio $\frac{K_{s1}}{K_{s0}}$ as a function of the thermal perturbation parameter γ. Results are shown for three different values of C_μ.

Since the expression of function A is too large, it is presented in Section F1 of the document for the sake of conciseness. Now, it is important to mention that the velocity field $\bar{u}$ is a combination of two profiles $\bar{u}_0$ and $\bar{u}_1$, i.e. $\bar{u} = \bar{u}_0 + \gamma \bar{u}_1$ while the $\bar{v}$ component is given by $\bar{v} = \gamma\, \bar{v}_1$. Accordingly, the correction factor K_s can be divided into two parts K_{s0} and K_{s1} i.e. $K_s = K_{s0} + K_{s1}$ indicating the contributions of the two velocity distributions $\bar{u}_0$ and $\bar{u}_1$ respectively. Therefore, the ratio $\frac{K_{s1}}{K_{s0}}$ signifies the relative contribution of the thermally perturbed flow field $(\bar{u}_1)$ to the mean advection speed correction factor. The variation of this ratio is plotted in figure S6 as a function of the thermal perturbation parameter γ. Higher the value of γ, more is the disturbance in the uniformity in the flow field, stronger is the axial dependence of the flow field, more is the generation of the $\bar{v}$ component thus leads to higher correction to the mean advection speed. Since our analysis is correct up to O(γ), we have observed linear dependence of the ratio $\frac{K_{s1}}{K_{s0}}$ with γ. As already discussed, increasing C_μ favors

more secondary flow generation resulting in a significant increment in the correction factor as observed in figure S6.

Case (b): *Temperature gradient applied in the transverse direction*

For temperature difference applied in the transverse direction, considering all previously-mentioned assumptions and simplifications (for the case of the axially applied thermal gradient), the governing equation of the temperature distribution reads as

$$\frac{\partial}{\partial \bar{y}}\left(\bar{k}\,\frac{\partial \theta}{\partial \bar{y}}\right)=0 \tag{S39}$$

and the corresponding temperature profile (asymptotic solution) is given by

$$\theta=\theta_0+\gamma\,\theta_1=\left(\bar{y}+1\right)+\frac{\gamma\,C_k}{2}\left(1-\bar{y}^2\right) \tag{S40}$$

Now, the governing equation for the transport of ionic species reads as

$$\frac{\partial}{\partial \bar{y}}\left\{\frac{D}{D^*}\left(\frac{\partial \bar{n}_i}{\partial \bar{y}}+\bar{S}_{Ti}\,\gamma\,\frac{\partial \theta}{\partial \bar{y}}\,\bar{n}_i+\frac{\bar{n}_i\,\bar{z}_i}{1+\gamma\,\theta}\,\frac{\partial \bar{\psi}}{\partial \bar{y}}\right)\right\}=0 \tag{S41}$$

which results in the following distribution of the ionic number concentration within the EDL

$$\bar{n}_+-\bar{n}_-\approx-\Delta\bar{S}_T\,\gamma\,\theta-\frac{2\bar{\psi}}{\left(1+\gamma\,\theta\right)}-2\,\gamma\,\frac{\partial \theta}{\partial y}\int\frac{\bar{\psi}}{\left(1+\gamma\,\theta\right)^2}d\bar{y} \tag{S42}$$

This is now used in the Poisson equation to obtain the potential distribution. The governing equations for the potential distribution are as follows

$$\left.\begin{aligned}&\mathrm{O}(1):\ \frac{\partial^2\bar{\psi}_0}{\partial \bar{y}^2}=\bar{\kappa}_0^2\,\bar{\psi}_0\\&\mathrm{O}(\gamma):\ \frac{\partial^2\bar{\psi}_1}{\partial \bar{y}^2}-\bar{\kappa}_0^2\,\bar{\psi}_1=\left\{C_\varepsilon-\left(1+\bar{S}_{Tavg}\right)\right\}\bar{\kappa}_0^2\,\theta_0\;\bar{\psi}_0+C_\varepsilon\,\frac{\partial \theta_0}{\partial \bar{y}}\,\frac{\partial \bar{\psi}_0}{\partial \bar{y}}+\bar{\kappa}_0^2\,\frac{\partial \theta_0}{\partial \bar{y}}\int\bar{\psi}_0\,d\bar{y}+\frac{\bar{\kappa}_0^2\,\Delta\bar{S}_T\,\theta_0}{2}\end{aligned}\right\} \tag{S43}$$

For potential distribution, unlike the case of axial temperature gradient, no closed-form solution is possible. So, one needs to either employ asymptotic approach (approximate solution) or can solve it numerically. The solutions of O(1) and O(γ) potential distributions are written as follows

$$\mathrm{O}(1):\qquad \bar{\psi}_0=\frac{\cosh\left(\bar{\kappa}_0\,\bar{y}\right)}{\cosh\left(\bar{\kappa}_0\right)}$$

$$\mathrm{O}(\gamma):\ \bar{\psi}_1=\left[\begin{aligned}&\left\{-\frac{f_1\left(\bar{y}\right)\cosh\left(\bar{\kappa}_0\,\bar{y}\right)}{8\,\bar{\kappa}_0\,\cosh\left(\bar{\kappa}_0\right)}-\frac{\Delta\bar{S}_T\,f_3\left(\bar{y}\right)}{4\,\bar{\kappa}_0}\right\}g_1\left(\bar{y}\right)\exp\left(-\bar{\kappa}_0\,\bar{y}\right)+c_1\exp\left(-\bar{\kappa}_0\,\bar{y}\right)+c_2\exp\left(\bar{\kappa}_0\,\bar{y}\right)\\&+\left\{-\frac{f_2\left(\bar{y}\right)g_2\left(\bar{y}\right)}{16\,\bar{\kappa}_0\cosh\left(\bar{\kappa}_0\right)}+\frac{\Delta\bar{S}_T\,f_4\left(\bar{y}\right)g_3\left(\bar{y}\right)}{4\,\bar{\kappa}_0\cosh\left(\bar{\kappa}_0\right)}\right\}\exp\left(\bar{\kappa}_0\,\bar{y}\right)-\frac{\left\{g_4\left(\bar{y}\right)\exp\left(\bar{\kappa}_0\,\bar{y}\right)-g_5\left(\bar{y}\right)\exp\left(-\bar{\kappa}_0\,\bar{y}\right)\right\}}{8\cosh\left(\bar{\kappa}_0\right)}\end{aligned}\right] \tag{S44}$$

The coefficients of equation (S44) are reported in Section F2 of the supplementary material.

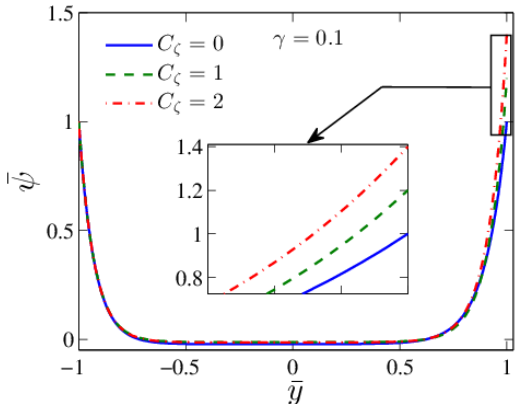

FIGURE S7. Potential distribution in the y-direction (at γ = 0.1) for transverse temperature gradient. Inset shows the zoomed view towards the top wall (i.e. close to $\bar{y}$ = 1).

Comparing the potential distribution profiles for longitudinal and transverse thermal gradients one can understand that the basic difference is the introduction of asymmetry through the temperature distribution (figure S7) which has its immediate effect on the potential distribution within the EDL. With increasing C_ζ, the magnitude of surface potential gets amplified significantly in the hot region while remaining unaffected in the cold region thus creating more asymmetry in the y-direction. This further influences the fluid advective motion through electrokinetic forcing thereby altering strongly the velocity distribution. Knowing the potential distribution, the flow field can now be obtained from the following governing equations

$$\mathrm{O}(1): \quad \frac{\partial^2 \bar{u}_0}{\partial \bar{y}^2} = \frac{\partial \bar{p}_0}{\partial \bar{x}} + \frac{\lambda}{\bar{\kappa}_0^2}\bar{E}_{x0}\frac{\partial^2 \bar{\psi}_0}{\partial \bar{y}^2} \tag{S45}$$

and

$$\mathrm{O}(\gamma): \quad \frac{\partial^2 \bar{u}_1}{\partial \bar{y}^2} - C_\mu \theta_0 \frac{\partial^2 \bar{u}_0}{\partial \bar{y}^2} - C_\mu \frac{\partial \theta_0}{\partial \bar{y}}\frac{\partial \bar{u}_0}{\partial \bar{y}} = \frac{\lambda}{\bar{\kappa}_0^2}\left[\begin{array}{l} \dfrac{\partial^2 \bar{\psi}_0}{\partial \bar{y}^2}\bar{E}_{x0}\,\theta_0\left(\bar{S}_{Tavg} - C_\varepsilon\right) + \dfrac{\partial^2 \bar{\psi}_0}{\partial \bar{y}^2}\bar{E}_{x1} \\ + \dfrac{\partial^2 \bar{\psi}_1}{\partial \bar{y}^2}\bar{E}_{x0} - \dfrac{\partial \theta_0}{\partial \bar{y}} C_\varepsilon \dfrac{\partial \bar{\psi}_0}{\partial \bar{y}}\bar{E}_{x0} \end{array}\right] \tag{S46}$$

The solution of these two equations subjected to no-slip boundary condition at the surfaces yields

$$\mathrm{O}(1): \bar{u}_0 = \frac{1}{2}\frac{\partial \bar{p}_0}{\partial \bar{x}}\left(\bar{y}^2 - 1\right) + \frac{\lambda}{\bar{\kappa}_0^2}\bar{E}_{x0}\left[\frac{\cosh\left(\bar{\kappa}_0 \bar{y}\right)}{\cosh\left(\bar{\kappa}_0\right)} - 1\right] \tag{S47}$$

$$\mathrm{O}(\gamma): \bar{u}_1 = \left.\begin{array}{l} C_\mu\left[\dfrac{\partial \bar{p}_0}{\partial \bar{x}}\left(\dfrac{\bar{y}^3}{3} + \dfrac{\bar{y}^2}{2}\right) + \dfrac{\lambda \bar{E}_{x0}\, f_7(\bar{y})}{\cosh\left(\bar{\kappa}_0\right)}\right] - \dfrac{C_\varepsilon \lambda \bar{E}_{x0}\, f_7(\bar{y})}{\cosh\left(\bar{\kappa}_0\right)} + \dfrac{\bar{E}_{x1}\lambda \cosh\left(\bar{\kappa}_0 \bar{y}\right)}{\bar{\kappa}_0^2 \cosh\left(\bar{\kappa}_0\right)} + \dfrac{\bar{S}_{Tavg}\lambda \bar{E}_{x0}\, f_6(\bar{y})}{\cosh\left(\bar{\kappa}_0\right)} \\ + \dfrac{\lambda \bar{E}_{x0}\Delta \bar{S}_T}{2}\left(\dfrac{\bar{y}^3}{3} + \dfrac{\bar{y}^2}{2}\right) + \dfrac{\lambda \bar{E}_{x0}\left(C_\varepsilon + 1\right)}{\bar{\kappa}_0^2}\dfrac{\sinh\left(\bar{\kappa}_0 \bar{y}\right)}{\cosh\left(\bar{\kappa}_0\right)} - \dfrac{\lambda \bar{E}_{x0}\, f_6(\bar{y})\, f_5}{\cosh\left(\bar{\kappa}_0\right)} + C_{u1}\bar{y} + \lambda \bar{E}_{x0} I_6 + C \end{array}\right\} \tag{S48}$$

The coefficients of the velocity distribution described by equation (S48) are given below

$$f_6(\bar{y})=\frac{\bar{\kappa}_0\,\bar{y}\cosh(\bar{\kappa}_0\,\bar{y})-2\sinh(\bar{\kappa}_0\,\bar{y})}{\bar{\kappa}_0{}^3}+\frac{\cosh(\bar{\kappa}_0\,\bar{y})}{\bar{\kappa}_0{}^2},\ f_7(\bar{y})=f_6(\bar{y}),\ f_8=2\bar{\kappa}_0-\tanh(\bar{\kappa}_0),$$

$$f_9=\bar{\kappa}_0-\tanh(\bar{\kappa}_0),\ f_{10}=(C_\varepsilon+1)\tanh(\bar{\kappa}_0),\ C=\begin{bmatrix}-\dfrac{\lambda\bar{E}_{x0}C_\mu f_8}{\bar{\kappa}_0{}^3}-\dfrac{5}{6}C_\mu\dfrac{\partial\bar{p}_0}{\partial\bar{x}}+\dfrac{C_\varepsilon\lambda\bar{E}_{x0}f_8}{\bar{\kappa}_0{}^3}-\dfrac{\bar{E}_{x1}\lambda}{\bar{\kappa}_0{}^2}-\dfrac{\lambda\bar{E}_{x0}\Delta\bar{S}_T}{3}\\ -\dfrac{\lambda\bar{E}_{x0}f_{10}}{\bar{\kappa}_0{}^2}+\dfrac{2\lambda\bar{E}_{x0}f_9}{\bar{\kappa}_0{}^3}\left(f_5-\bar{S}_{Tavg}\right)-C_{u1}-\lambda\bar{E}_{x0}I_7\end{bmatrix}$$

Now, the induced streaming field ($\bar{E}_x$) can be evaluated by using the electroneutrality condition similarly as mentioned in the case of axial temperature gradient

$$\mathrm{O}(1):\ \chi\bar{E}_{x0}\int_{-1}^{1}\bar{\psi}_0\,d\bar{y}+Pe_i\int_{-1}^{1}\bar{u}_0\,\bar{\psi}_0\,d\bar{y}=0 \tag{S49}$$

$$\mathrm{O}(\gamma):\left(2\bar{S}_{Tavg}\bar{E}_{x0}+\chi\bar{E}_{x0}\Delta\bar{S}_T\right)\int_{-1}^{1}\theta_0\,d\bar{y}+2\bar{E}_{x0}\int_{-1}^{1}\left\{\chi\left(\bar{\psi}_1-\bar{\psi}_0\theta_0\right)-\theta_0\bar{\psi}_0(1-C_D)\right\}d\bar{y}+2\chi\bar{E}_{x1}\int_{-1}^{1}\bar{\psi}_0\,d\bar{y}$$
$$+2\chi\bar{E}_{x0}\int_{-1}^{1}\left\{\frac{\partial\theta_0}{\partial\bar{y}}\int_{-1}^{1}\bar{\psi}_0\,d\bar{y}\right\}d\bar{y}+2Pe_i\int_{-1}^{1}\left\{\bar{u}_0\frac{\partial\theta_0}{\partial\bar{y}}\int_{-1}^{1}\bar{\psi}_0\,d\bar{y}\right\}d\bar{y}+2Pe_i\int_{-1}^{1}\begin{Bmatrix}\bar{\psi}_0\bar{u}_1+\bar{\psi}_1\bar{u}_0\\ -\bar{u}_0\bar{\psi}_0\theta_0+\dfrac{1}{2}\Delta\bar{S}_T\bar{u}_0\bar{\psi}_0\end{Bmatrix}d\bar{y}=0 \tag{S50}$$

The final forms of the induced streaming fields ($\bar{E}_x$) for O(1) and O(γ) are written below

$$\bar{E}_{x0}=\frac{2Pe_i\dfrac{\partial\bar{p}_0}{\partial\bar{x}}\left\{\bar{\kappa}_0-\tanh(\bar{\kappa}_0)\right\}}{\left[Pe_i\,\lambda\left\{\dfrac{\bar{\kappa}_0}{\cosh^2(\bar{\kappa}_0)}-\tanh(\bar{\kappa}_0)\right\}+2\,\bar{\kappa}_0^2\,\chi\tanh(\bar{\kappa}_0)\right]} \tag{S51}$$

and

$$\bar{E}_{x1}=-\left(\alpha_{32}+\alpha_{30}\bar{E}_{x0}\right)/\alpha_{31} \tag{S52}$$

with the coefficients of equation (S52) shown in Section F2 of the supplementary material.

A.4 *Fluid rheology*

Now, we focus on the alteration of hydrodynamics and the associated streaming field caused by the inclusion of rheological aspects of fluid. Towards this, the constitutive form of viscoelastic fluid has been chosen for which we have taken into account the simplified Phan-Thien Tanner (sPTT) model, typically employed to model the rheological characteristics of viscoelastic fluids. Here, the basic difference with Newtonian fluid lies in the expressions of the stress tensors (Afonso *et al.* 2009; Arcos *et al.* 2018; Bautista *et al.* 2013)

$$\left.\begin{aligned}2\mu_{eff}\frac{\partial u}{\partial x}&=F\tau_{xx}+\lambda_{eff}\left(u\frac{\partial\tau_{xx}}{\partial x}+v\frac{\partial\tau_{xx}}{\partial y}-2\frac{\partial u}{\partial x}\tau_{xx}-2\frac{\partial u}{\partial y}\tau_{yx}\right)\\ 2\mu_{eff}\frac{\partial v}{\partial y}&=F\tau_{yy}+\lambda_{eff}\left(u\frac{\partial\tau_{yy}}{\partial x}+v\frac{\partial\tau_{yy}}{\partial y}-2\frac{\partial v}{\partial x}\tau_{xy}-2\frac{\partial v}{\partial y}\tau_{yy}\right)\\ \mu_{eff}\left(\frac{\partial u}{\partial y}+\frac{\partial v}{\partial x}\right)&=F\tau_{xy}+\lambda_{eff}\left(u\frac{\partial\tau_{xy}}{\partial x}+v\frac{\partial\tau_{xy}}{\partial y}-\frac{\partial u}{\partial y}\tau_{yy}-\frac{\partial v}{\partial x}\tau_{xx}\right)\end{aligned}\right\} \tag{S53}$$

One important thing to note here that, in presence of temperature gradient, not only fluid viscosity but also fluid relaxation time start to become temperature-dependent and interestingly, the extent of viscoelasticity of fluid is governed by these two parameters - viscosity and

relaxation time. In equation (S53), F is the stress coefficient function, which for the linear PTT model, takes the form $F = 1 + \delta \lambda_{eff} \left(\tau_{xx} + \tau_{yy} \right) / \mu_{eff}$ where δ represents the extensibility of viscoelastic fluid (here δ is chosen to be equal to unity). Here, μ_{eff} and λ_{eff} are viscosity and relaxation time of the fluid which are assumed to be function of temperature as $\mu_{eff} = \mu_{ref} \exp\left[-\omega_1 \left(T - T_{ref} \right) \right]$ and $\lambda_{eff} = \lambda_{ref} \exp\left[-\omega_4 \left(T - T_{ref} \right) \right]$ respectively. The dimensionless form of fluid relaxation time is $\bar{\lambda} = \lambda_{eff} / \lambda_{ref} = \exp\left(-\gamma C_\lambda \theta \right)$ with C_λ being the sensitivity of relaxation time with temperature. Unlike the Newtonian fluid, evaluation of the leading order streaming potential $\left(\bar{E}_{x0} \right)$ in case of a viscoelastic fluid involves a cubic equation in the form of $A \bar{E}_{x0}^{\,3} + B \bar{E}_{x0}^{\,2} + C \bar{E}_{x0} + D = 0$ (the expressions for *A*, *B*, *C*, and *D* can be found in Section F3 of the supplementary material) in which the real root has been chosen for further calculations while the other two roots are complex conjugate to each other and thus discarded.

One important non-dimensional number associated with the flow of viscoelastic fluids is Deborah number (*De*) which determines the degree of viscoelasticity of a fluid defined as $De = \lambda_{ref} \kappa_{ref} u_c$. Keeping other parameters (κ_{ref}, u_c) fixed, the value of Deborah number (*De*) can lie in between 10^{-1} and 1 depending on fluid relaxation time (λ_{ref}) (which may vary due to factors like polymer concentration, polymer molecular weight, etc.). Accordingly, we have chosen *De* in our analysis to vary in between 0 to 1 (with *De* = 0 representing the results of a Newtonian fluid) while obtaining the results. Meanwhile, the stress-tensors in case of viscoelastic fluid are made dimensionless as follows

$$\bar{\tau}_{xx} = \frac{\tau_{xx} h}{\mu_{ref} u_c}, \bar{\tau}_{yy} = \frac{\tau_{yy} h}{\mu_{ref} u_c}, \bar{\tau}_{xy} = \frac{\tau_{xy} h}{\mu_{ref} u_c}$$

For temperature gradient applied in the *x*-direction, the momentum equations for different degree of perturbations are given in the following

$$\mathrm{O}(1): \frac{\partial \bar{\tau}_{xy0}}{\partial \bar{y}} = \frac{\partial \bar{p}_0}{\partial \bar{x}} + \frac{\lambda}{\bar{\kappa}_0^2} \bar{E}_{x0} \frac{\partial^2 \bar{\psi}_0}{\partial \bar{y}^2} \tag{S54}$$

$$\mathrm{O}(\gamma): \frac{\partial \bar{\tau}_{xy1}}{\partial \bar{y}} = \frac{\lambda}{\bar{\kappa}_0^2} \left[\frac{\partial^2 \bar{\psi}_0}{\partial \bar{y}^2} \bar{E}_{x0} \theta_0 \left(\bar{S}_{Tavg} - C_\varepsilon \right) + \frac{\partial^2 \bar{\psi}_0}{\partial \bar{y}^2} \bar{E}_{x1} + \frac{\partial^2 \bar{\psi}_1}{\partial \bar{y}^2} \bar{E}_{x0} - \frac{1}{2} C_\varepsilon \frac{\partial \theta_0}{\partial \bar{x}} \left(\frac{\partial \bar{\psi}_0}{\partial \bar{y}} \right)^2 - \frac{1}{2} \frac{\partial \theta_0}{\partial \bar{x}} \bar{\psi}_0^2 \left(1 + \bar{S}_{Tavg} \right) \right] \tag{S55}$$

where the stress tensors $\bar{\tau}_{xy0}$ and $\bar{\tau}_{xy1}$ are related to the velocity gradients $\frac{\partial \bar{u}_0}{\partial \bar{y}}$ and $\frac{\partial \bar{u}_1}{\partial \bar{y}}$ as

$$\frac{\partial \bar{u}_0}{\partial \bar{y}} = \bar{\tau}_{xy0} + \frac{2 \delta De^2}{\bar{\kappa}_0^2} \bar{\tau}_{xy0}^{\,3} \text{ and } \frac{\partial \bar{u}_1}{\partial \bar{y}} - C_\mu \theta_0 \frac{\partial \bar{u}_0}{\partial \bar{y}} = \bar{\tau}_{xy1} + \frac{2 \delta De^2}{\bar{\kappa}_0^2} \left\{ 3 \bar{\tau}_{xy0}^{\,2} \bar{\tau}_{xy1} + 2 \bar{\tau}_{xy0}^{\,3} \theta_0 \left(C_\mu - C_\lambda \right) \right\} \tag{S56}$$

For the case of transverse thermal gradient, the governing momentum equations can be written as

$$\mathrm{O}(1): \frac{\partial \bar{\tau}_{xy0}}{\partial \bar{y}} = \frac{\partial \bar{p}_0}{\partial \bar{x}} + \frac{\lambda}{\bar{\kappa}_0^2} \bar{E}_{x0} \frac{\partial^2 \bar{\psi}_0}{\partial \bar{y}^2} \tag{S57}$$

$$\text{and } \mathrm{O}(\gamma): \frac{\partial \bar{\tau}_{xy1}}{\partial \bar{y}} = \frac{\lambda}{\bar{\kappa}_0^2}\left[\frac{\partial^2 \bar{\psi}_0}{\partial \bar{y}^2}\bar{E}_{x0}\theta_0\left(\bar{S}_{Tavg} - C_\varepsilon\right) + \frac{\partial^2 \bar{\psi}_0}{\partial \bar{y}^2}\bar{E}_{x1} + \frac{\partial^2 \bar{\psi}_1}{\partial \bar{y}^2}\bar{E}_{x0} - \frac{\partial \theta_0}{\partial \bar{y}}C_\varepsilon \frac{\partial \bar{\psi}_0}{\partial \bar{y}}\bar{E}_{x0}\right] \quad \text{(S58)}$$

$$\text{where } \frac{\partial \bar{u}_0}{\partial \bar{y}} = \bar{\tau}_{xy0} + \frac{2\delta De^2}{\bar{\kappa}_0^2}\bar{\tau}_{xy0}{}^3 \text{ and } \frac{\partial \bar{u}_1}{\partial \bar{y}} - C_\mu \theta_0 \frac{\partial \bar{u}_0}{\partial \bar{y}} = \bar{\tau}_{xy1} + \frac{2\delta De^2}{\bar{\kappa}_0^2}\left\{3\bar{\tau}_{xy0}{}^2\bar{\tau}_{xy1} + 2\bar{\tau}_{xy0}{}^3\theta_0\left(C_\mu - C_\lambda\right)\right\} \quad \text{(S59)}$$

One interesting thing to note that, for the special case of $C_\mu = C_\lambda$, the expressions relating the stress tensor and velocity gradient get simplified resulting in a reduction of non-linearity in the constitutive equation. This also indicates the attenuation of the degree of viscoelasticity of the fluid. Since the stress-tensors in the constitutive form of a viscoelastic fluid are inherently non-linear in nature, the final form of the velocity profiles (for both longitudinal and transverse temperature gradient) are quite large and thus not included in the supplementary material. The MATLAB script files containing the expressions can be made available upon request.

Section B. Results considering the temperature dependence of diffusivity of ions

The dependence of the diffusivity of ions with temperature can be written as $\bar{D} = D/D_{ref} = \left[1 + C_D\gamma\theta\right]$ (Ghonge *et al.* 2013) with C_D representing its temperature-sensitivity. Since, temperature increases gradually (following a linear relationship) in the *x*-direction for axially applied thermal gradient, the diffusivity of ions also increases in a similar way. If there is

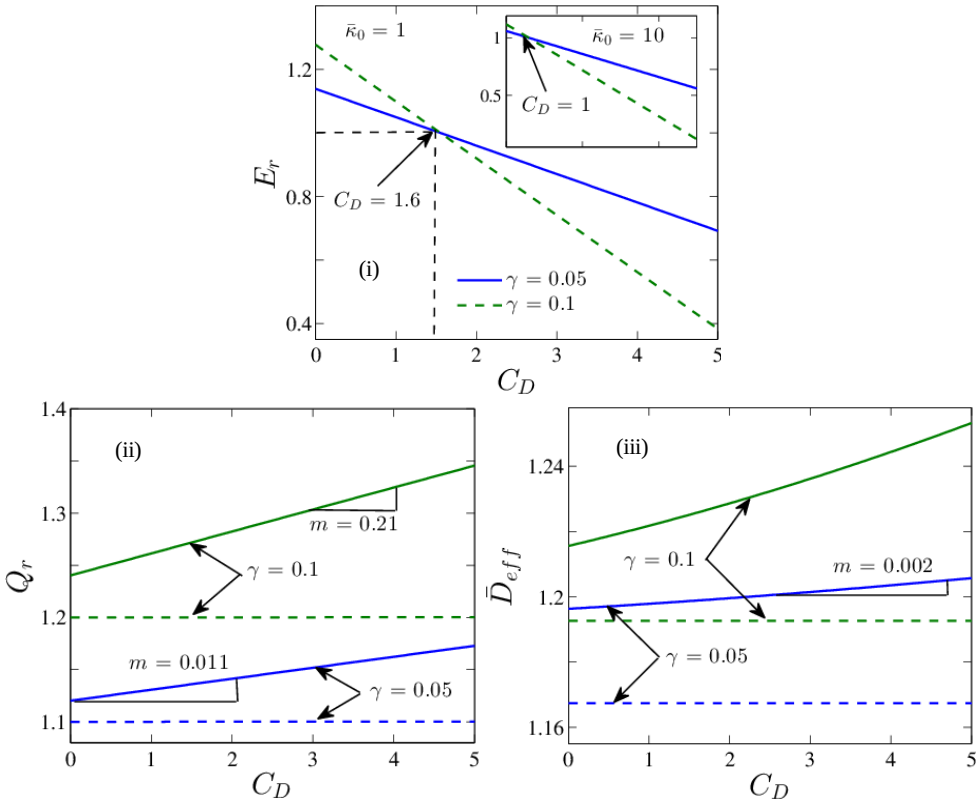

FIGURE S8. The effect of temperature sensitivity of diffusion coefficient (C_D) on (i) streaming potential ratio (E_r), (ii) flow rate ratio (Q_r) and dispersion coefficient ratio ($\bar{D}_{eff}$) , respectively.

a difference between the diffusivity of co-ions and counter-ions, ions having higher diffusivity migrates much faster than the other thus creating an axial separation between them which results in an augmentation of the streaming potential. Now, the enhanced diffusivity in the presence of thermal gradient creates more migration of both cations and anions thus creating a hindrance in the axial separation between them. This results in a significant reduction in the net streaming potential. As shown in figure S8 (i), for lower thermal perturbation (γ = 0.05), streaming potential ratio (E_r) decreases from ~ 1.1 times to ~ 0.7 times as C_D is increased from 0 to 5 (evaluated at $\bar{\kappa}_0$ = 1). At higher γ, the effect of thermo-electric perturbation to the flow field becomes more prominent and accordingly, the dependence of E_r on C_D becomes stronger (E_r decreases from ~ 1.3 to ~ 0.4 with increasing C_D). Also, a cross-over between the graphs of γ = 0.05 and γ = 0.1 can be seen at C_D = 1.6. For higher $\bar{\kappa}_0$, similar reduction of E_r with increasing C_D (inset of figure S8 (i)) can be noticed with cross-over occurring earlier at C_D = 1. The reduced volumetric suppression due to lower induced streaming field results in an increment in the flow rate ratio (Q_r) from 1.12 to 1.17 as C_D is changed from 0 to 5. At higher thermal perturbation (at γ = 0.1), more is the thermally-induced migration of both ions resulting in further lessening of streaming potential. Therefore, as C_D is increased from 0 to 5, the flow rate ratio (Q_r) is enhanced from 1.24 to 1.35 (figure S8 (ii)). For dispersion coefficient ratio ($\bar{D}_{eff}$), trends at lower γ (γ = 0.05) are qualitatively similar to the variations of flow rate ratio (Q_r) with reduced slopes indicating weaker dependence with C_D (figure S8 (iii)). However, at higher γ (γ = 0.1), $\bar{D}_{eff}$ follows a non-linear dependence with C_D because of amplified sensitivity of diffusivity with temperature resulting in a significant increment on the net flow velocity.

Section C1. The reasoning behind the choice of the ranges of the dimensionless parameters

While expressing the results, we have used the following ranges of the dimensionless parameters: $0 \le \gamma$ (thermal perturbation parameter) ≤ 0.1, $10^{-1} \le C_\mu$ (sensitivity coefficient of viscosity) ≤ 10, $10^{-1} \le C_\varepsilon$ (sensitivity coefficient of electrical permittivity) ≤ 10, C_k (sensitivity coefficient of thermal conductivity) = 1, $-0.3 \le \chi$ (diffusivity difference between ions) ≤ 0, $0 \le \Delta\bar{S}_T$ (difference in Soret coefficients between ions) ≤ 1, $1 \le \bar{\kappa}_0$ (inverse of the EDL thickness) ≤ 10, $0 \le -\partial\bar{p}_0/\partial\bar{x}$ (strength of imposed pressure gradient) ≤ 10, $0 \le C_D$ (sensitivity coefficient of diffusivity of ions) ≤ 5, $0 \le C_\zeta$ (sensitivity coefficient of zeta potential) ≤ 4 and $0 \le De$ (Deborah number) ≤ 1. The reason behind choosing these ranges along with the corresponding dimensional values of these parameters are discussed in the following:

In our study, the parameter γ is used to take into account the effect of thermal perturbation to the flow field and the induced streaming potential which is defined as the ratio of the temperature difference to the cold side temperature (which is chosen as the reference temperature), .i.e. $\gamma = \Delta T/T_C$. The upper limit of γ is chosen as 0.1. Since T_C ~ 298.15 K (i.e. room temperature is chosen as reference temperature), it indicates that the maximum temperature difference (ΔT) in our study is chosen to be ~ 30 K approximately. This upper limit is chosen by keeping in mind the under-prediction of the perturbation solution at a higher value of γ. Besides, as highlighted in the literature, 25 K temperature difference (ΔT) can result in a significant alteration in fluid physical properties like viscosity, thermal conductivity, electrical permittivity, etc. (Lide 2009, Dietzel & Hardt 2017).

Now C_μ is the dimensionless parameter indicating the temperature sensitivity of fluid viscosity. The reduction in the fluid viscosity for typical aqueous solutions [] for a temperature range of 25 K (starting from the reference temperature 298 K) can be fitted in the exponential form $\mu = \mu_{ref} \exp\left[-\omega_1\left(T - T_{ref}\right)\right]$ where μ_{ref} is the reference fluid viscosity evaluated at the reference temperature T_{ref}. The corresponding the dimensionless form of this expression is $\bar{\mu} = \mu/\mu_{ref} = \exp\left(-\gamma C_\mu \theta\right)$ where $\gamma = \Delta T/T_C$ and $C_\mu = \omega_1 T_C$ with ω_1 denoting the relative change of viscosity with temperature. For 25 K temperature difference, the value of ω_1 (which is nothing but $-\left(1/\mu\right)\cdot\left(\partial\mu/\partial T\right)$) is found to be 15.7 x 10^{-3} K^{-1} (Lide 2009, Dietzel & Hardt 2017) and the value of its corresponding dimensionless parameter (i.e. C_μ) turns out to be ~ 4.68 Keeping in mind this, although we have chosen a range of $10^{-1} \leq C_\mu \leq 10$ to report some results, the final graph which depicts the significant augmentation in dispersion coefficient by a combination of all involving parameters under the physically realizable scenario, we have chosen the value of C_μ as 5.

Similarly, the reduction of the electrical permittivity of fluid with temperature can be correlated in a similar exponential form: $\varepsilon = \varepsilon_{ref} \exp\left[-\omega_2\left(T - T_{ref}\right)\right]$ and the corresponding non-dimensional form becomes $\bar{\varepsilon} = \varepsilon/\varepsilon_{ref} = \exp\left(-\gamma C_\varepsilon \theta\right)$ where $C_\varepsilon = \omega_2 T_C$ denoting dimensionless parameter for relative change of electrical permittivity with temperature. For the same 25 K temperature difference (ΔT), the value of ω_2 ($\omega_2 = -\left(1/\varepsilon\right)\cdot\left(\partial\varepsilon/\partial T\right)$) is found to be 4.35 x 10^{-3} K^{-1} (Lide 2009, Dietzel & Hardt 2017) and C_ε becomes ~ 1.29. Therefore, although a range of $10^{-1} \leq C_\varepsilon \leq 10$ is used to show some results indicating its effect, for the final graph representing the massive augmentation in dispersion coefficient, $C_\varepsilon = 1$ is used.

The same reasoning can be applied for other parameters like C_k representing the relative change of fluid thermal conductivity with temperature. The dimensional and corresponding dimensionless form of thermal conductivity reads as $k = k_{ref} \exp\left[\omega_3\left(T - T_{ref}\right)\right]$ and $\bar{k} = k/k_{ref} = \exp\left(\gamma C_k \theta\right)$ respectively with $C_k = \omega_3 T_C$. For ΔT = 25 K, ω_3 ($\omega_3 = \left(1/k\right)\cdot\left(\partial k/\partial T\right)$) turns out to be ~ 2.41 x 10^{-3} K^{-1} (Lide 2009, Dietzel & Hardt 2017) and C_k ~ 0.72. Hence, $C_k = 1$ is chosen while obtaining the temperature distribution. Also, higher C_k indicates more sensitivity of thermal conductivity which may eventually result in a departure from the linear temperature distribution.

Similarly, the coefficient of the relative change of diffusivity of ions $\left(1/D\right)\cdot\left(\partial D/\partial T\right)$ for 25 K temperature difference (ΔT) is ~ 19.1 x 10^{-3} K^{-1} (Lide 2009, Dietzel & Hardt 2017) and C_D becomes ~ 5.69. Therefore, we have chosen the value of C_D to be 5 while showing its effect on the flow field and the dispersion coefficient in Section B of the supplementary material.

The parameter C_ζ shows the sensitivity of the zeta potential with temperature. The reason for choosing this specific range (supported with experimental reference) is highlighted in Section A.2 of the supplementary material.

Now we recall the definition of the parameter χ ($\chi = \frac{D_+ - D_-}{D_+ + D_-}$) which indicates the difference in diffusivities between cation and anions. Let us consider aqueous NaCl solution as an example. As reported in the literature, the diffusivity values of Na^+ and Cl^- ions are 1.334 × 10^{-9} m^2 s^{-1} and 2.032 × 10^{-9} m^2 s^{-1} (Zhang et al 2019, Haynes et al. 2014) respectively and thus, the value of χ becomes ~ -0.207. Similarly, for the KCl solution (where diffusivity of K^+ is 1.957× 10^{-9} m^2 s^{-1}), the value of χ turns out to be ~ -0.019. For LiCl solution (diffusivity of Li^+ is 1.029× 10^{-9} m^2 s^{-1}(Zhang et al 2019, Haynes et al. 2014)), the value of χ becomes -0.328. Accordingly, we have chosen the range of - $0.3 \leq \chi \leq 0$ while showing the effect of χ on the streaming potential.

Next, we explain the range of the parameter $\Delta\bar{S}_T$ which denotes the difference in Soret coefficients between cations and anions. Soret coefficient (S_T) is the ratio of the thermophoretic mobility to the diffusivity of the ions ($S_T = \frac{Q_i}{N_A k_B T_C^{\,2}}$ is the dimensional form and $\bar{S}_T = S_T T_C$ is the dimensionless form) which characterizes the response of the ions upon the applied temperature gradient. Choosing the same example, i.e. aqueous NaCl solution, molar heat of transport (Q_i) of Na^+ and Cl^- ions are 3.46 KJ mol^{-1} and 0.53 KJ mol^{-1} (Zhang et al 2019, Agar et al. 1989) respectively. Therefore, the value of $\Delta\bar{S}_T$ becomes ~ 1.18. Similarly, for LiCl solution, since the values of Q_i are the same for Li^+ and Cl^- ions, $\Delta\bar{S}_T$ vanishes. Hence, the range of $0 \leq \Delta\bar{S}_T \leq 1$ is chosen while showing its effect on the streaming potential.

The dimensionless parameter $-\partial\bar{p}_0/\partial\bar{x}$ signifies the strength of the imposed pressure gradient. $-\partial\bar{p}_0/\partial\bar{x} = 0$ represents the scenario of the flow in absence of an external pressure gradient where the imposed temperature gradient (ΔT) solely governs the flow physics. For the value of $-\partial\bar{p}_0/\partial\bar{x}$ = 10, the corresponding dimensional value of the pressure gradient turns out to be ~ 10^6 Pa m^{-1} which is typically used in experimental studies of electrokinetic streaming field-induced flow (Heyden et al. 2007).

The dimensionless parameter $\bar{\kappa}_0$ indicates the inverse of the electrical double layer (EDL) thickness where $\bar{\kappa}_0$ = 10 implies that the thickness of the EDL is 10 times thinner as compared to the channel height. Using the definition of $\kappa_0 = \sqrt{\frac{2 n_\infty z^2 e^2}{\varepsilon_{ref} k_B T}}$, this value $\bar{\kappa}_0 = \kappa_0 h$ can be attained for bulk ionic number concentration n_∞ = 6.023 × 10^{20} mol^{-1}.

To explain the range of Deborah number associated with the flow of viscoelastic fluids, first, we invoke the definition of Deborah number (De) $De = \lambda_{ref} \kappa_{ref} u_c$. While showing the results for viscoelastic fluids in Figures 3a-3b, we have chosen the respective scales of velocity (u_c) as O(10^{-4}) ms^{-1}, the inverse of the electrical double layer (EDL) thickness (κ_{ref}) as 10^7 m^{-1}, fluid relaxation time (λ_{ref}) as 10^{-4} s to 10^{-3} s such that the value of Deborah number (De) lies in between 0.1 and 1.

Another non-dimensional parameter related to viscoelastic fluid is C_λ representing the reduction of the fluid relaxation time with temperature. As shown in previous experimental studies (Pan et al. 2018), this reduction can be correlated in the exponential form $\lambda_{eff} = \lambda_{ref} \exp\left[-\omega_4 \left(T - T_{ref}\right)\right]$ and the corresponding dimensionless form $\bar{\lambda} = \lambda_{eff} / \lambda_{ref} = \exp\left(-\gamma C_\lambda \theta\right)$. As discussed later in Section E2 of the supplementary material, the relative change of fluid relaxation time with temperature $\omega_4 = -\left(1/\lambda_R\right) \cdot \left(d\lambda_R / dT\right) = C_\lambda / T_C$ comes out to be of the order of O(10^{-1}) K^{-1} and thus, the value of C_λ turns out to be close to ~ 3 (approximately). Accordingly, we have chosen C_λ = 3 while representing the results of the dispersion coefficient for viscoelastic fluids (as shown in figure 3b (iii) of the main paper).

Section C2. Comparison between asymptotic approach and exact/numerical solution

As mentioned in the main manuscript, both approximate and exact solutions are obtained for the axially applied thermal gradient for the case of a Newtonian fluid. Figure S9(i) depicts the comparison of volumetric flow rate ratios between the asymptotic (approximate) and exact solutions as a function of C_μ which denotes the sensitivity of fluid viscosity with temperature. The volume flow rate ratio (Q_r) is defined as the ratio of the net throughput because of the combined action of imposed pressure gradient and temperature gradient to that due to the sole action of a pressure gradient. Here C_μ is varied over two decades ranging from 10^{-1} to 10^{1} while keeping other parameters constant. As evident, the asymptotic solution closely approximates the exact solution up to C_μ = 3. Beyond this critical value of C_μ, a large deviation between these two solutions is observed with asymptotic approach under-predicting the results significantly at higher C_μ. In figure S9(ii), comparison of the same has been shown for varying γ, which denotes

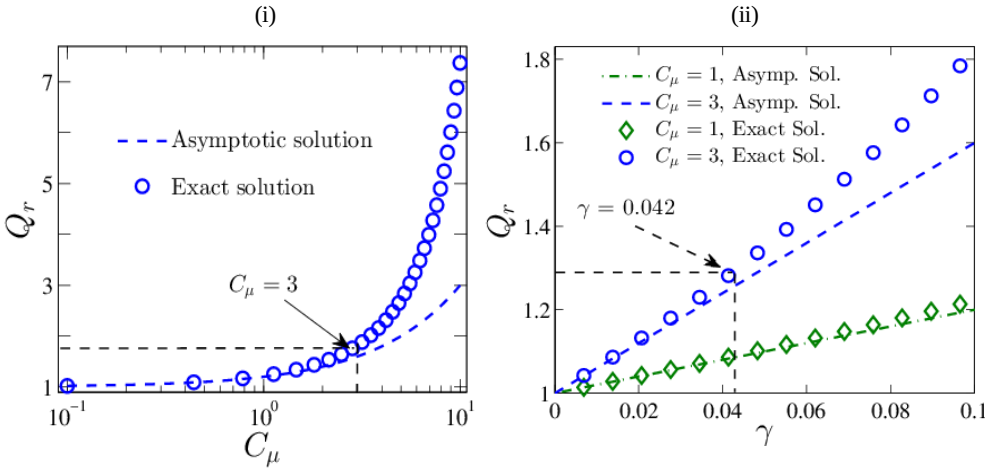

FIGURE S9. Volume flow rate ratio (Q_r) with (i) C_μ and (ii) γ respectively. Symbols show the results obtained from exact solution while lines are for asymptotic solution.

the ratio of the imposed temperature difference with respect to the reference temperature, i.e. quantification of the degree of thermal perturbation imposed. In this context, it is necessary to note that our asymptotic analysis is corrected up to first order in γ. Therefore, our findings can capture the linear thermal effect only. For lower C_μ, the asymptotic solution approximates the exact solution reasonably well while at higher C_μ, deviation takes place between the two solutions with asymptotic solution under-predicting volumetric flow rate beyond γ = 0.042.

For the case of transverse thermal gradient, since no exact solution is possible, a comparison between the asymptotic approach and the numerical solution has been done and is presented in figure S10. Since no closed-form solution for the flow field is possible for the case of the transverse temperature gradient, numerical solution (this is performed using the finite element solver COMSOL Multiphysics) has been carried out to check the validity of the asymptotic solution. First, the temperature distribution (θ) in the transverse direction ($\bar{y}$) is shown where the asymptotic solution closely matches the numerical solution for the lower C_k. Here also (similar to the case of axial temperature gradient), higher the value of C_k, more is the departure from the linear variation, more is the deviation between the two solutions as depicted in the inset (zoomed view for C_k = 10) of figure S10 (i). For potential distribution, predictions of two solutions are very close in the electroneutral region while deviation can be observed in the region close to the wall where the thermal effects are at its prominence on altering the potential profile. Also, this deviation gets amplified (as visible in the inset of figure S10 (ii)) when one increases the value of C_ε i.e. enhancing the sensitivity of electrical permittivity with temperature. Now, the comparison of the flow rate ratio (Q_r) dependence on the thermal perturbation parameter γ is shown in figure S10 (iii) where γ is varying from 0 to 0.1. Since the asymptotic approach is truncated up to the first order of perturbation, it is expected to get a linear dependence of the results on perturbation parameter γ. Here, the asymptotic solution matches closely with the numerical solution for the lower value of C_μ. As one starts increasing C_μ, the deviation between the two solutions starts to become noticeable (figure S10 (iii)). For C_μ = 3, this deviation can be seen beyond γ = 0.06 because of the inability of the asymptotic solution to capture the non-linear dependence of the flow rate with imposed thermal gradient. Now keeping γ fixed, C_μ is varied from 10^{-1} to 10 to check its influence on altering the flow rate. In the region $10^{-1} \leq C_\mu \leq 3$, two solutions closely match each other and beyond C_μ = 3, under-prediction in flow rate ratio (Q_r) by the asymptotic solution can be noticed (figure S10 (iv)).

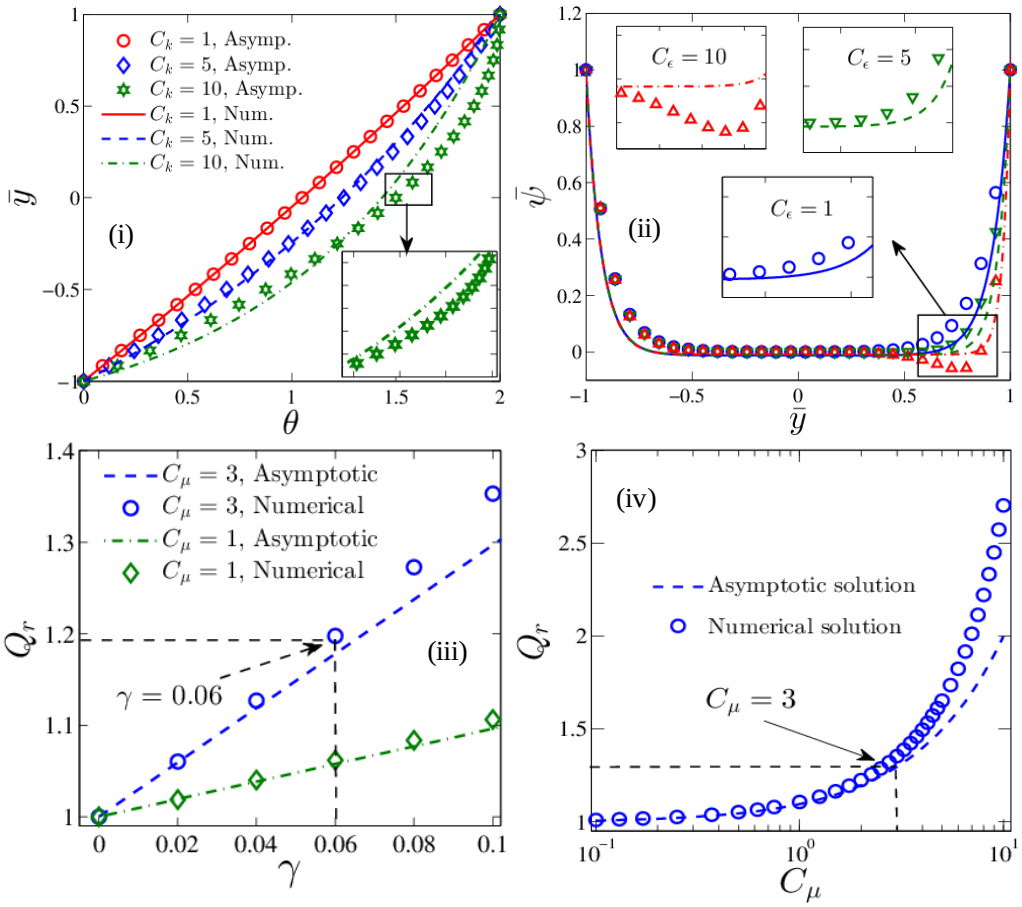

FIGURE S10. Comparison between asymptotic and numerical solution for transverse thermal gradient. (i) Temperature distribution and (ii) potential distribution in the *y*-direction. (iii) Flow rate ratio (Q_r) with perturbation parameter γ, (iv) flow rate ratio (Q_r) with varying C_μ.

Section D. Results for the case of transverse temperature gradient

In the case of temperature gradient applied in the transverse direction, the primary driving force for flow actuation is the axially applied pressure gradient while the contribution from the imposed thermal gradient (ΔT) is secondary through physical property alteration and introducing a permittivity-variation induced body force (this term is $C_\varepsilon\left(\partial\bar{\varepsilon}/\partial\bar{y}\right)\left(\partial\theta/\partial\bar{y}\right)$ as observed in the *x*-component of the momentum equation S46). Apart from this, a concentration gradient in the transverse direction is also induced because of the imposed temperature difference which creates a transverse migration of the ions from the hot region to the cold region (mathematically this can be observed from equation (S41) of the supplementary material which tells us that in the electro-neutral (i.e. ϕ = 0) region, $\left(1/\bar{n}_i\right)\left(\partial\bar{n}_i/\partial\bar{y}\right) = -\bar{S}_{Ti}\,\gamma\left(\partial\theta/\partial\bar{y}\right)$). This migration acts as a resistance in the axial separation between the ions thus creating a weaker streaming field. A further source of alteration in the streaming potential upon the applied thermal gradient comes from factors like modulated viscous resistance of flow, change in effective EDL thickness, permittivity variation induced alteration in streaming current (as previously discussed), etc.

Contrary to the case of axial thermal gradient, here the flow physics is strongly dependent on the parameter χ which indicates the difference in diffusivities between the counter-ions and co-ions. Decreasing the value of χ indicates more diffusivity of the co-ions than counter-ions in the upstream section. This leads to more migration of the co-ions in the upstream section, resulting in a reduction of the streaming potential. As depicted in inset I of figure S11a (i), streaming potential ratio (*Er*) decreases twice from 4 to 2 as χ is changing from -0.1 to -0.3. As χ decreases, the magnitude of the maximum velocity increases more than twice, as observed in figure S11a (i). Interestingly, for χ = -0.3, the position of maxima is close to the channel centreline while for χ = -0.1, this is shifted away from the channel centreline towards the right i..e. towards the direction of the thermal gradient. For χ = -0.1, the velocity profile is slightly deviating from the parabolic behavior because of the generation of stronger streaming field-induced backflow. As χ is decreasing, a lesser generation of streaming potential makes the effect of pressure gradient predominant and velocity distribution follows parabolic behavior. Here, the effect of χ on the flow field is observed only in the higher degree of confinement of channel (observed at $\bar{\kappa}_0 = 1$) and gets diminished with decreasing the extent of confinement (i.e. larger region of electro-neutrality). The inset II of figure S11a (i) shows that increasing $\bar{\kappa}_0$ (i.e. decreasing confinement) from 1 to 10 makes the effect of χ on flow-field insignificant. With decreasing χ, there is a negligible difference between the magnitude of maximum velocity as shown by the zoomed view in inset II.

Keeping χ constant, the velocity distribution for varying C_μ is shown in figure S11a (ii). Since C_μ signifies the sensitivity of fluid viscosity with temperature, higher the value of C_μ, higher is the reduction of the viscosity, lower is the resistance to drive the flow. Because of the strengthened advective current, streaming potential ratio (E_r) is increased slightly as C_μ is increased from 1 to 5. For lower C_μ, the velocity profile is parabolic in nature while at higher C_μ, the enhanced sensitivity of fluid viscosity creates a strong departure from the parabolic distribution with the maxima being shifted towards the hot region. Increasing $\bar{\kappa}_0$ ensures lesser penetration of EDL in the bulk resulting in lowering the net streaming potential thereby enhancing the magnitude of the flow velocity to some extent as depicted by the dotted lines in figure S11a (ii).

Figure S11a (iii) shows the transverse variation of the velocity field with increasing C_ε. Here, C_ε indicates the sensitivity of permittivity with temperature. The contribution of C_ε primarily comes through the alteration in the potential distribution upon increasing C_ε and through the permittivity-induced forcing term in the fluid momentum transport. Here, streaming potential ratio (E_r) decreases (inset I of figure S11a (iii)) slightly with increasing C_ε resulting in a small increment in the velocity magnitude. Similar to the effect of χ, here also increasing $\bar{\kappa}_0$ from 1 to 10 makes the effect of C_ε on the flow field inconsequential as evident from inset II (where zoomed view of maximum velocity is presented) of figure S11a (iii).

The variation of the velocity field in the *y*-direction for different $\Delta\bar{S}_T$ is shown in figure S11a (iv) where $\Delta\bar{S}_T$ means the difference in thermophoretic mobilities between cations and anions. Increasing $\Delta\bar{S}_T$ implies higher thermophoretic mobility of counter-ions than co-ions which leads to preferential migration of the counter-ions towards the cold region. This leads to an ionic redistribution resulting in an asymmetry in the potential distribution within EDL. On observing the momentum equation S46, one can understand that the role of $\Delta\bar{S}_T$ comes through

the charge distribution alteration (via the modulated EDL thickness and the term $\left\{C_\varepsilon - \left(1+\bar{S}_{Tavg}\right)\right\} \bar{\kappa}_0^2 \theta_0 \bar{\psi}_0$) which further perturbs the fluid advection motion. This, in turn, influences the advection current and the induced streaming field. Accordingly, the streaming potential ratio (E_r) increases from ~ 1.8 times to ~ 2.05 times as one increases $\Delta\bar{S}_T$ from 0 to 1 following a linear dependence. The enhanced streaming field induces more backward flow thus lowering the magnitude of the flow velocity as observed in figure S11a (iv) for $\Delta\bar{S}_T = 1$.

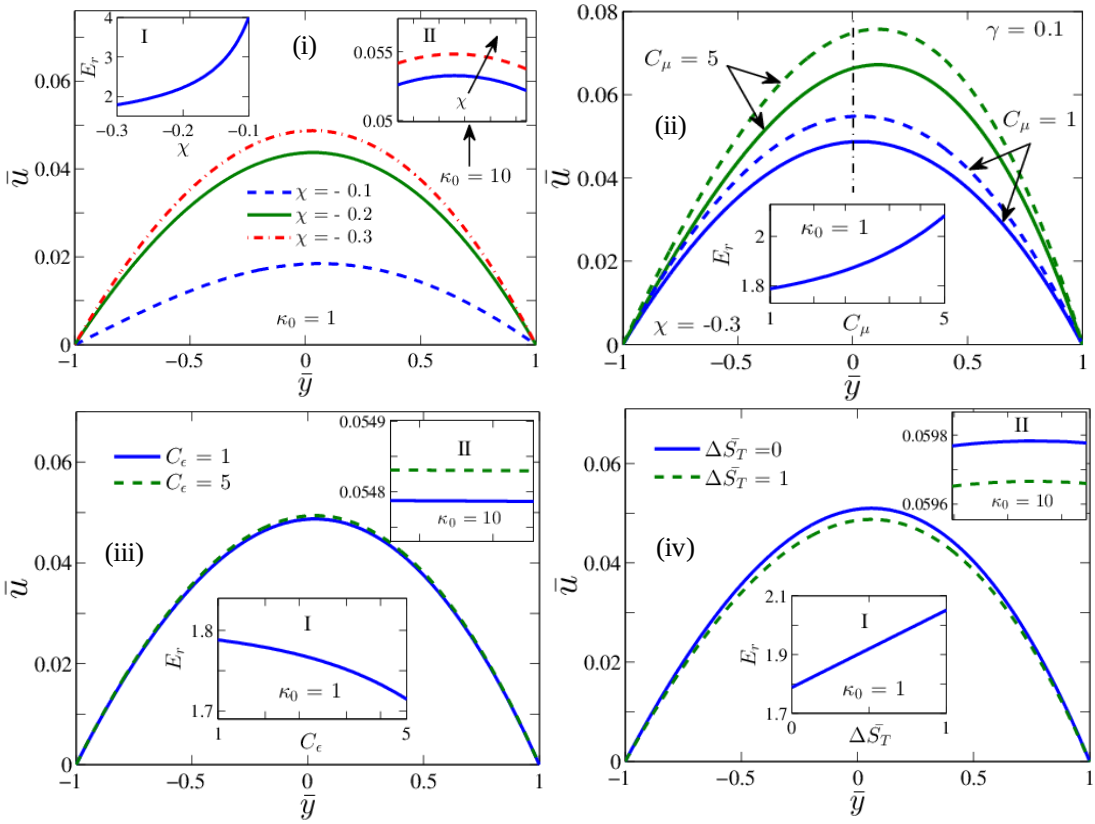

FIGURE S11a. Velocity distribution in the *y*-direction for varying (i) χ, (ii) C_μ, (iii) C_ε and (iv) $\Delta\bar{S}_T$ respectively (evaluated at $-\partial\bar{p}_0/\partial\bar{x} = 0.1$).

As discussed in the case of an axial thermal gradient, any perturbation to the flow field is strongly reflected in the associated dispersion coefficient because of its strong dependence on the flow velocity. By inspecting the velocity distributions demonstrated by figure S11a, one general observation can be made that the effect of most of the parameters (except C_μ) on the flow field is noticeable only under higher confinement (i.e. at lower $\bar{\kappa}_0$) and becomes negligible at higher $\bar{\kappa}_0$. Apart from $\bar{\kappa}_0$, C_μ is another important parameter whose effect on the flow field is far more significant compared to other parameters (C_ε, $\Delta\bar{S}_T$) not only by altering the magnitude of the flow velocity but also creating a strong departure from the parabolic distribution. Accordingly, in figure S11b we have incorporated the variation of dispersion coefficient ratio ($\bar{D}_{eff}$) with two parameters C_μ and $\bar{\kappa}_0$. Similar to axial ΔT, drastic reduction in flow resistance with increasing C_μ is reflected in figure S11b (i) where $\bar{D}_{eff}$ is increased 3 times as C_μ is varying from 1 to 10.

The reduced strength of electrokinetic forces with increasing $\bar{\kappa}_0$ lowers the thermo-electric perturbation to the flow field and hence, dispersion coefficient ratio ($\bar{D}_{eff}$) (at γ = 0.1) reduces from 1.19 to 1.18 as $\bar{\kappa}_0$ is changed from 1 to 10 with alteration being suppressed beyond $\bar{\kappa}_0$ = 4.4. Corresponding results for lower γ are similar with saturation occuring at higher $\bar{\kappa}_0$.

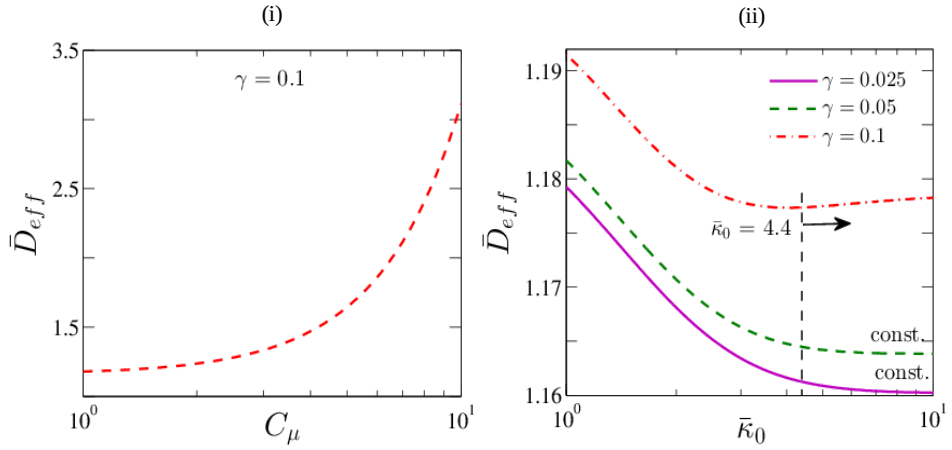

FIGURE S11b. (i) Variation of dispersion coefficient ratio ($\bar{D}_{eff}$) with C_μ, (ii) variation of the same with $\bar{\kappa}_0$ for different γ.

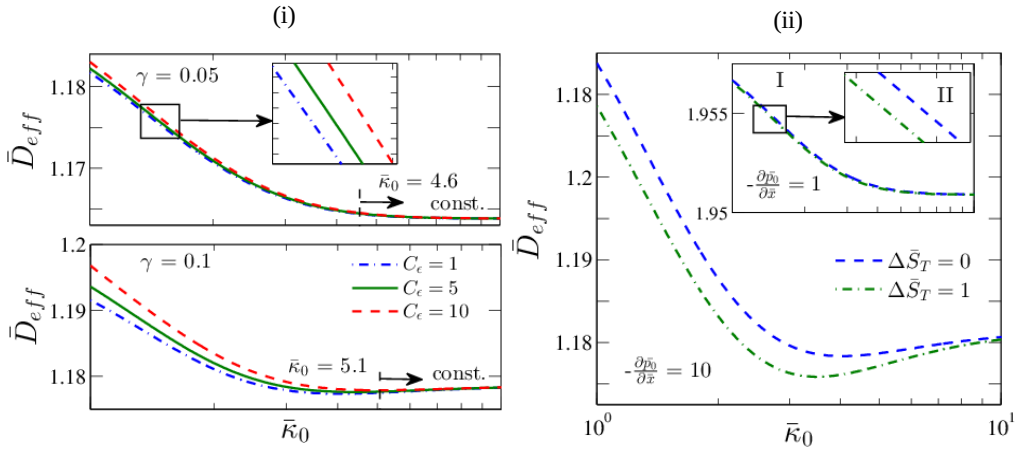

FIGURE S11c. Variation of $\bar{D}_{eff}$ with $\bar{\kappa}_0$ for different values of (i) C_ε and (ii) $\Delta \bar{S}_T$

Now, the effect of two other parameters C_ε and $\Delta \bar{S}_T$ are shown in figure S11c where the reduced streaming potential with increasing C_ε results in increasing the dispersion coefficient. However, C_ε turns out to be less effective at lower thermal perturbation (γ = 0.05) and noticeable effect can only be observed at higher γ (figure S11c (i)). Similarly, higher volumetric suppression due to enhanced streaming potential with increasing $\Delta \bar{S}_T$ lowers the dispersion coefficient with $\Delta \bar{S}_T$ becoming influential only at a higher strength of pressure gradient (figure S11c (ii)).

Section E1. Results in the case of fluid relaxation time varying with polymer concentration

In the rheological characterization of polymeric fluid, Zimm's definition of relaxation time (λ_z) has been widely used which tells that the fluid relaxation time is independent of the polymer

concentration. However, some experimental studies (Tirtaatmadja et al (2006)) have reported that even for solutions in the dilute regime, fluid relaxation time can vary with the polymer concentration with the effective relaxation time (λ_{eff}) showing one order of magnitude higher value than Zimm's relaxation time (at higher polymer concentration).

While showing the results for viscoelastic fluids in figures 3a-3b of the revised manuscript, we have chosen the respective scales of velocity (u_c) as O(10^{-4}) ms^{-1}, the inverse of the electrical double layer (EDL) thickness (κ_{ref}) as 10^7 m^{-1}, fluid relaxation time (λ_{ref}) as 10^{-4} s to 10^{-3} s such that the value of Deborah number (*De*) lies in between 0.1 and 1. Now, to incorporate the effective change of fluid relaxation time with polymer concentration (as shown by Tirtaatmadja et al (2006)) on our results, we should take into account both the changes in fluid relaxation time as well as the viscosity enhancement with increasing polymer concentration. In this context, we recall the definition of the characteristic velocity scale (u_c) which is inversely proportional to the fluid viscosity μ_{ref}. We have used the relaxation time and viscosity data from table 2 of this mentioned paper where properties for aqueous Polyethylene Oxide solution (M_w = 1 x 10^6 g mol^{-1}) are given. We have calculated the Deborah number (*De*) values for different polymer concentrations (*c*) ranging from $c/c^* = 0.01$ to $c/c^* = 0.63$ where *c** denotes the overlap concentration above which a transition from dilute to semi-dilute regime takes place.

The variations of the streaming potential ratio (E_r), volumetric flow rate ratio (Q_r) and dispersion coefficient ratio ($\bar{D}_{eff}$) as a function of c/c^* are shown in figure S12. As the polymer concentration (*c*) is increased gradually, both the fluid relaxation time and viscosity increase. The relative change of fluid relaxation time and viscosity with increasing polymer concentration are shown in insets I and II of figure S12 (a). It is clear from these insets that the rate of increase in relaxation time is much higher as compared to that of viscosity.

Now, Deborah number (*De*) is defined as the ratio of the elastic to viscous forces and hence, as *c* increases, the relative strength of elasticity increases which enhances the degree of viscoelasticity of the fluid thereby leading to a slight increment in the streaming potential for C_μ = 1, C_λ = 1. C_μ and C_λ denote the relative sensitivity of fluid relaxation time and viscosity with temperature. Increased streaming potential induces more backward electrokinetic flow in the reverse direction and as the dispersion coefficient is more susceptible to change in flow velocity, it decreases slightly as c/c^* is increased from 0.01 to 0.63. Next, we have evaluated the same at higher C_μ and lower C_λ (i.e. at C_μ = 3, C_λ = 1). Higher C_μ at one side strongly enhances the streaming potential (figure S12(a)) and thus the backward electrokinetic flow. However, the viscous resistance to the flow decreases at a much higher rate such that it overweighs the effect of reverse electrokinetic flow and $\bar{D}_{eff}$ increases up to 1.8 times as c/c^* is changed from 0.01 to

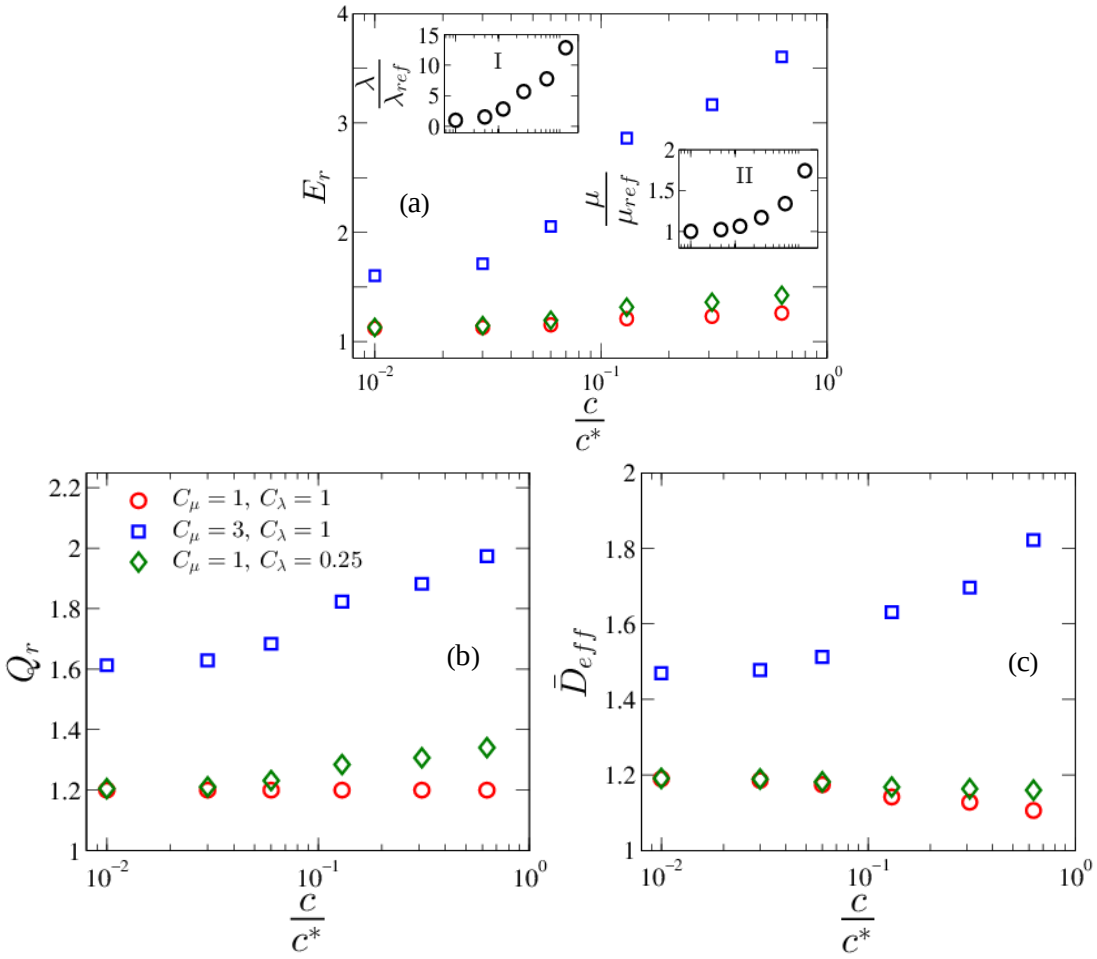

FIGURE S12: The variation of (a) streaming potential ratio (E_r), (b) volume flow rate ratio (Q_r) and (c) dispersion coefficient ratio ($\bar{D}_{eff}$) as a function of polymer concentration (for polymeric solution in the dilute regime). The relaxation time (λ) and viscosity (μ) values are taken from the experimental work of Tirtaatmadja et al. (2006).

0.63 (shown in figure S12(c))**.** Now, decreasing the value of C_λ indicates less reduction of fluid relaxation time with temperature indicating more extent of viscoelasticity of fluid thus increasing the dispersion coefficient ratio ($\bar{D}_{eff}$) slightly as C_λ is changed from 1 to 0.25. Dependence of Q_r on C_μ and C_λ remains similar to that for $\bar{D}_{eff}$ where instead of decreasing, a slight increment of Q_r is observed for C_μ = 1, C_λ = 0.25 while Q_r remains constant for C_μ = 1, C_λ = 1 where two opposing factors C_μ and C_λ nullify each other (figure S12(b)).

Section E2. Part1: Flow rate variation of viscoelastic fluids for axial temperature gradient

For axially applied temperature gradient, the flow rate ratio (Q_r) variation with Deborah number (De) is highlighted in figure S13 for two varying factors C_μ and C_λ respectively. At one side, increasing C_μ induces more streaming potential leading to the net volumetric suppression due to reverse electrokinetic flow, on the other hand, viscous resistance in the flow decreases

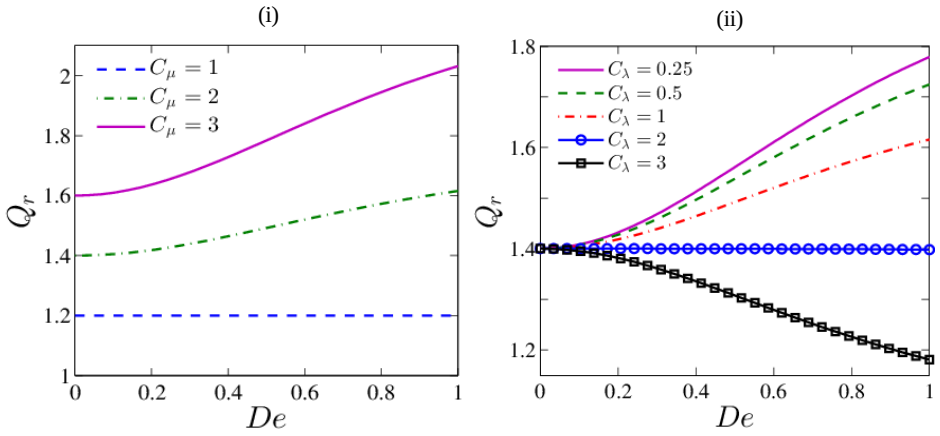

FIGURE S13. Volume flow rate ratio (Q_r) with De for different (i) C_μ and (ii) C_λ

significantly. Hence, net throughput through the microchannel is determined by their relative strengths. For the lower value of C_μ, Q_r remains almost unaffected with the variation of De (at C_μ = 1). However, with increasing C_μ, Q_r increases sharply with an enhancement up to ~ 2.03 times can be noticed at C_μ = 3 (figure S13 (i)). Similarly, increasing C_λ has an inverse effect on the flow rate as Q_r decreases with De from 1.78 times to 1.18 times as C_λ is changed from 0.25 to 3. Since the net streaming potential reduces beyond C_λ = 1, reduced volumetric suppression makes Q_r still higher than unity at C_λ = 3 (figure S13 (ii)).

Section E2. Part2: Dependence of fluid relaxation time with temperature

For dilute polymeric solutions, fluid relaxation time is described by the well-known Zimm's relaxation time which is independent of the polymer concentration (Del Giudice *et al.* 2015, 2017). Previous experimental studies have reported that Zimm's relaxation time is inversely proportional to the fluid temperature (Del Giudice *et al.* 2015, 2017; Pan *et al.* 2018). In this study, we have used the following dependence of fluid relaxation time with temperature $\lambda_{eff} = \lambda_{ref} \exp\left[-\omega_4\left(T - T_{ref}\right)\right]$ which, in the dimensionless form, can be expressed as $\bar{\lambda} = \lambda_{eff}/\lambda_{ref} = \exp\left(-\gamma C_\lambda \theta\right)$.

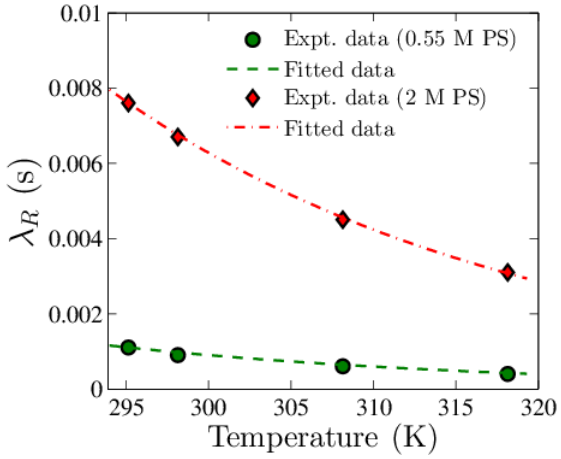

FIGURE S14. Dependence of fluid relaxation time with temperature. Reported experimental results are fitted considering the exponential function used in the present analysis (Pan et al. 2018).

For a representative example, experimental results of relaxation time reduction with temperature for two different samples (dilute Polystyrene samples (PS) of Molecular weights 0.55 M and 2 M respectively) (Pan *et al.* 2018) have been chosen. We have fitted this variation with our chosen exponential form and the experimental data points match reasonably well using the above-mentioned correlation (figure S14) where the value of the relative change of fluid relaxation time with temperature $-\left(1/\lambda_R\right)\left(d\lambda_R/dT\right)$ is found to be of the order of O(10^{-1}) K^{-1} which in turn equals to C_λ/T_C. For the reference value $T_C = 298.15\,\mathrm{K}$, the value of the coefficient C_λ turns out to be close to ~ 3 (approximately). Accordingly, we have chosen $C_\lambda = 3$ while representing the results of dispersion coefficient for viscoelastic fluids (as shown in figure 3b (iii) of the main paper).

Section E3. Results for viscoelastic fluids in case of a transverse temperature gradient

For the transverse thermal gradient, variations of dispersion coefficient ratio ($\bar{D}_{eff}$) with Deborah number (*De*) are shown in figure S15 for two important factors associated with the flow of viscoelastic fluids, .i.e. C_μ and C_λ respectively. For a lower value of C_μ, two counter-acting effects of viscous resistance of flow and elasticity-mediated perturbation to the flow field are of comparable magnitude and dispersion coefficient ratio ($\bar{D}_{eff}$) decreases gradually (from 1.17 to 1.06) with Deborah number (*De*). Similar to the case of an axial thermal gradient, increasing C_μ strongly influences the dispersion coefficient with an enhancement up to ~ 1.9 times can be seen as C_μ is increased from 1 to 5 (figure S15 (i)). For lower C_λ (C_λ = 0.25), less is the elasticity-induced disturbance to the flow field

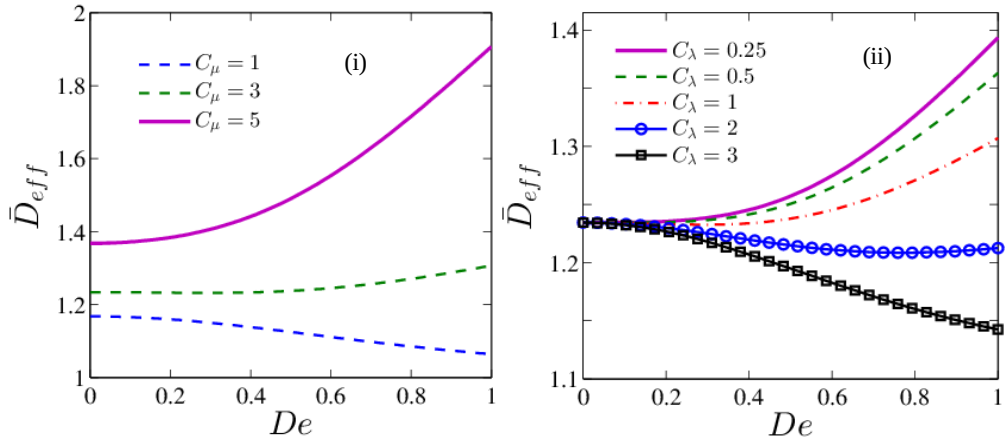

FIGURE S15. Variation of dispersion coefficient ratio ($\bar{D}_{eff}$) with Deborah number (*De*) for different (i) C_μ and (ii) C_λ respectively (for the case of transverse thermal gradient).

making the effect of C_μ (i.e. lower viscous resistance of flow) dominant over C_λ resulting in an increment up to ~ 1.4 times (figure S15 (ii)). As one starts increasing C_λ, its effect on the flow field and resulting dispersion coefficient starts to become important which lowers the dispersion coefficient ratio ($\bar{D}_{eff}$) from 1.4 to 1.3 as C_λ is changed from 0.25 to 1. Beyond C_λ = 1, increasing C_λ has its inverse effect on dispersion coefficient as $\bar{D}_{eff}$ undergoes a reduction from ~ 1.23 to ~ 1.14 when C_λ is increased from 1 to 3 indicating its pronounced effect in governing the hydrodynamics and the resulting dispersion coefficient (figure S15 (ii)).

Section F1. Coefficients involved in the streaming potential expression

The coefficients of the streaming potential described by equation (S28) are given in the following

$$\gamma_1 = -2\,\chi\,\theta_0\,\gamma_{57}, \gamma_2 = -2, \gamma_3 = 2\theta_0, \gamma_4 = 2\chi\,\gamma_{57}, \gamma_5 = \gamma_1, \gamma_6 = -2\gamma_{57}, \gamma_7 = -\left(1+\chi\right)\Delta\bar{S}_T, \gamma_8 = \left(1+\chi\right)\gamma_{57}\,\Delta\bar{S}_T,$$

$$\gamma_9 = 2\,\gamma_{57}\left(\bar{S}_{T-} - \bar{S}_{Tavg}\right), \gamma_{10} = -\frac{\gamma_9\,\chi}{\gamma_{57}}, \gamma_{11} = -\frac{\gamma_{49}}{2\,\bar{\kappa}_0\cosh^2\left(\bar{\kappa}_0\right)}, \gamma_{12} = -\theta_0\gamma_{11}, \gamma_{13} = -2\chi\,\gamma_{11}, \gamma_{15} = -2\,\theta_0\,\gamma_{11},$$

$$\gamma_{14} = -\frac{\gamma_{10}\,\gamma_{11}}{2}, \gamma_{16} = -\frac{\gamma_{54}}{3\bar{\kappa}_0\cosh^3\left(\bar{\kappa}_0\right)}, \gamma_{17} = \chi\left[\frac{2}{\bar{\kappa}_0}\sinh\left(\bar{\kappa}_0\right)\left(f_1+f_2\right) + C_{\varepsilon eff}\left(1-\gamma_{57}\right) - \frac{3C_{\varepsilon eff}\,\gamma_{57}}{4}\right],$$

$$\gamma_{18} = \left[-\frac{\gamma_{49}\left(f_1+f_2\right)}{\bar{\kappa}_0\cosh\left(\bar{\kappa}_0\right)} - \frac{C_{\varepsilon eff}\,\gamma_{50}}{8\bar{\kappa}_0\cosh^2\left(\bar{\kappa}_0\right)} - \frac{3C_{\varepsilon eff}}{4\bar{\kappa}_0}\gamma_{11}\right], \gamma_{19} = \theta_0\frac{\partial\bar{p}_0}{\partial\bar{x}}\left[-\frac{\gamma_{51}}{\bar{\kappa}_0{}^3} + \gamma_{57}\right], \gamma_{20} = -\frac{\theta_0\,\lambda\,\gamma_{49}}{\bar{\kappa}_0{}^3\cosh^2\left(\bar{\kappa}_0\right)},$$

$$\gamma_{21} = \frac{2\,\theta_0\,\lambda\,\gamma_{57}}{\bar{\kappa}_0{}^2}, \gamma_{22} = \frac{\lambda\,f_1\,\gamma_{49}}{\bar{\kappa}_0{}^3\cosh\left(\bar{\kappa}_0\right)}, \gamma_{23} = \gamma_{22}\frac{f_2}{f_1}, \gamma_{24} = \frac{\lambda\,C_{\varepsilon eff}\,\gamma_{50}}{8\bar{\kappa}_0{}^3\cosh^2\left(\bar{\kappa}_0\right)}, \gamma_{25} = -\frac{\lambda\,C_{\varepsilon eff}\,\gamma_{49}}{4\bar{\kappa}_0{}^3\cosh^2\left(\bar{\kappa}_0\right)}, \gamma_{26} = \frac{\gamma_{25}}{2},$$

$$\gamma_{27} = -\frac{2\,\lambda\,f_1}{\bar{\kappa}_0{}^3}\sinh\left(\bar{\kappa}_0\right), \gamma_{28} = -\frac{2\,\lambda\,f_2}{\bar{\kappa}_0{}^3}\sinh\left(\bar{\kappa}_0\right), \gamma_{29} = -\frac{\lambda\,C_{\varepsilon eff}\,\gamma_{55}}{\bar{\kappa}_0{}^3\cosh\left(\bar{\kappa}_0\right)}, \gamma_{30} = \frac{\lambda\,C_{\varepsilon eff}\,\gamma_{57}}{2\,\bar{\kappa}_0{}^2}, \gamma_{31} = \frac{\gamma_{30}}{2},$$

$$\gamma_{32} = \begin{bmatrix} -\frac{\partial\bar{p}_0}{\partial\bar{x}}\frac{\gamma_{58}}{2\bar{\kappa}_0{}^3}\left(f_1+f_2\right) - \frac{C_{\varepsilon eff}}{4\bar{\kappa}_0{}^3}\frac{\partial\bar{p}_0}{\partial\bar{x}}\gamma_{51} + \frac{C_{\varepsilon eff}\,\gamma_{58}}{16\bar{\kappa}_0{}^3\cosh\left(\bar{\kappa}_0\right)}\frac{\partial\bar{p}_0}{\partial\bar{x}} + \frac{C_{\varepsilon eff}\,\gamma_{56}}{2\bar{\kappa}_0{}^3\cosh\left(\bar{\kappa}_0\right)} \\ -\frac{\partial\bar{p}_0}{\partial\bar{x}}\frac{\sinh\left(\bar{\kappa}_0\right)}{\bar{\kappa}_0}\left(f_1+f_2\right) + \frac{3}{8}\frac{\partial\bar{p}_0}{\partial\bar{x}}C_{\varepsilon eff}\gamma_{57} - \frac{\partial\bar{p}_0}{\partial\bar{x}}\frac{C_{\varepsilon eff}\,\gamma_{55}}{2\bar{\kappa}_0\cosh\left(\bar{\kappa}_0\right)} \end{bmatrix}, \gamma_{33} = \frac{\beta_2\,\lambda\,\gamma_{49}}{\bar{\kappa}_0{}^3\cosh^2\left(\bar{\kappa}_0\right)},$$

$$\gamma_{34} = \frac{\beta_3\,\beta_1\,\gamma_{49}}{\bar{\kappa}_0\cosh^2\left(\bar{\kappa}_0\right)}, \gamma_{35} = \frac{\beta_4}{\bar{\kappa}_0{}^4\cosh\left(\bar{\kappa}_0\right)}\left[\gamma_{49}\left\{\bar{\kappa}_0\left(\beta_7+\beta_8+\beta_9-\beta_{11}\right)-2\beta_{10}\right\} + \frac{\gamma_{50}\,\beta_{10}}{4}\right], \gamma_{36} = \frac{\gamma_{34}}{\beta_1},$$

$$\gamma_{37} = \left[\left\{\frac{\left(\bar{\kappa}_0{}^2\beta_5 - \beta_6\right)}{2\bar{\kappa}_0{}^3\cosh^2\left(\bar{\kappa}_0\right)} + \frac{\beta_2}{\bar{\kappa}_0{}^3}\frac{\partial\bar{p}_0}{\partial\bar{x}}\right\}\gamma_{51} - \left\{\frac{\left(\bar{\kappa}_0{}^2\beta_5 + \beta_6\right)}{2\bar{\kappa}_0{}^3\cosh^2\left(\bar{\kappa}_0\right)}\right\}\gamma_{54}\right], \gamma_{38} = \frac{1}{\bar{\kappa}_0}, \gamma_{39} = \left[-\frac{\beta_2}{2}\frac{\partial\bar{p}_0}{\partial\bar{x}} + \beta_5\,\beta_{13} + \beta_6\,\beta_{14}\right],$$

$$\gamma_{40} = \left[-\frac{\beta_2\,\lambda}{\bar{\kappa}_0{}^2} - \beta_3\,\beta_1 - \beta_4\,\beta_{18} + \frac{\beta_4\,\beta_{12}}{\bar{\kappa}_0}\right], \gamma_{41} = -\beta_3, \gamma_{42} = 2\,\gamma_{38}\,\gamma_{39}\tanh\left(\bar{\kappa}_0\right), \gamma_{43} = 2\,\gamma_{38}\,Pe_i\,\gamma_{40}\tanh\left(\bar{\kappa}_0\right),$$

$$\gamma_{44} = 2\,\gamma_{38}\,\gamma_{41}\,Pe_i\tanh\left(\bar{\kappa}_0\right), \gamma_{45} = \left[\begin{pmatrix}\gamma_1+\gamma_3+\gamma_5+\gamma_{12}+\\ \gamma_{15}+\gamma_{17}+\gamma_{18}+\gamma_{43}\end{pmatrix} + Pe_i\begin{Bmatrix}\gamma_{20}+\gamma_{21}+\gamma_{22}+\gamma_{23}+\gamma_{24}+\gamma_{25}+\gamma_{26}+\gamma_{27}\\ +\gamma_{28}+\gamma_{29}+\gamma_{30}+\gamma_{31}+\gamma_{33}+\gamma_{34}+\gamma_{35}\end{Bmatrix}\right],$$

$$\gamma_{46} = \left[\gamma_2+\gamma_4+\gamma_{11}+\gamma_{44}+Pe_i\,\gamma_{36}\right], \gamma_{47} = \left[\gamma_{19}+\gamma_{32}+\gamma_{37}+\gamma_{42}\right], \gamma_{48} = \left[\gamma_6+\gamma_7+\gamma_8+\gamma_9+\gamma_{10}+\gamma_{13}+\gamma_{14}+\gamma_{16}\right],$$

$$\gamma_{49} = \left[\bar{\kappa}_0 + \cosh\left(\bar{\kappa}_0\right)\sinh\left(\bar{\kappa}_0\right)\right], \gamma_{50} = \left[2\bar{\kappa}_0\cosh\left(2\bar{\kappa}_0\right) - \sinh\left(2\bar{\kappa}_0\right)\right], \gamma_{51} = \left[\bar{\kappa}_0{}^2\tanh\left(\bar{\kappa}_0\right) - 2\bar{\kappa}_0 + 2\tanh\left(\bar{\kappa}_0\right)\right],$$

$$\gamma_{52} = \left(\bar{\kappa}_0{}^2 - 2\bar{\kappa}_0 + 2\right), \gamma_{53} = \left(\bar{\kappa}_0{}^2 + 2\bar{\kappa}_0 + 2\right), \gamma_{54} = \left[\left\{\cosh^2\left(\bar{\kappa}_0\right)+2\right\}\sinh\left(\bar{\kappa}_0\right)\right], \gamma_{55} = \left[\bar{\kappa}_0\cosh\left(\bar{\kappa}_0\right) - \sinh\left(\bar{\kappa}_0\right)\right],$$

$$\gamma_{56} = \begin{bmatrix}\bar{\kappa}_0{}^3\cosh\left(\bar{\kappa}_0\right) - 3\bar{\kappa}_0{}^2\sinh\left(\bar{\kappa}_0\right)\\ +6\bar{\kappa}_0\cosh\left(\bar{\kappa}_0\right) - 6\sinh\left(\bar{\kappa}_0\right)\end{bmatrix}, \gamma_{57} = \frac{\tanh\left(\bar{\kappa}_0\right)}{\bar{\kappa}_0}, \gamma_{58} = \left[\exp\left(-\bar{\kappa}_0\right)\gamma_{53} - \exp\left(\bar{\kappa}_0\right)\gamma_{52}\right]$$

Expression of the function *A*

The expression of function A is given below

$$A = +\left(\frac{\partial \bar{p}_0}{\partial \bar{x}}\right)\frac{1}{96\beta_{23}{}^2\bar{\kappa}_0{}^4\cosh(\bar{\kappa}_0)\gamma_{46}}\begin{bmatrix}96\beta_{23}{}^3\beta_4\gamma_{46}C_1(\beta_8-\beta_{11})\exp(-\bar{\kappa}_0\bar{y})\\+384(P_1+P_2+P_3)\exp(-2\bar{\kappa}_0)\bar{y}^2+96(P_4+P_5)\bar{\kappa}_0\end{bmatrix}+P_6+C_6\bar{y}+C_7$$

where C_6 and C_7 are the integration constants which are obtained using the previously mentioned boundary conditions. Now, the expressions for P_1 - P_6 are presented below

$$P_1 = 16\beta_{23}{}^2\bar{\kappa}_0\exp(2\bar{\kappa}_0)\begin{bmatrix}\begin{bmatrix}24\gamma_{41}\beta_{23}\beta_{26}Pe_i\lambda\bar{x}C_1+12C_\mu\lambda\bar{x}\beta_{23}{}^2\gamma_{46}\bar{\kappa}_0C_1+6\beta_4C_1\gamma_{46}\beta_{12}\beta_{23}{}^2+24\gamma_{41}C_\mu Pe_i\lambda\bar{x}\beta_{24}C_1\\+2\bar{\kappa}_0{}^3\beta_{23}{}^2\left[3C_1(2\bar{x}\gamma_{46}C_2\beta_3+\gamma_{41}\gamma_{62}Pe_i+4\gamma_{41}\bar{x}+\beta_{18}\beta_4\gamma_{46}+\gamma_{41}\gamma_{63})+2C_\mu\bar{x}\gamma_{46}+3\gamma_{41}Pe_i\gamma_{60}\right]\\+3C_1\bar{\kappa}_0{}^2\begin{bmatrix}-\beta_4\beta_{12}\beta_{23}{}^2\gamma_{46}+4\gamma_{41}\beta_{23}\bar{x}\beta_{24}\\+8\bar{x}\gamma_{41}\beta_{24}(1+Pe_iC_2\beta_3)\end{bmatrix}+12\gamma_{41}Pe_i\bar{x}\beta_{25}(C_\mu-1)\beta_{23}\end{bmatrix}\\+12\gamma_{41}\bar{\kappa}_0\beta_{23}\beta_{26}\begin{bmatrix}-Pe_i\gamma_{38}\left[(2\bar{x}C_2\beta_3+\beta_4\beta_{18})C_1+C_\mu\bar{x}\right]\bar{\kappa}_0{}^2-2C_\mu Pe_i\lambda\bar{x}\gamma_{38}C_1\\+\left[(Pe_i\beta_{12}\beta_4\gamma_{38}-4\chi\bar{x})C_1+Pe_i\bar{x}\right]\bar{\kappa}_0{}^2\end{bmatrix}\end{bmatrix},$$

$$P_2 = \beta_{23}\exp(3\bar{\kappa}_0)\begin{bmatrix}\begin{bmatrix}+192\beta_3\beta_{26}Pe_i\lambda\bar{x}\beta_{23}C_1+48\beta_{23}{}^2\left[\left[\gamma_{62}Pe_i+2(2-C_2\gamma_{46})\bar{x}+\gamma_{63}\right]C_1+Pe_i\gamma_{60}\right]\beta_3\bar{\kappa}_0{}^3\\+96\beta_{29}\bar{x}\beta_{24}\beta_3C_1\bar{\kappa}_0{}^2-48\beta_{23}{}^2\left[\beta_4(2\beta_7+\beta_9+\beta_{10})\beta_{23}+2\bar{x}\lambda C_\mu\right]\gamma_{46}C_1\bar{\kappa}_0\\+144\beta_{10}\beta_{23}{}^3\gamma_{46}C_1\beta_4+96\bar{x}\beta_{25}Pe_i\beta_3(C_\mu-1)\beta_{23}+192\bar{x}\beta_{24}C_1Pe_i\lambda C_\mu\beta_3\end{bmatrix}\\+96\beta_{23}\beta_{26}\begin{bmatrix}-Pe_i\gamma_{38}\left[(2\bar{x}C_2\beta_3+\beta_4\beta_{18})C_1+C_\mu\bar{x}\right]\bar{\kappa}_0{}^2-2C_\mu Pe_i\lambda\bar{x}\gamma_{38}C_1\\+\left[(Pe_i\beta_{12}\beta_4\gamma_{38}-4\chi\bar{x})C_1+Pe_i\bar{x}\right]\bar{\kappa}_0\end{bmatrix}\bar{\kappa}_0\beta_3\end{bmatrix},$$

$$P_3 = -48\beta_{23}\exp(\bar{\kappa}_0)\begin{bmatrix}\begin{bmatrix}4\beta_3\beta_{26}Pe_i\lambda\bar{x}\beta_{23}C_1+\beta_{23}{}^2\beta_3\bar{\kappa}_0{}^3\left[\left[\gamma_{62}Pe_i+2(2-C_2\gamma_{46})\bar{x}+\gamma_{63}\right]C_1+Pe_i\gamma_{60}\right]\\+2\bar{x}\beta_{24}\beta_3C_1\bar{\kappa}_0{}^2(\beta_{23}+2+2Pe_iC_2\beta_3)-\beta_{23}{}^2\gamma_{46}C_1\bar{\kappa}_0\left[\beta_4(2\beta_8+\beta_9-\beta_{10}-2\beta_{11})\beta_{23}+2\bar{x}\lambda C_\mu\right]\\+3\beta_{10}\beta_{23}{}^3\gamma_{46}C_1\beta_4+2\bar{x}\beta_{25}Pe_i\beta_3(C_\mu-1)\beta_{23}+4\bar{x}\beta_{24}C_1Pe_i\lambda C_\mu\beta_3\end{bmatrix}\\+2\bar{\kappa}_0\beta_3\beta_{23}\beta_{26}\begin{bmatrix}-Pe_i\gamma_{38}\left[(2\bar{x}C_2\beta_3+\beta_4\beta_{18})C_1+C_\mu\bar{x}\right]\bar{\kappa}_0{}^2-2C_\mu Pe_i\lambda\bar{x}\gamma_{38}C_1\\+\left[(Pe_i\beta_{12}\beta_4\gamma_{38}-4\chi\bar{x})C_1+Pe_i\bar{x}\right]\bar{\kappa}_0\end{bmatrix}\end{bmatrix},$$

$$P_4 = +\frac{\cosh(\bar{\kappa}_0\bar{y})}{\bar{\kappa}_0{}^2}\begin{bmatrix}-2\beta_{23}\bar{\kappa}_0\beta_3\beta_{26}\begin{bmatrix}-Pe_i\gamma_{38}\left[(2\bar{x}C_2\beta_3+\beta_4\beta_{18})C_1+C_\mu\bar{x}\right]\bar{\kappa}_0{}^2\\+\left[(Pe_i\beta_{12}\beta_4\gamma_{38}-4\chi\bar{x})C_1+Pe_i\bar{x}\right]\bar{\kappa}_0-2C_\mu Pe_i\lambda\bar{x}\gamma_{38}C_1\end{bmatrix}\\-\beta_{23}{}^2\beta_3\bar{\kappa}_0{}^3\left[\left[\gamma_{62}Pe_i+2(2-C_2\gamma_{46})\bar{x}+\gamma_{63}\right]C_1+Pe_i\gamma_{60}\right]-4\bar{x}\beta_{24}C_1Pe_i\lambda C_\mu\beta_3\\-2\beta_{29}\bar{x}\beta_{24}\beta_3C_1\bar{\kappa}_0{}^2-4\beta_3\beta_{26}Pe_i\lambda\bar{x}\beta_{23}C_1+2\beta_{23}{}^2\gamma_{46}C_1\bar{\kappa}_0(2\bar{x}\lambda C_\mu+\beta_9\beta_{23}\beta_4)\\-2\beta_{10}\beta_{23}{}^3\gamma_{46}C_1\beta_4-2\bar{x}\beta_{25}Pe_i\beta_3(C_\mu-1)\beta_{23}\end{bmatrix},$$

$$P_5=\frac{\beta_{23}}{12\bar{\kappa}_0}\begin{bmatrix}12\beta_{10}\beta_{23}^{\,2}\beta_4\gamma_{46}C_1F_4(\bar{y})\bar{\kappa}_0^{\,2}+12\beta_4C_1\gamma_{46}\beta_{23}^{\,2}\beta_7\exp(\bar{\kappa}_0\bar{y})-24\gamma_{41}\beta_{23}\beta_{26}Pe_i\lambda\bar{x}C_1\bar{y}^2\bar{\kappa}_0\\-12C_\mu\lambda\bar{x}\beta_{23}^{\,2}\gamma_{46}\bar{\kappa}_0^{\,2}C_1\bar{y}^2-12\bar{x}\bar{\kappa}_0\gamma_{41}Pe_i\left[\beta_{25}(C_\mu-1)\beta_{23}+2\beta_{24}C_1\lambda C_\mu\right]\bar{y}^2\\-12\beta_{23}\beta_{26}\gamma_{41}\bar{\kappa}_0^{\,2}\bar{y}^2\begin{bmatrix}-Pe_i\gamma_{38}\left[(2\bar{x}C_2\beta_3+\beta_4\beta_{18})C_1+C_\mu\bar{x}\right]\bar{\kappa}_0^{\,2}\\+\left[(Pe_i\beta_{12}\beta_4\gamma_{38}-4\chi\bar{x})C_1+Pe_i\bar{x}\right]\bar{\kappa}_0-2C_\mu Pe_i\lambda\bar{x}\gamma_{38}C_1\end{bmatrix}\\+\beta_{23}^{\,2}\bar{\kappa}_0^{\,4}\begin{bmatrix}-6C_1\bar{y}^2(2\bar{x}\gamma_{46}C_2\beta_3+\gamma_{41}\gamma_{62}Pe_i+4\gamma_{41}\bar{x}+\beta_{18}\beta_4\gamma_{46}+\gamma_{41}\gamma_{63})\\-6\gamma_{41}Pe_i\gamma_{60}\bar{y}^2+C_\mu\bar{x}\gamma_{46}(\bar{y}^4-6\bar{y}^2)\end{bmatrix}\\-2C_1\bar{\kappa}_0^{\,3}\left[\beta_4\beta_{12}\gamma_{46}\beta_{23}^{\,2}(\bar{y}^3-3\bar{y}^2)+6\gamma_{41}\beta_{23}\bar{x}\beta_4\bar{y}^2+12\bar{x}\gamma_{41}\beta_{24}(1+Pe_iC_2\beta_3)\bar{y}^2\right]\end{bmatrix},$$

$$P_6=+\frac{\exp(-2\bar{\kappa}_0)\bar{y}^2}{192\beta_{23}^{\,2}\bar{\kappa}_0^{\,3}\gamma_{46}}\begin{bmatrix}4\bar{\kappa}_0\exp(2\bar{\kappa}_0)\begin{bmatrix}\left[-2\bar{\kappa}_0^{\,4}\gamma_{46}\beta_3C_\varepsilon+6\gamma_{46}\beta_6+144\bar{\kappa}_0^{\,2}\left[8\beta_{23}^{\,2}\beta_{30}+(3\beta_3C_\varepsilon+4\beta_6)\gamma_{46}\right]\right]\\+48\bar{\kappa}_0^{\,2}Pe_i\gamma_{38}\beta_{27}\beta_{23}\gamma_{41}\beta_{26}\end{bmatrix}\\+48\bar{\kappa}_0^{\,2}\beta_3\left[(Pe_i\gamma_{61}+2\gamma_{48})\beta_{23}+2Pe_i\gamma_{38}\beta_{27}\beta_{26}\right]\exp(3\bar{\kappa}_0)+3\gamma_{46}\exp(4\bar{\kappa}_0)\beta_{28}\\-3\left[\left[16\beta_{23}\bar{\kappa}_0^{\,2}\beta_3(Pe_i\gamma_{61}+2\gamma_{48})\exp(\bar{\kappa}_0)+\gamma_{46}\beta_{28}\right]+32\bar{\kappa}_0^{\,2}Pe_i\gamma_{38}\beta_3\beta_{27}\beta_{26}\exp(\bar{\kappa}_0)\right]\end{bmatrix}$$

$$-\frac{1}{48\beta_{23}^{\,2}\bar{\kappa}_0^{\,4}\gamma_{46}}\begin{bmatrix}3\gamma_{46}\beta_{28}\left[\cosh^2(\bar{\kappa}_0\bar{y})+\bar{\kappa}_0^{\,2}\bar{y}^2\right]+48(2\gamma_{38}Pe_i\beta_{26}\beta_{27}+\beta_{23}Pe_i\gamma_{61}+2\gamma_{48}\beta_{23})\bar{\kappa}_0^{\,2}\beta_3\cosh(\bar{\kappa}_0\bar{y})\\+\bar{\kappa}_0^{\,4}\begin{bmatrix}24(2\gamma_{41}\gamma_{48}-\beta_3C_\varepsilon\beta_{13}\gamma_{46}+\gamma_{41}Pe_i\gamma_{61}-2\beta_{14}\beta_6\gamma_{46})\beta_{23}^{\,2}\bar{y}^2\\+2\bar{y}^4\gamma_{46}\beta_6-\bar{y}^4\gamma_{46}C_\varepsilon\beta_3\bar{\kappa}_0^{\,2}+48\beta_{23}\beta_{26}\gamma_{41}\beta_{27}\gamma_{38}Pe_i\bar{y}^2\end{bmatrix}\end{bmatrix}$$

Some of the coefficients of these expressions are presented below while the remaining coefficients are already reported in section F1 of the supplementary material.

$$\beta_{24}=\frac{1}{2}\bar{\kappa}_0+\frac{1}{2}\beta_{23}\beta_{26},\beta_{25}=\bar{\kappa}_0^{\,2}\beta_{26}-2\bar{\kappa}_0\beta_{23}+2\beta_{26},\beta_{26}=\sinh(\bar{\kappa}_0),\beta_{27}=(\beta_3C_\varepsilon\beta_{13}+2\beta_6\beta_{14}),$$

$$\beta_{28}=(\beta_3\bar{\kappa}_0^{\,2}C_\varepsilon+2\beta_6),\beta_{29}=(\beta_{23}+2+2Pe_iC_2\beta_3),\beta_{30}=\begin{pmatrix}-\beta_3C_\varepsilon\beta_{13}\gamma_{46}+\gamma_{41}Pe_i\gamma_{61}\\-2\beta_{14}\beta_6\gamma_{46}+2\gamma_{41}\gamma_{48}\end{pmatrix},$$

$$\gamma_{59}=\gamma_{22}+\gamma_{23}+\gamma_{24}+\gamma_{25}+\gamma_{26}+\gamma_{27}+\gamma_{28}+\gamma_{29}+\gamma_{30}+\gamma_{31},\gamma_{62}=\gamma_{20}+\gamma_{35}+\gamma_{49},\ \gamma_{63}=\gamma_{17}+\gamma_{18},$$

$$\gamma_{60}=\frac{f_1}{2\bar{\kappa}_0^{\,3}}\begin{bmatrix}\exp(\bar{\kappa}_0)(\bar{\kappa}_0^{\,2}-2\bar{\kappa}_0+2)\\-\exp(-\bar{\kappa}_0)(\bar{\kappa}_0^{\,2}+2\bar{\kappa}_0+2)\end{bmatrix}-\frac{f_2}{2\bar{\kappa}_0^{\,3}}\left[\exp(-\bar{\kappa}_0)(\bar{\kappa}_0^{\,2}+2\bar{\kappa}_0+2)-\exp(\bar{\kappa}_0)(\bar{\kappa}_0^{\,2}-2\bar{\kappa}_0+2)\right]$$

$$+\frac{1}{16}\frac{C_{\varepsilon_{eff}}}{\bar{\kappa}_0^{\,3}\beta_{23}}\left[\exp(-\bar{\kappa}_0)(\bar{\kappa}_0^{\,2}+2\bar{\kappa}_0+2)-\exp(\bar{\kappa}_0)(\bar{\kappa}_0^{\,2}-2\bar{\kappa}_0+2)\right]-\frac{C_{\varepsilon_{eff}}(\bar{\kappa}_0^{\,2}\beta_{26}-2\bar{\kappa}_0\beta_{23}+2\beta_{26})}{4\bar{\kappa}_0^{\,3}\beta_{23}}$$

$$+\frac{C_{\varepsilon_{eff}}(\bar{\kappa}_0^{\,3}\beta_{23}-3\bar{\kappa}_0^{\,2}\beta_{26}+6\bar{\kappa}_0\beta_{23}-6\beta_{26})}{2\bar{\kappa}_0^{\,3}\beta_{23}}-\frac{f_1\beta_{26}}{\bar{\kappa}_0}-\frac{f_2\beta_{26}}{\bar{\kappa}_0}+\frac{C_{\varepsilon_{eff}}\gamma_{57}}{4}+\frac{C_{\varepsilon_{eff}}\beta_{26}}{8\bar{\kappa}_0\beta_{23}}-\frac{1}{2}C_{\varepsilon_{eff}}\frac{(\bar{\kappa}_0\beta_{23}-\beta_{26})}{\bar{\kappa}_0\beta_{23}},$$

$$\gamma_{61}=-\beta_3C_\varepsilon\frac{(\beta_{26}\beta_{23}^{\,2}+2\beta_{26})}{6\bar{\kappa}_0\beta_{23}^{\,3}}+\frac{\beta_3C_\varepsilon\beta_{25}}{2\bar{\kappa}_0\beta_{23}^{\,3}}-\lambda(1+\bar{S}_{Tavg})\frac{(\beta_{26}\beta_{23}^{\,2}+2\beta_{26})}{6\beta_{23}^{\,3}\bar{\kappa}_0^{\,3}}-\frac{\lambda(1+\bar{S}_{Tavg})\beta_{25}}{2\bar{\kappa}_0^{\,4}\beta_{23}^{\,3}}$$

Section F2. The coefficients of equation (S44) and equation (S52)

The coefficients of potential distribution described by equation (S44) are as follows

$$f_1(\bar{y})=\left\{-2f_5(\bar{y}+1)\,\bar{\kappa}_0+\bar{S}_{Tavg}+C_\varepsilon+3\right\},\ f_2(\bar{y})=2f_5(\bar{y}+1)\bar{\kappa}_0+\bar{S}_{Tavg}+C_\varepsilon+3,\ f_3(\bar{y})=-1+\bar{\kappa}_0(\bar{y}+1),$$

$$f_4(\bar{y})=1+\bar{\kappa}_0(\bar{y}+1),\ f_5=\left(-C_\varepsilon+1+\bar{S}_{Tavg}\right),\ g_1(\bar{y})=\sinh(\bar{\kappa}_0\,\bar{y})+\cosh(\bar{\kappa}_0\,\bar{y}),$$

$$g_2(\bar{y})=\sinh(2\bar{\kappa}_0\,\bar{y})-\cosh(2\bar{\kappa}_0\,\bar{y}),\ g_3(\bar{y})=\sinh(\bar{\kappa}_0\,\bar{y})\sinh(\bar{\kappa}_0)-\cosh(\bar{\kappa}_0\,\bar{y})\cosh(\bar{\kappa}_0),$$

$$g_4(\bar{y})=\left\{f_5(\bar{y}+2)\,\bar{\kappa}_0-2C_\varepsilon-2\right\}\bar{y},\ g_5(\bar{y})=\left\{f_5(\bar{y}+2)\,\bar{\kappa}_0-\bar{S}_{Tavg}+3C_\varepsilon+1\right\}\bar{y},$$

$$c_1=c_{1part1}+c_{1part2}+c_{1part3},\ c_{1part1}=\frac{\bar{S}_{Tavg}\left[\left\{1-(4\bar{\kappa}_0+1)\alpha_{40}{}^4\right\}+\left\{1+(4\bar{\kappa}_0+1)\alpha_{40}{}^4\right\}\tanh(2\bar{\kappa}_0)\right]}{32\bar{\kappa}_0\,\alpha_{37}\,\alpha_{40}{}^2\tanh(2\bar{\kappa}_0)},$$

$$c_{1part2}=\frac{\Delta\bar{S}_T}{16\bar{\kappa}_0\,\alpha_{37}\,\alpha_{40}{}^2}\left[\left\{-1+\alpha_{40}{}^2\left\{2\bar{\kappa}_0-2-(2\bar{\kappa}_0+1)\alpha_{40}{}^2\right\}\right\}+\left\{-1+\alpha_{40}{}^2\left\{2\bar{\kappa}_0+(2\bar{\kappa}_0+1)\alpha_{40}{}^2\right\}\right\}\frac{\alpha_{37}{}^2}{\alpha_{45}\,\alpha_{40}{}^2}\right],$$

$$c_{1part3}=\frac{\left\{C_\varepsilon(2\bar{\kappa}_0+1)-\bar{S}_{Tavg}(2\bar{\kappa}_0-1)-(2\bar{\kappa}_0-3)\right\}}{16\alpha_{37}\,\bar{\kappa}_0}+\frac{\left[\begin{array}{l}C_\varepsilon\left\{1+(4\bar{\kappa}_0-1)\alpha_{40}{}^4\right\}\\+\left\{3-(4\bar{\kappa}_0+3)\alpha_{40}{}^4\right\}\end{array}\right]}{32\alpha_{37}\,\bar{\kappa}_0\tanh(2\bar{\kappa}_0)\,\alpha_{40}{}^2}+\frac{\left[\begin{array}{l}C_\varepsilon\left\{1-(4\bar{\kappa}_0-1)\alpha_{40}{}^4\right\}\\+\left\{3+(4\bar{\kappa}_0+3)\alpha_{40}{}^4\right\}\end{array}\right]}{32\alpha_{37}\,\bar{\kappa}_0\,\alpha_{40}{}^2}$$

$$+\frac{1}{96\alpha_{37}\,\alpha_{35}\,\alpha_{40}{}^2}\left[\begin{array}{l}\bar{S}_{Tavg}\left\{\bar{\kappa}_0\left(3+\alpha_{40}{}^4\right)-6\alpha_{40}{}^2\left(2\alpha_{37}{}^2+2\bar{\kappa}_0-1\right)\right\}\\+3\left\{(\bar{\kappa}_0-2)-\alpha_{40}{}^2\left\{4\alpha_{37}{}^2+4\bar{\kappa}_0+2+(2-3\bar{\kappa}_0)\alpha_{40}{}^2\right\}\right\}\\-3C_\varepsilon\left\{(\bar{\kappa}_0+2)-\alpha_{40}{}^2\left\{4\alpha_{37}{}^2+4\bar{\kappa}_0-6-(3\bar{\kappa}_0+2)\alpha_{40}{}^2\right\}\right\}\end{array}\right],$$

$$c_2=c_{2part1}+c_{2part2}+c_{2part3}+c_{2part4},\ c_{2part1}=\frac{4\bar{\kappa}_0-3}{32\alpha_{38}\,\bar{\kappa}_0\,\alpha_{40}{}^2}+\frac{1}{32\alpha_{37}\,\alpha_{45}}\left(\frac{3\bar{\kappa}_0+1}{\alpha_{40}{}^2}-4\bar{\kappa}_0+4\right),$$

$$c_{2part2}=\frac{4\bar{\kappa}_0-3}{32\alpha_{37}\,\bar{\kappa}_0\,\alpha_{40}{}^2},c_{2part3}=-\frac{1}{32\alpha_{37}\,\alpha_{45}\,\bar{\kappa}_0}\left[\left\{3\left(\alpha_{45}-\alpha_{37}{}^2\right)-\bar{\kappa}_0(\bar{\kappa}_0+1)\exp(2\bar{\kappa}_0)\right\}\right],$$

$$c_{2part4}=\frac{\left(1+\bar{S}_{Tavg}-C_\varepsilon\right)}{8\alpha_{37}\tanh(2\bar{\kappa}_0)}+\frac{1}{16\bar{\kappa}_0\,\alpha_{37}}\left\{C_\varepsilon(2\bar{\kappa}_0-1)-\bar{S}_{Tavg}(2\bar{\kappa}_0+1)-(2\bar{\kappa}_0+3)\right\}$$

$$+\frac{C_\varepsilon}{32\alpha_{37}\,\alpha_{45}\,\bar{\kappa}_0\,\alpha_{40}{}^2}\left[\begin{array}{l}\alpha_{40}{}^2\left\{\bar{\kappa}_0(3\bar{\kappa}_0+2)\alpha_{40}{}^2-(4\bar{\kappa}_0+1)\left(\alpha_{37}{}^2+\alpha_{45}\right)\right\}-3\bar{\kappa}_0(\bar{\kappa}_0-1)\\+\left\{\bar{\kappa}_0(\bar{\kappa}_0+2)+\alpha_{40}{}^2\left\{\alpha_{37}{}^2-\alpha_{45}-\bar{\kappa}_0(\bar{\kappa}_0-3)\right\}\right\}\alpha_{40}{}^2\end{array}\right]$$

$$-\frac{\Delta\bar{S}_T}{16\alpha_{37}\,\alpha_{45}\,\bar{\kappa}_0\,\alpha_{40}{}^2}\left[\left(\alpha_{37}{}^2+\alpha_{45}\right)(2\bar{\kappa}_0-1)+2\left\{\alpha_{37}\,\bar{\kappa}_0-\alpha_{38}(\bar{\kappa}_0+1)\right\}\alpha_{37}\,\alpha_{40}{}^2-\left(\alpha_{45}-\alpha_{37}{}^2\right)\alpha_{40}{}^4\right]$$

$$+\frac{\bar{S}_{Tavg}}{32\alpha_{37}\,\alpha_{45}\,\bar{\kappa}_0\,\alpha_{40}{}^2}\left[\left\{\begin{array}{l}(4\bar{\kappa}_0-1)\left(\alpha_{37}{}^2+\alpha_{45}\right)\\\left(3\bar{\kappa}_0-1-3\bar{\kappa}_0\,\alpha_{40}{}^2\right)\bar{\kappa}_0\end{array}\right\}-\left\{\frac{\bar{\kappa}_0{}^2}{\alpha_{40}{}^2}-\alpha_{37}{}^2+\alpha_{45}-\bar{\kappa}_0(\bar{\kappa}_0-1)\alpha_{40}{}^4\right\}\right]$$

Coefficients involved in the expressions of steaming potential (equation (S52)) are shown below

$$\alpha_1 = 4\bar{S}_{Tavg}, \alpha_2 = 2\chi\,\Delta\bar{S}_T, \alpha_3 = -4\chi\,\frac{\alpha_{39}}{\bar{\kappa}_0}, \alpha_4 = -\alpha_3, \alpha_5 = -\frac{4\alpha_{39}}{\bar{\kappa}_0}, \alpha_6 = -\frac{2}{3}Pe_i\,\Delta\bar{S}_T\,\frac{\partial\bar{p}_0}{\partial\bar{x}}, \alpha_7 = \frac{2Pe_i\,\Delta\bar{S}_T\lambda}{\bar{\kappa}_0^{\,3}}\left(\alpha_{39}-\bar{\kappa}_0\right),$$

$$\alpha_8 = -\frac{4Pe_i}{\bar{\kappa}_0^{\,4}}\frac{\partial\bar{p}_0}{\partial\bar{x}}\left(\alpha_{39}-\bar{\kappa}_0\right), \alpha_9 = -\frac{2Pe_i\,\lambda}{\bar{\kappa}_0^{\,2}\alpha_{37}^{\,2}} + \frac{2Pe_i\,\lambda\,\alpha_{39}}{\bar{\kappa}_0^{\,3}}, \alpha_{10} = 2\chi I_1, \alpha_{25} = \frac{2\lambda Pe_i}{a_{37}},$$

$$\alpha_{11} = \frac{\lambda Pe_i\,\alpha_{40}}{64\alpha_{42}\,\alpha_{45}}\left[-16\,\Delta\bar{S}_T\,\alpha_{42} + \left\{\bar{S}_{Tavg}\left(40\bar{\kappa}_0^{\,2}-18\bar{\kappa}_0+1\right)+\left(40\bar{\kappa}_0^{\,2}-18\bar{\kappa}_0+3\right)-C_\varepsilon\left(40\bar{\kappa}_0^{\,2}-18\bar{\kappa}_0-1\right)\right\}\alpha_{43}\right],$$

$$\alpha_{12} = \frac{Pe_i\lambda}{64\alpha_{40}\,\alpha_{42}\,\alpha_{45}}\left[\left\{16\Delta\bar{S}_T + \frac{\left(40\bar{\kappa}_0^{\,2}+18\bar{\kappa}_0-3\right)\alpha_{43}}{\bar{\kappa}_0^{\,5}\,\alpha_{37}^{\,3}}\right\}\alpha_{42} + \left\{\left(40\bar{\kappa}_0^{\,2}+18\bar{\kappa}_0-1\right)\bar{S}_{Tavg} - \left(40\bar{\kappa}_0^{\,2}+18\bar{\kappa}_0+1\right)C_\varepsilon\right\}\alpha_{43}\right],$$

$$\alpha_{13} = -\frac{Pe_i\,\lambda\,\alpha_{40}^{\,2}\,C_5}{4\alpha_{43}}, \alpha_{14} = \frac{Pe_i\,\lambda\,C_5}{4\alpha_{40}^{\,2}\,\alpha_{43}}, \alpha_{17} = -\frac{Pe_i\,\lambda\,\alpha_{40}^{\,4}C_5}{8\alpha_{43}}, \alpha_{18} = \frac{\lambda\,Pe_i\,C_5}{8\alpha_{40}^{\,4}\,\alpha_{43}}, \alpha_{24} = \frac{2\,Pe_i\,\lambda}{\alpha_{37}\,\alpha_{41}}\left(\bar{\kappa}_0+\alpha_{38}\,\alpha_{37}\right),$$

$$\alpha_{15} = \left(Pe_i\lambda\alpha_{40}^{\,3}/64\alpha_{42}\alpha_{43}\right)\left[-16\,\Delta\bar{S}_T\,\alpha_{42} - \left(8\bar{\kappa}_0^{\,2}-18\bar{\kappa}_0-1\right)C_\varepsilon\,\alpha_{43} + \left(8\bar{\kappa}_0^{\,2}-18\bar{\kappa}_0+1\right)\bar{S}_{Tavg}\,\alpha_{43} + \left(8\bar{\kappa}_0^{\,2}-18\bar{\kappa}_0+3\right)\alpha_{43}\right],$$

$$\alpha_{16} = \frac{Pe_i\,\lambda}{64\alpha_{40}^{\,3}\,\alpha_{42}\,\alpha_{43}}\left[16\,\Delta\bar{S}_T\,\alpha_{42} - \frac{\left(8\bar{\kappa}_0^{\,2}+18\bar{\kappa}_0+1\right)C_\varepsilon\,\alpha_{43}\,\alpha_{42}}{\bar{\kappa}_0^{\,5}\,\alpha_{37}^{\,3}} + \left(8\bar{\kappa}_0^{\,2}+18\bar{\kappa}_0-1\right)\bar{S}_{Tavg}\,\alpha_{43} + \left(8\bar{\kappa}_0^{\,2}+18\bar{\kappa}_0-3\right)\alpha_{43}\right],$$

$$\alpha_{19} = \left(Pe_i\,\lambda/8\bar{\kappa}_0^{\,3}\,\alpha_{37}^{\,2}\right)\left[16\alpha_{37}\,\bar{\kappa}_0\left(C_5+\Delta\bar{S}_T\,\alpha_{37}\right) - C_\varepsilon\left(6\bar{\kappa}_0+1\right)+\bar{S}_{Tavg}\left(6\bar{\kappa}_0-1\right)+3\left(2\bar{\kappa}_0-1\right)\right],$$

$$\alpha_{21} = \frac{Pe_i}{6\bar{\kappa}_0^{\,2}\,\alpha_{37}^{\,3}}\frac{\partial\bar{p}_0}{\partial\bar{x}}\left(-9C_5+4\Delta\bar{S}_T\,\bar{\kappa}_0^{\,2}\alpha_{37}^{\,3}\right), \alpha_{22} = 2\frac{Pe_i}{\alpha_{37}}\frac{\partial\bar{p}_0}{\partial\bar{x}}\frac{C_\mu}{\bar{\kappa}_0^{\,3}}\left(\bar{\kappa}_0^{\,2}\alpha_{38}-2\bar{\kappa}_0\,\alpha_{37}+2\alpha_{38}\right), \alpha_{26} = -\frac{5\,Pe_i\,C_\mu}{3\alpha_{37}}\left(\frac{\partial\bar{p}_0}{\partial\bar{x}}\right),$$

$$\alpha_{28} = -\frac{2\,\lambda\,Pe_i}{\bar{\kappa}_0^{\,2}\alpha_{37}}, \alpha_{29} = \alpha_{27} - \frac{2Pe_i}{\alpha_{37}}\left(\lambda\,I_7+C_{u1}\right), I_1 = \frac{\left(C_\varepsilon\,\alpha_{33}+\bar{S}_{Tavg}\,\alpha_{34}-16\,\Delta\bar{S}_T\,\alpha_{40}\,\alpha_{37}\,\bar{\kappa}_0^{\,2}+C_5\,\alpha_{35}+\alpha_{36}\right)}{16\alpha_{40}\,\alpha_{37}\,\bar{\kappa}_0^{\,2}},$$

$$\alpha_{20} = \frac{\alpha_{40}\,Pe_i}{32\,\alpha_{42}}\left(\frac{\partial\bar{p}_0}{\partial\bar{x}}\right)\left[\left(-8\bar{\kappa}_0^{\,3}+90\bar{\kappa}_0^{\,2}-27\bar{\kappa}_0-1\right)C_\varepsilon + \left(8\bar{\kappa}_0^{\,3}-90\bar{\kappa}_0^{\,2}+33\bar{\kappa}_0-1\right)\bar{S}_{Tavg} + \left(8\bar{\kappa}_0^{\,3}-90\bar{\kappa}_0^{\,2}+39\bar{\kappa}_0-3\right)\right]$$

$$+\frac{Pe_i}{32\,\alpha_{40}\,\alpha_{42}}\left(\frac{\partial\bar{p}_0}{\partial\bar{x}}\right)\left[\left(8\bar{\kappa}_0^{\,3}+90\bar{\kappa}_0^{\,2}+33\bar{\kappa}_0+1\right)C_\varepsilon - \left(8\bar{\kappa}_0^{\,3}+90\bar{\kappa}_0^{\,2}+27\bar{\kappa}_0-1\right)\bar{S}_{Tavg} - \left(8\bar{\kappa}_0^{\,3}+90\bar{\kappa}_0^{\,2}+21\bar{\kappa}_0-3\right)\right]$$

$$-\frac{Pe_i\,\alpha_{40}^{\,2}\,C_5}{2\alpha_{43}}\frac{\partial\bar{p}_0}{\partial\bar{x}}\left(2\bar{\kappa}_0-1\right) - \frac{Pe_i\,C_5}{2\alpha_{43}\,\alpha_{40}^{\,2}}\frac{\partial\bar{p}_0}{\partial\bar{x}}\left(2\bar{\kappa}_0+1\right) - \frac{Pe_i\,C_5\,\alpha_{40}^{\,4}}{4\alpha_{43}}\left(\bar{\kappa}_0-1\right)\frac{\partial\bar{p}_0}{\partial\bar{x}} - Pe_i\,\frac{\exp\left(-4\bar{\kappa}_0\right)}{4\alpha_{43}}\left(\bar{\kappa}_0+1\right)\frac{\partial\bar{p}_0}{\partial\bar{x}}C_5$$

$$-\frac{Pe_i\,\alpha_{40}^{\,3}}{32\,\alpha_{42}}\left(\frac{\partial\bar{p}_0}{\partial\bar{x}}\right)\left[\left(8\bar{\kappa}_0^{\,3}+30\bar{\kappa}_0^{\,2}+29\bar{\kappa}_0+1\right)C_\varepsilon - \left(8\bar{\kappa}_0^{\,3}-30\bar{\kappa}_0^{\,2}+31\bar{\kappa}_0-1\right)\bar{S}_{Tavg} - \left(8\bar{\kappa}_0^{\,3}-30\bar{\kappa}_0^{\,2}+33\bar{\kappa}_0-3\right)\right]$$

$$+\frac{Pe_i}{32\,\alpha_{42}\,\alpha_{40}^{\,3}}\left(\frac{\partial\bar{p}_0}{\partial\bar{x}}\right)\left[\left(8\bar{\kappa}_0^{\,3}+30\bar{\kappa}_0^{\,2}+31\bar{\kappa}_0+1\right)C_\varepsilon - \left(8\bar{\kappa}_0^{\,3}+30\bar{\kappa}_0^{\,2}+29\bar{\kappa}_0-1\right)\bar{S}_{Tavg} - \left(8\bar{\kappa}_0^{\,3}+30\bar{\kappa}_0^{\,2}+27\bar{\kappa}_0-3\right)\right],$$

$$\alpha_{23} = \frac{2\,Pe_i\,\lambda}{\alpha_{37}\,\alpha_{41}}\left[\left(C_\mu-C_\varepsilon\right)\left(\bar{\kappa}_0+\alpha_{37}\,\alpha_{38}\right)+\bar{S}_{Tavg}\left(\bar{\kappa}_0+\alpha_{37}\,\alpha_{38}\right)+\frac{\chi\,\Delta\bar{S}_T\,\alpha_{41}}{2\bar{\kappa}_0^{\,3}\lambda}\left(\bar{\kappa}_0^{\,2}\,\alpha_{38}-2\bar{\kappa}_0\,\alpha_{37}+2\alpha_{38}\right)+C_{\varepsilon eff}\left(\bar{\kappa}_0+\alpha_{37}\,\alpha_{38}\right)\right],$$

$$\alpha_{27} = \frac{2\,Pe_i\,\lambda}{\alpha_{37}\,\bar{\kappa}_0^{\,3}}\left[\left(C_\mu-C_\varepsilon\right)\left(2\bar{\kappa}_0-\alpha_{39}\right)-2\,\bar{S}_{Tavg}\left(\bar{\kappa}_0-\alpha_{39}\right)-\frac{1}{3}\Delta\bar{S}_T\,\bar{\kappa}_0-C_{\varepsilon eff}\,\bar{\kappa}_0\right], \alpha_{31} = \alpha_4+\alpha_{24}+\alpha_{28},$$

$$\alpha_{30} = \begin{bmatrix}\alpha_1+\alpha_2+\alpha_3+\alpha_5+\alpha_7+\alpha_9+\alpha_{10}+\left(\alpha_{23}+\alpha_{25}\,I_9\right)+\alpha_{29}\\ +\left(\alpha_{11}+\alpha_{12}+\alpha_{13}+\alpha_{14}+\alpha_{15}+\alpha_{16}+\alpha_{17}+\alpha_{18}+\alpha_{19}\right)\end{bmatrix}, a_{32} = \alpha_6+\alpha_8+\alpha_{20}+\alpha_{21}+\alpha_{22}+\alpha_{26}, C_5 = c_1+c_2,$$

$$\alpha_{33}=4\bar{\kappa}_0\,{\alpha_{40}}^2\left(2\bar{\kappa}_0-7\right)+4\bar{\kappa}_0\left(2\bar{\kappa}_0+7\right)-{\alpha_{40}}^2+1,\alpha_{45}=\alpha_{37}\,\alpha_{38},\alpha_{34}=-8{\bar{\kappa}_0}^2\left({\alpha_{40}}^2+1\right)+\left(14\bar{\kappa}_0-1\right)\left({\alpha_{40}}^2-1\right),$$

$$\alpha_{35}=16\alpha_{37}\,\bar{\kappa}_0\left({\alpha_{40}}^2-1\right),\alpha_{36}=-8{\bar{\kappa}_0}^2\left({\alpha_{40}}^2+1\right)+\left({\alpha_{40}}^2-1\right)\left(14\bar{\kappa}_0-3\right),\alpha_{37}=\cosh\left(\bar{\kappa}_0\right),\alpha_{38}=\sinh\left(\bar{\kappa}_0\right),$$

$$\alpha_{39}=\tanh\left(\bar{\kappa}_0\right),\alpha_{40}=\exp\left(\bar{\kappa}_0\right),\alpha_{41}={\bar{\kappa}_0}^3\,\alpha_{37},\alpha_{42}={\bar{\kappa}_0}^4\,{\alpha_{37}}^3,\alpha_{43}={\bar{\kappa}_0}^3\,{\alpha_{37}}^3,\alpha_{44}={\bar{\kappa}_0}^4\,\alpha_{37},C_{\varepsilon eff}=\left\{C_\varepsilon-\left(1+\bar{S}_{Tavg}\right)\right\},$$

$$I_7=\frac{\left\{-\left(3\bar{\kappa}_0+5\right)C_\varepsilon\,\bar{\kappa}_0+\left(3{\bar{\kappa}_0}^2+7\bar{\kappa}_0+4\right)\bar{S}_{Tavg}+\left(8c_2\,\alpha_{41}/{\bar{\kappa}_0}^2\right)+\left(3{\bar{\kappa}_0}^2+9\bar{\kappa}_0+8\right)\right\}}{8\alpha_{40}\,\alpha_{41}}+\left\{\begin{matrix}\left(12\bar{\kappa}_0+1\right)\alpha_{37}\\-\left(4\bar{\kappa}_0+15\right)\alpha_{38}\end{matrix}\right\}\Big/\left(16\alpha_{41}\right)-\frac{\Delta\bar{S}_T}{3}$$

$$+\left(\frac{\alpha_{40}}{8\alpha_{41}}\right)\left\{\begin{matrix}\left(3{\bar{\kappa}_0}^2-6\bar{\kappa}_0+2\right)C_\varepsilon-\left(3{\bar{\kappa}_0}^2-8\bar{\kappa}_0+6\right)\bar{S}_{Tavg}\\+\left(8c_1\,\alpha_{41}/{\bar{\kappa}_0}^2\right)-\left(3{\bar{\kappa}_0}^2-10\bar{\kappa}_0+10\right)\end{matrix}\right\}+\left\{\begin{matrix}\left(4\bar{\kappa}_0+11\right)\alpha_{38}\\-\left(12\bar{\kappa}_0+5\right)\alpha_{37}\end{matrix}\right\}\left(\frac{C_\varepsilon}{16\alpha_{41}}\right)+\left\{\begin{matrix}3\left(4\bar{\kappa}_0+11\right)\alpha_{37}\\-\left(4\bar{\kappa}_0+5\right)\alpha_{38}\end{matrix}\right\}\left(\frac{\bar{S}_{Tavg}}{16\alpha_{41}}\right),$$

$$C_{u1}=\left[\begin{matrix}\left\{-\left(2{\bar{\kappa}_0}^2+7\bar{\kappa}_0+10\right)\exp\left(-\bar{\kappa}_0\right)+\left(2{\bar{\kappa}_0}^2-7\bar{\kappa}_0+10\right)\alpha_{40}-6\bar{\kappa}_0\,\alpha_{37}+\left(2\bar{\kappa}_0+13\right)\alpha_{38}\right\}\bar{S}_{Tavg}\\+16\left(\alpha_{38}-\bar{\kappa}_0\,\alpha_{37}\right)C_\mu\,\alpha_{40}+16\alpha_{37}\,\bar{\kappa}_0\,\alpha_{38}\left(c_2-c_1\right)\alpha_{40}\\+\left\{\left(2{\bar{\kappa}_0}^2+3\bar{\kappa}_0+2\right)-\left(2{\bar{\kappa}_0}^2-3\bar{\kappa}_0+2\right){\alpha_{40}}^2+6\alpha_{37}\,\bar{\kappa}_0\,\alpha_{40}-\left(18\bar{\kappa}_0-5\right)\alpha_{38}\,\alpha_{40}\right\}C_\varepsilon\\+\left\{-\left(2{\bar{\kappa}_0}^2+11\bar{\kappa}_0+8\right)+\left(2{\bar{\kappa}_0}^2-11\bar{\kappa}_0+18\right){\alpha_{40}}^2+10\alpha_{37}\,\bar{\kappa}_0\,\alpha_{40}-\left(14\bar{\kappa}_0+17\right)\alpha_{38}\,\alpha_{40}\right\}\end{matrix}\right]\frac{\bar{E}_{x0}\,\lambda}{16\alpha_{40}\,\alpha_{41}}-\frac{C_\mu}{3}\left(\frac{\partial\bar{p}_0}{\partial\bar{x}}\right),$$

$$I_9=\left(\frac{C_5}{{\bar{\kappa}_0}^2}\right)+\frac{C_5\left\{\alpha_{38}+\sinh\left(3\bar{\kappa}_0\right)\right\}}{4\alpha_{41}}+\frac{1}{2}\frac{\Delta\bar{S}_T}{{\bar{\kappa}_0}^2\,\alpha_{37}}+\frac{\left\{\left(22\bar{\kappa}_0-3\right)+\left(22\bar{\kappa}_0-1\right)\bar{S}_{Tavg}-\left(22\bar{\kappa}_0+1\right)C_\varepsilon\right\}}{16\alpha_{41}}$$

$$+\left[8\Delta\bar{S}_T\,\bar{\kappa}_0\left({\bar{\kappa}_0}^2+2\bar{\kappa}_0+2\right)+C_\varepsilon\left(8{\bar{\kappa}_0}^2+26\bar{\kappa}_0+1\right)-\bar{S}_{Tavg}\left(8{\bar{\kappa}_0}^2+26\bar{\kappa}_0-1\right)-\left(8{\bar{\kappa}_0}^2+26\bar{\kappa}_0-3\right)\right]\left(\frac{1}{64{\alpha_{40}}^2\alpha_{44}}\right)$$

$$-\left[8\Delta\bar{S}_T\,\bar{\kappa}_0\left({\bar{\kappa}_0}^2-2\bar{\kappa}_0+2\right)-C_\varepsilon\left(8{\bar{\kappa}_0}^2-26\bar{\kappa}_0-1\right)+\bar{S}_{Tavg}\left(8{\bar{\kappa}_0}^2-26\bar{\kappa}_0+1\right)+\left(8{\bar{\kappa}_0}^2-26\bar{\kappa}_0+3\right)\right]\left({\alpha_{40}}^2/64\alpha_{44}\right),$$

$$I_6=\left[\left\{\begin{matrix}-\bar{y}\left(\bar{y}+2\right){\bar{\kappa}_0}^2\\-\left(\bar{y}+4\right)\bar{\kappa}_0\end{matrix}\right\}C_\varepsilon+\left\{\begin{matrix}\bar{y}\left(\bar{y}+2\right){\bar{\kappa}_0}^2\\+\left(3\bar{y}+4\right)\bar{\kappa}_0+4\end{matrix}\right\}\bar{S}_{Tavg}+\left(\frac{8\alpha_{41}C2}{{\bar{\kappa}_0}^2}\right)+\left\{\begin{matrix}\bar{y}\left(\bar{y}+2\right){\bar{\kappa}_0}^2\\+\left(5\bar{y}+4\right)\bar{\kappa}_0+8\end{matrix}\right\}\right]\left\{\frac{\exp\left(-\bar{\kappa}_0\bar{y}\right)}{8\alpha_{41}}\right\}$$

$$+\left[\left\{\begin{matrix}\bar{y}\left(\bar{y}+2\right){\bar{\kappa}_0}^2\\-2\left(\bar{y}+2\right)\bar{\kappa}_0+2\end{matrix}\right\}C_\varepsilon+\left\{\begin{matrix}-\bar{y}\left(\bar{y}+2\right){\bar{\kappa}_0}^2\\+4\left(\bar{y}+1\right)\bar{\kappa}_0-6\end{matrix}\right\}\bar{S}_{Tavg}+\left(\frac{8\alpha_{41}C1}{{\bar{\kappa}_0}^2}\right)+\left\{\begin{matrix}-\bar{y}\left(\bar{y}+2\right)\bar{\kappa}_0^2\\+\left(6\bar{y}+4\right)\bar{\kappa}_0-10\end{matrix}\right\}\right]\left\{\frac{\exp\left(\bar{\kappa}_0\,\bar{y}\right)}{8\alpha_{41}}\right\}$$

$$-\frac{1}{12}\bar{y}^3\left(\bar{y}+3\right)\Delta\bar{S}_T-\left[\left\{6\left(\bar{y}+1\right)\bar{\kappa}_0+5\right\}\cosh\left(\bar{\kappa}_0\,\bar{y}\right)-\left\{2\left(\bar{y}+1\right)\bar{\kappa}_0+11\right\}\sinh\left(\bar{\kappa}_0\,\bar{y}\right)\right]\left(\frac{C_\varepsilon}{16\alpha_{41}}\right)$$

$$+\left[\begin{matrix}\left\{6\left(\bar{y}+1\right)\bar{\kappa}_0+3\right\}\cosh\left(\bar{\kappa}_0\,\bar{y}\right)\\-\left\{2\left(\bar{y}+1\right)\bar{\kappa}_0+13\right\}\sinh\left(\bar{\kappa}_0\,\bar{y}\right)\end{matrix}\right]\left(\frac{\bar{S}_{Tavg}}{16\alpha_{41}}\right)+\left[\begin{matrix}\left\{6\left(\bar{y}+1\right)\bar{\kappa}_0+1\right\}\cosh\left(\bar{\kappa}_0\,\bar{y}\right)\\-\left\{2\left(\bar{y}+1\right)\bar{\kappa}_0+15\right\}\sinh\left(\bar{\kappa}_0\,\bar{y}\right)\end{matrix}\right]\left(\frac{1}{16\alpha_{41}}\right)$$

Section F3. Coefficients of the cubic equation for determining $\bar{E}_{x0}$ in viscoelastic fluids

For axial temperature gradient, coefficients of the cubic equation $A{\bar{E}_{x0}}^3+B{\bar{E}_{x0}}^2+C\,\bar{E}_{x0}+D=0$ involved in the estimation of $\bar{E}_{x0}$ (evaluated at $C_D = 0$) are given below

$$A=-\left[\begin{array}{l}32\left\{\cosh^2\left(\bar{\kappa}_0\right)-3\right\}\cosh\left(\bar{\kappa}_0\right)\left\{\exp\left(5\bar{\kappa}_0\right)-\exp\left(3\bar{\kappa}_0\right)\right\}\\-\left[16\exp\left(2\bar{\kappa}_0\right)-72\bar{\kappa}_0\exp\left(4\bar{\kappa}_0\right)-16\exp\left(6\bar{\kappa}_0\right)+\left\{\exp\left(8\bar{\kappa}_0\right)-1\right\}\right]\end{array}\right]\frac{\delta\lambda^3 Pe_i\exp\left(-4\bar{\kappa}_0\right)De^2}{48\bar{\kappa}_0{}^7\cosh^4\left(\bar{\kappa}_0\right)},$$

$$B=-\left[\begin{array}{l}9\left\{4\cosh^2\left(\bar{\kappa}_0\right)-8\bar{\kappa}_0\sinh\left(\bar{\kappa}_0\right)\cosh\left(\bar{\kappa}_0\right)-\left(10\bar{\kappa}_0+13\right)\right\}\exp\left(3\bar{\kappa}_0\right)\\-9\left\{4\cosh^2\left(\bar{\kappa}_0\right)-8\bar{\kappa}_0\sinh\left(\bar{\kappa}_0\right)\cosh\left(\bar{\kappa}_0\right)+\left(10\bar{\kappa}_0-13\right)\right\}\exp\left(5\bar{\kappa}_0\right)\\-\left\{\left(6\bar{\kappa}_0-5\right)\exp\left(7\bar{\kappa}_0\right)+\exp\left(\bar{\kappa}_0\right)\left(6\bar{\kappa}_0+5\right)\right\}\end{array}\right]\frac{\delta\lambda^2 Pe_i\exp(-4\bar{\kappa}_0)De^2}{24\bar{\kappa}_0{}^7\cosh^3\left(\bar{\kappa}_0\right)}\left(\frac{\partial\bar{p}_0}{\partial\bar{x}}\right),$$

$$C=-\left[\begin{array}{l}4\left[\left\{6\left(\bar{\kappa}_0{}^2+2\right)\cosh\left(\bar{\kappa}_0\right)-12\bar{\kappa}_0\sinh\left(\bar{\kappa}_0\right)\right\}\left\{\exp\left(5\bar{\kappa}_0\right)-\exp\left(3\bar{\kappa}_0\right)\right\}\right]\\-\left[\begin{array}{l}-3\left(2\bar{\kappa}_0{}^2+6\bar{\kappa}_0+7\right)\exp\left(2\bar{\kappa}_0\right)+8\left(\bar{\kappa}_0{}^2+6\right)\bar{\kappa}_0\exp\left(4\bar{\kappa}_0\right)\\+3\left(2\bar{\kappa}_0{}^2-6\bar{\kappa}_0+7\right)\exp\left(6\bar{\kappa}_0\right)\end{array}\right]\end{array}\right]\frac{\delta\lambda Pe_i\exp\left(-4\bar{\kappa}_0\right)De^2}{4\bar{\kappa}_0{}^7\cosh^2\left(\bar{\kappa}_0\right)}\left(\frac{\partial\bar{p}_0}{\partial\bar{x}}\right)^2$$

$$+\frac{1}{8\bar{\kappa}_0{}^7\cosh^2\left(\bar{\kappa}_0\right)}\left[\begin{array}{l}-2\lambda Pe_i\exp\left(-4\bar{\kappa}_0\right)\left[\begin{array}{l}4\bar{\kappa}_0{}^4\cosh\left(\bar{\kappa}_0\right)\left\{\exp\left(5\bar{\kappa}_0\right)-\exp\left(3\bar{\kappa}_0\right)\right\}-4\bar{\kappa}_0{}^5\exp\left(4\bar{\kappa}_0\right)\\+\bar{\kappa}_0{}^4\left\{\exp\left(6\bar{\kappa}_0\right)-\exp\left(2\bar{\kappa}_0\right)\right\}\exp\left(6\bar{\kappa}_0\right)\end{array}\right]\\-\bar{\kappa}_0{}^6\left[\begin{array}{l}4\exp\left(2\bar{\kappa}_0\right)\left\{\bar{\kappa}_0\exp\left(-2\bar{\kappa}_0\right)-2\cosh\left(\bar{\kappa}_0\right)\exp\left(-\bar{\kappa}_0\right)\chi\right\}+16\bar{\kappa}_0\cosh^2\left(\bar{\kappa}_0\right)\\+8\chi\cosh\left(\bar{\kappa}_0\right)\exp\left(-\bar{\kappa}_0\right)+\exp\left(-2\bar{\kappa}_0\right)\left\{\exp\left(4\bar{\kappa}_0\right)-1\right\}\end{array}\right]\end{array}\right],$$

$$D=-\left[\left(\bar{\kappa}_0{}^3+3\bar{\kappa}_0{}^2+6\bar{\kappa}_0+6\right)\exp\left(3\bar{\kappa}_0\right)+\left(\bar{\kappa}_0{}^3-3\bar{\kappa}_0{}^2+6\bar{\kappa}_0-6\right)\exp\left(5\bar{\kappa}_0\right)\right]\frac{2\delta Pe_i\exp\left(-4\bar{\kappa}_0\right)De^2}{\bar{\kappa}_0{}^7\cosh\left(\bar{\kappa}_0\right)}\left(\frac{\partial\bar{p}_0}{\partial\bar{x}}\right)^3$$

$$-\left[\bar{\kappa}_0{}^4\left(\bar{\kappa}_0+1\right)\exp\left(3\bar{\kappa}_0\right)+\bar{\kappa}_0{}^4\left(\bar{\kappa}_0-1\right)\exp\left(5\bar{\kappa}_0\right)\right]\frac{Pe_i\exp\left(-4\bar{\kappa}_0\right)}{\bar{\kappa}_0{}^7\cosh\left(\bar{\kappa}_0\right)}\left(\frac{\partial\bar{p}_0}{\partial\bar{x}}\right)$$

REFERENCES

AFONSO, A. M., ALVES, M. A., & PINHO, F. T. (2009). Analytical solution of mixed electro-osmotic/pressure driven flows of viscoelastic fluids in microchannels. *Journal of Non-Newtonian Fluid Mechanics*, **159**(1–3), 50–63.

AGAR, J. N., MOU, C. Y., & LIN, J. L. (1989). Single-ion heat of transport in electrolyte solutions: a hydrodynamic theory. *The Journal of Physical Chemistry*, **93**(5), 2079-2082.

ARCOS, J. C., MÉNDEZ, F., BAUTISTA, E. G., & BAUTISTA, O. (2018). Dispersion coefficient in an electro-osmotic flow of a viscoelastic fluid through a microchannel with a slowly varying wall zeta potential. *Journal of Fluid Mechanics*, **839**, 348–386.

BAUTISTA, O., SÁNCHEZ, S., ARCOS, J. C., & MÉNDEZ, F. (2013). Lubrication theory for electro-osmotic flow in a slit microchannel with the Phan-Thien and Tanner model. *Journal of Fluid Mechanics*, **722**, 496–532.

CHU, H. C. W., GAROFF, S., PRZYBYCIEN, T. M., TILTON, R. D., & KHAIR, A. S. (2019). Dispersion in steady and time-oscillatory two-dimensional flows through a parallel-plate channel. *Physics of Fluids*, **31**(2), 1-18.

DEL GIUDICE, F., D'AVINO, G., GRECO, F., DE SANTO, I., NETTI, P. A., & MAFFETTONE, P. L. (2015). Rheometry-on-a-chip: measuring the relaxation time of a viscoelastic liquid through particle migration in microchannel flows. *Lab on a Chip*, **15**(3), 783–792.

DEL GIUDICE, F., HAWARD, S. J., & SHEN, A. Q. (2017). Relaxation time of dilute polymer

solutions: A microfluidic approach. *Journal of Rheology*, **61**(2), 327–337.
DIETZEL, M., & HARDT, S. (2016). Thermoelectricity in Confined Liquid Electrolytes. *Physical Review Letters*, **116**(22), 225901.
DIETZEL, M., & HARDT, S. (2017). Flow and streaming potential of an electrolyte in a channel with an axial temperature gradient. *Journal of Fluid Mechanics*, **813**, 1060–1111.
D. R. LIDE. (2005). *CRC Handbook of Chemistry and Physics*, FL: CRC Press, Boca Raton,.
GHONGE, T., CHAKRABORTY, J., DEY, R., & CHAKRABORTY, S. (2013). Electrohydrodynamics within the electrical double layer in the presence of finite temperature gradients. *Physical Review E - Statistical, Nonlinear, and Soft Matter Physics*, **88**(5), 1–12.
HAYNES, W.M., LIDE, D.R. BRUNO, T.J. (2014). CRC Handbook of Chemistry and Physics, CRC Press, Boca Raton, 2014.
ISHIDO, T., & MIZUTANI, H. (1981). Experimental and theoretical basis of electrokinetic phenomena in rock-water systems and its applications to geophysics. *Journal of Geophysical Research*, **86**(B3), 1763.
NG, C. O. (2006). Dispersion in steady and oscillatory flows through a tube with reversible and irreversible wall reactions. *Proceedings of the Royal Society A: Mathematical, Physical and Engineering Sciences*, **462** (2066), 481–515.
PAN, S., NGUYEN, D. A., DÜNWEG, B., SUNTHAR, P., SRIDHAR, T., & RAVI PRAKASH, J. (2018). Shear thinning in dilute and semidilute solutions of polystyrene and DNA. *Journal of Rheology*, **62**(4), 845–867.
REPPERT, P. M. (2003). Temperature-dependent streaming potentials: 1. Theory. *Journal of Geophysical Research*, **108** (B11), 2546.
REVIL, A., PEZARD, P. A., & GLOVER, P. W. J. (2003). Streaming potential in porous media: 1. Theory of the zeta potential. *Journal of Geophysical Research: Solid Earth*, **104**(B9), 20021–20031.
TIRTAATMADJA, V., MCKINLEY, H. G., & COOPER-WHITE, J. J. (2006). Drop formation and breakup of low viscosity elastic fluids: Effects of molecular weight and concentration. *Physics of Fluids*, **18**(4).
VAN DER HEYDEN, F. H., BONTHUIS, D. J., STEIN, D., MEYER, C., & DEKKER, C. (2007). Power generation by pressure-driven transport of ions in nanofluidic channels. *Nano letters*, **7**(4), 1022-1025.
ZHANG, W., WANG, Q., ZENG, M., & ZHAO, C. (2019). Thermoelectric effect and temperature-gradient-driven electrokinetic flow of electrolyte solutions in charged nanocapillaries. *International Journal of Heat and Mass Transfer*, **143**, 118569.